PACIFIC EARTHQUAKE ENGINEERING
RESEARCH CENTER

New Ground Motion Selection Procedures and Selected Motions for the PEER Transportation Research Program

Jack W. Baker
Ting Lin
Shrey K. Shahi
Department of Civil and Environmental Engineering
Stanford University

Nirmal Jayaram
Risk Management Solutions, Inc.

PEER 2011/03
MARCH 2011

New Ground Motion Selection Procedures and Selected Motions for the PEER Transportation Research Program

Jack W. Baker
Ting Lin
Shrey K. Shahi
Department of Civil and Environmental Engineering
Stanford University

Nirmal Jayaram
Risk Management Solutions, Inc.

PEER Report 2011/03
Pacific Earthquake Engineering Research Center
College of Engineering
University of California, Berkeley

March 2011

ABSTRACT

The primary goal of this project was to develop strategies for selecting standardized sets of ground motions for use by the Pacific Earthquake Engineering Research Center's Transportation Research Program. The broad research activities of the Transportation Research Program require ground motions for use in a variety of applications, including analysis of structural and geotechnical systems at locations throughout California (or other active areas where seismic hazard is dominated by mid- to large-magnitude crustal earthquakes at near to moderate distances). The systems of interest may be sensitive to excitation at a wide range of periods, and some sites of interest may have the potential to experience near-fault directivity pulses. A unique aspect of this project is that these are not structure-specific and site-specific goals, so many ground motion selection techniques developed in previous research efforts are not directly applicable here.

This report summarizes the approaches that were developed to meet these goals and describes the properties of the ground motion sets that were selected. To develop some of the ground motion sets, a new selection algorithm is proposed that allows the user to select a set of ground motions whose response spectra match a target mean and variance; this new algorithm is also described. The project thus provides several useful sets of standardized ground motions, as well as a new approach to select alternate sets to meet user-specific needs.

ACKNOWLEDGMENTS

This work was supported by the State of California through the Transportation Research Program of the Pacific Earthquake Engineering Research Center (PEER). Any opinions, findings, and conclusion or recommendations expressed in this material are those of the authors and do not necessarily reflect those of the funding agency.

The authors thank Curt Haselton, Tom Shantz, Nilesh Shome, Peter Stafford and an anonymous reviewer for their helpful reviews of Section 2 during the process of its review as a journal manuscript. Thanks also to Curt Haselton for providing the structural models used for the example analyses in Section 2. Feedback from many Transportation Research Program researchers, which was invaluable in identifying user needs and data documentation requirements, is also appreciated.

CONTENTS

LIST OF FIGURES

LIST OF TABLES

1 STUDY OVERVIEW

1.1 INTRODUCTION

Efforts in recent decades to understand the properties of earthquake ground motions that affect geotechnical and structural systems have led to insights for structure-specific ground motion selection in performance-based earthquake engineering (PBEE). Current practice selects ground motions whose intensity (measured by an Intensity Measure or IM) is exceeded with some specified probability at a given site, and whose other properties are also appropriate (as typically determined by probabilistic seismic hazard and deaggregation calculations). See, for example, Krawinkler et al. (2003) Stewart et al. (2002), Mavroeidis et al. (2004), Kramer and Mitchell (2006), Kennedy et al. (1984), Bazzurro et al. (1998), Baker and Cornell (2006), and Haselton et al. (2009) among many others for progress and recommendations on structure-specific ground motion selection.

Research on this topic has focused primarily on cases where the structure and location of interest is known (so that ground motions can be selected and modified with specific structural properties and seismic hazard information in mind). The PEER Transportation Research Program (*peer.berkeley.edu/transportation/*), in contrast, is studying a wide variety of structural and geotechnical systems at a wide range of locations; this research would benefit from having a standardized set of ground motions to facilitate comparative evaluations. Even in situations where a specific location might be of interest, the Transportation Research Program often evaluates alternative structural systems (with differing periods of vibration) for potential use at a given location, so ground motion selection techniques that depend upon knowledge of structural periods are not applicable. Other techniques are thus needed to choose 'appropriate' ground motion sets for this research program. This document describes the process used to select three standardized ground motion sets intended for use by PEER and documents the properties of the selected ground motions. Because the ground motions are not structure-specific or site-specific,

it may be useful for the user to pre-process these ground motions prior to using them for structural analysis (e.g., by scaling the motions) or to post-process the structural analysis results (e.g., by using regression analysis to identify trends in structural response as a function of ground motion intensity parameters). The selected ground motions described in this report and some additional descriptive data for these motions are available electronically at *www.stanford.edu/~bakerjw/PEER_gms.html*.

1.2 OBJECTIVES

The goal of this project was to select several standardized sets of ground motions to be used in the PEER Transportation Research Program to analyze a variety of structural and geotechnical systems potentially located in active seismic regions such as California. Because of the wide variety of uses for these ground motions, as discussed above it is not feasible to use the site-specific/structure-specific ground motion selection methods most frequently proposed in recent research. Despite the generality of this objective, the scope of the ground motion selection were constrained as follows:

- Although the sites of interest will vary, we were generally interested in high-seismicity sites that may experience strong ground motions from mid- to large-magnitude earthquakes at close distances.
- Some sites of interest may be located nearby active faults and have the potential to experience near-fault directivity.
- Given that there are a variety of structures to be studied, some of which are also sensitive excitation at a wide range of periods, focusing on a specific period or narrow range of periods when selecting ground motions is not likely to be useful.
- The primary period range of interest was between 0 and 3 secs, with secondary interest in periods as long as 5 secs.
- It was assume that the users would be willing and able to utilize a relatively large number of ground motions (i.e., dozens to hundreds) in order identify probability distributions and statistical trends in system responses.

- Three-component ground motions were desired.

With these objectives and criteria in mind, four ground motion sets were selected and described in Section 0 below.

Site and structure-specific ground-motion selection methods often involve selecting a set of ground motions whose response spectra match a site-specific target response spectrum. That approach is not applicable here, because no single target spectrum is available. Instead, we selected ground motions with a variety of spectral shapes. This ensured that ground motions with a range of properties were available to analysts (and captured ground motion aleatory variability in the case that the analyst is interested in response from the scenario earthquake) and that variability in ground motion durations and directivity pulse periods (when applicable) was also present in the selected ground motions. Thus, previous research into the effect of spectral shape and directivity pulse properties on structural response (e.g., Baker and Cornell 2006; Rodriguez-Marek and Bray 2006) could also be incorporated using these ground motions. To achieve this goal, ground motions were selected such that the mean and variance of their logarithmic response spectra match that predicted for a 'generic earthquake scenario' typical of high-seismicity sites in California. This type of approach required selecting ground motions with specified variability in their response spectra and other parameters. As no algorithm currently exists to to easily incorporate such variability, a new algorithm was devised and is described in Section 2.

1.3 GROUND MOTION LIBRARY

All ground motions and associated metadata were obtained from the PEER Next Generation Attenuation (NGA) Project ground motion library (Chiou et al. 2008)., Available online at *http://peer.berkeley.edu/nga*, this library contains 3551 multi-component ground motions from 173 earthquakes. The earthquakes range in magnitudes from 4.3 to 7.9 and are primarily from shallow crustal earthquakes observed in seismically active regions of the world. The NGA project made a significant effort to carefully process these ground motion recordings (including filtering, baseline correcting, and verification of metadata such as associated source-site-distances and near surface site conditions). For this project, the selected ground motions were

rotated from their as-recorded orientations (the orientations provided by PEER) to strike-normal and strike-parallel orientations. The strike orientations used when performing this rotation come from the NGA Flatfile.

1.4 DOCUMENTATION OF SELECTED GROUND MOTIONS

The following sections of report summarize the procedures used to select ground motions and provide some summary data of the selected motions. The most detailed documentation of these motions, however, comes from the ground motion time histories themselves, as well as metadata, e.g., magnitudes, distances, and response spectra. A brief summary of the ground motion properties is provided in Appendix A, which provides a few metadata fields for each selected ground motion. A more complete set of information is available from the project website (*http://peer.berkeley.edu/transportation/publications_data.html*), including complete time histories, response spectra for all three components of each ground motion, etc. The appendix tables and project website also list an 'NGA Record Sequence Number' for each ground motion, which matches a corresponding field in the much more complete NGA Flatfile (*http://peer.berkeley.edu/nga/documentation.html*). Additional information not in the current NGA Flatfile, such as directivity pulse periods, scale factors (if applicable), and ε values, are included in the appendix tables or in spreadsheets posted at the project website.

2 A COMPUTATIONALLY EFFICIENT GROUND-MOTION SELECTION ALGORITHM FOR MATCHING A TARGET RESPONSE SPECTRUM MEAN AND VARIANCE[1]

2.1 INTRODUCTION

The 'broadband' ground motion sets discussed in Section 0 below were selected so that their response spectra (more precisely, their logarithmic response spectra) match a target mean and variance. Given that no practical algorithm was available to perform such a procedure, such an algorithm was developed to facilitate this task. This section presents a brief description of the new ground motion selection algorithm. This new selection algorithm probabilistically generates multiple response spectra from a target distribution, and then selects recorded ground motions whose response spectra individually match the simulated response spectra. A greedy optimization technique further improves the match between the target and the sample means and variances. The proposed algorithm is used to select ground motions for the analysis of sample structures in order to assess the impact of considering ground-motion variance on the structural response estimates. The implications for code-based design and PBEE are discussed.

The unique feature of this new approach is that it is able to produce a set of ground motions matching both a target mean and target variance of a log response spectrum, as opposed to most methods which match only a mean spectrum (e.g., Beyer and Bommer 2007; Shantz 2006; Watson-Lamprey and Abrahamson 2006). A notable exception is the algorithm of Kottke and Rathje (2008), but the technique developed here is more suitable to the current task because

[1] This section is adapted from Jayaram et al. (2011) with slightly modified text in some sections to more directly address the specific ground motion selection results presented below

it works easily with the large ground motion catalog considered here, does not require ground motion scaling, and reproduces desired correlations among response spectral values at pairs of periods.

Selecting a set of ground motions to match only a target mean response spectrum is computationally inexpensive, since it can be done by choosing time histories whose response spectra individually deviate the least from the target response spectrum. The deviation can be measured using the sum of squared differences between the response spectrum of the record and the target response spectrum (e.g., AMEC Geomatrix Inc. 2009; Youngs et al. 2006).

When matching a target mean and a target variance, however, it is not adequate to treat ground motions individually, but rather requires comparisons of the mean and variance of *sets* of ground motions to the target values. That is, the suitability of a particular ground motion can only be determined in the context of the complete ground-motion set in which it might be included. Generally, there are an intractably large number of possible ground-motion sets; therefore, identifying the best set is a computationally-expensive combinatorial optimization problem (Naeim et al. 2004). Although there are no automated procedures currently available to select ground motions that match the response spectrum mean and variance, one notable work in this regard is that of Kottke and Rathje (2008), who proposed a semi-automated procedure that first selects ground motions based on matching the mean spectrum, and subsequently applies individual scale factors on the ground motions to achieve the target variance. This technique is limited, however, as it does not easily scale to work with large ground-motion datasets and cannot be used for the selection of unscaled ground motions.

Besides the broadband selection cases discussed in Section 0, another important case where response spectrum variance may be important is the conditional mean spectrum (CMS), which is derived by conditioning on spectral acceleration at only a single period, $S_a(T^*)$ so the response spectra at other periods have variance (Baker 2011). To demonstrate the generality of this new algorithm and its relevance to cases beyond the broadband selection of Section 0, this section includes example results where the proposed algorithm is used to select ground motions matching a CMS for the purpose of estimating the seismic response of sample single-degree-of-freedom (SDOF) and multiple-degree-of-freedom (MDOF) structures[2]. The results are used to

[2] A description of this algorithm that selects the "Set #1A" ground motions described below as the example application is provided in Jayaram and Baker (2010).

demonstrate the algorithm and to assess the impact of considering ground-motion variance on the structural response estimates. The implications for code-based design and PBEE are discussed.

2.2 GROUND-MOTION SELECTION ALGORITHM

The objective of the proposed algorithm is to select a suite of ground motions whose response spectra have a specified mean and variance. This algorithm is based on the empirically verified observation that the set of logarithmic spectral accelerations ($\ln S_a$) at various periods is a random vector that follows a multivariate normal distribution (Jayaram and Baker 2008). The first step in this algorithm is to parameterize the multivariate normal distribution of $\ln S_a$'s at multiple periods. The parameters of the multivariate normal distribution are the means and variances of the $\ln S_a$'s at all periods, and the correlations between the $\ln S_a$'s at all pairs of periods. Equivalently, the distribution can be parameterized using the means of the $\ln S_a$'s and the covariances between the $\ln S_a$'s at all pairs of periods. In order to achieve the desired properties in the selected ground motions, these parameters should be set to their target values (i.e., target means and variances for the ground motions to be selected). A subsequent section illustrates this parameterization.

Once the distribution means and covariances are set equal to the desired target values, a Monte Carlo simulation is used to probabilistically generate response spectra from the above mentioned multivariate normal distribution. This can be performed using a standard function in many programming languages. The number of response spectra to be simulated equals the desired number of ground motions. For each simulated response spectrum, a ground motion with a similar response spectrum is then selected. The similarity between a ground-motion response spectrum and a Monte Carlo simulated response spectrum is evaluated using the sum of squared errors (SSE) described below:

$$SSE = \sum_{j=1}^{P} \left(\ln S_a(T_j) - \ln S_a^{(s)}(T_j) \right)^2 \tag{1}$$

where $\ln S_a(T_j)$ is the logarithmic spectral acceleration of the (optionally scaled) ground motion in consideration at period T_j, $\ln S_a^{(s)}(T_j)$ is the target $\ln S_a$ at period T_j from the simulated response spectrum, p is the number of periods considered, and SSE is the sum of squared errors

(which is a measure of dissimilarity). The measure of similarity defined by Equation 1 is not unique, and discussion of other measures of similarity can be found in Beyer and Bommer (2007) and Buratti et al. (2011). The selection is done by computing SSE for each ground motion in the database, and then choosing the ground motion having the smallest SSE. Other ground motion properties can also be accounted for at this stage, e.g., by considering only ground motions falling within a specified range of magnitudes and distances. Note that this is identical to comparison procedures currently used, except that here we are comparing to simulated spectra rather than a target mean spectrum.

The mean and the variance of the simulated response spectra will approximately match the corresponding target values because they were sampled from the desired distribution. This match will be nearly exact if a large number of spectra are simulated and will be approximate otherwise. Since the simulated response spectra have approximately the desired mean and variance, the response spectra selected using this approach will also have approximately the desired mean and variance. Additionally, this ground-motion selection approach also ensures that the selected set has the target correlation structure (i.e., correlation between $\ln S_a$'s at pairs of periods) specified while parameterizing the distribution of the response spectrum. This implies that in the particular case where the logarithmic response spectrum follows a multivariate normal distribution, the proposed algorithm actually matches the entire response spectrum distribution. Another advantage of this approach is that this algorithm allows the selection of unscaled ground motions (Jayaram and Baker 2010).

As mentioned above, when ground motions are selected using the approach described above, the sample means and variances may deviate slightly from the target values, particularly when the number of ground motions selected is small. Therefore, a 'greedy' optimization technique is used to further improve the match between the sample and the target means and variances. In this approach, each ground motion selected previously is replaced one at a time with a ground motion from the database that causes the best improvement in the match between the target and the sample means and variances. If none of the potential replacements causes an improvement, the original ground motion is retained. The mismatch is estimated as the sum of squared differences between the target and the sample means and variances over the period range of interest. The deviation of the set mean and variance from the target mean and variance (denoted SSE_s) is estimated as follows:

$$SSE_s = \sum_{j=1}^{p}\left[\left(\hat{m}_{\ln S_a(T_j)} - \mu^{(t)}_{\ln S_a(T_j)}\right)^2 + w\left(\hat{s}_{\ln S_a(T_j)} - \sigma^{(t)}_{\ln S_a(T_j)}\right)^2\right] \tag{2}$$

where SSE_s is the sum of squared errors of the set (which is the parameter to be minimized), $\hat{m}_{\ln S_a(T_j)}$ is the set mean lnS_a at period T_j, $\mu^{(t)}_{\ln S_a(T_j)}$ is the target mean lnS_a at period T_j, $\hat{s}_{\ln S_a(T_j)}$ is the set standard deviation of the lnS_a at period T_j, $\sigma^{(t)}_{\ln S_a(T_j)}$ is the target standard deviation of the lnS_a at period T_j, w is a weighting factor indicating the relative importance of the errors in the standard deviation and the mean (one possible value for w is 1, but it can be chosen depending on the desired accuracy in the match between the sample and the target means and standard deviations), and p is the number of periods (T_j) at which the error is computed.

The set mean and standard deviation can be calculated as follows:

$$\hat{m}_{\ln S_a(T_j)} = \frac{1}{n}\sum_{i=1}^{n} \ln S_{a_i}(T_j) \tag{3}$$

$$\hat{s}_{\ln S_a(T_j)} = \sqrt{\frac{1}{n-1}\sum_{i=1}^{n}\left(\ln S_{a_i}(T_j) - \hat{m}_{\ln S_a(T_j)}\right)^2} \tag{4}$$

where $\ln S_{a_i}(T_j)$ denotes the lnS_a of the i^{th} record in the set at period T_j, and n denotes the number of records in the set.

Note that the greedy optimization technique does not explicitly account for the correlation structure of selected sets. This correction structure is captured in the initial selection step, and is approximately retained after the greedy optimization as well.

The steps involved in the greedy optimization technique are summarized below.

- Step 1: Set j = 1.
- Step 2: Set i = 1. Denote the SSE_s of the set as $SSE_{s,old}$
- Step 3: If the ith database ground motion (G_i) is not already present in the set, replace the jth ground motion in the set with G_i. Compute $SSE_{s,i}$ (i.e., the SSE_s of the set after the replacement is carried out).

- Step 4: Reverse the replacement carried out in Step 3. Increment *i* by 1.
- Step 5: If *i* is less than or equal to the size of the ground-motion database, go to Step 3. Otherwise, identify the ground motion $\tilde{i}$ that results in the minimum value of $SSE_{s,\tilde{i}}$. If $SSE_{s,\tilde{i}} < SSE_{s,old}$, replace the *j*th ground motion in the set with the $\tilde{i}$ th ground motion in the database.
- Step 6: Increment *j* by 1. If *j* is less than the size of the set, go to Step 2. Otherwise, terminate the algorithm.

This is called a 'greedy' optimization technique because it maximizes the improvement in match between the target and sample at each iteration without necessarily achieving a global optimum solution. In this application, the initial simulation and selection steps result in a ground motion set that is already approximately optimal (for reasonably large sets). Once a near-optimal set has been selected, only this greedy technique is necessary to find a solution that is essentially globally optimal. Observational experience suggests that this algorithm never produces sets of ground motions with poor matches between the sample and the target means and variances (even for sets with as few as 10 ground motions, as illustrated in a subsequent section).

Appendix B, "An Alternate Ground-Motion Selection Algorithm," describes an alternate selection algorithm that does not require knowledge of the response spectrum distribution or the correlation structure.

2.3 ILLUSTRATIVE GROUND-MOTION SELECTION

This section describes applying the proposed algorithm to select structure-specific ground motions that have a specified spectral acceleration at the structure's fundamental period. In this example, the target response spectrum mean and covariance matrices are obtained using the conditional mean spectrum (CMS) method (Baker 2011), which provides the mean and variance (and correlations) of the response spectrum conditioned on the specified spectral acceleration. Note that while this example uses the targets from the CMS method, the proposed algorithm can be used with any arbitrary target mean and covariance (e.g., Jayaram and Baker 2010).

2.3.1 Parameterization of the Target Response Spectrum Distribution

As described in the previous section, the first step in the algorithm is to parameterize the multivariate normal distribution of the $\ln S_a$'s using the means and the variances of the spectral accelerations (chosen to equal the target mean and the target variance respectively) and the correlations between the spectral accelerations at two different periods. The steps involved in parameterizing the distribution using the CMS method are listed below.

- Step 1: Determine the target spectral acceleration (S_a) at a given period T^* (e.g., the fundamental period of the structure), and the associated magnitude (M), distance to source (R) and $\varepsilon(T^*)$, where $\varepsilon(T^*)$ is the number of standard deviations by which a given $\ln S_a$ differs from the mean predicted (by a ground-motion model) $\ln S_a$ at the period of interest T^*. In general,

$$\varepsilon(T) = \frac{\ln S_a(T) - \mu_{\ln S_a(T)}}{\sigma_{\ln S_a(T)}} \tag{5}$$

  where $\ln S_a(T)$ is the ground motion's logarithmic spectral acceleration at period T, and $\mu_{\ln S_a(T)}$ and $\sigma_{\ln S_a(T)}$ are the predicted mean and standard deviation, respectively, of $\ln S_a(T)$ given M, R, etc. (e.g., Campbell and Bozorgnia 2008). The values of M, R and $\varepsilon(T^*)$, can be obtained from deaggregation (e.g., USGS 2008).

- Step 2: For all T_j of interest, compute the unconditional mean and the unconditional standard deviation of the response spectrum, given M and R. In other words, compute $\mu_{\ln S_a(T)}$ and $\sigma_{\ln S_a(T)}$.

- Step 3: Compute the mean of $\left(\ln S_a(T_1), \ln S_a(T_2), ..., \ln S_a(T_n)\right)$ conditioned on $\varepsilon(T^*)$. This mean matrix (denoted μ) is computed as follows:

$$\boldsymbol{\mu} = \begin{bmatrix} \mu_{\ln S_a(T_1)} + \rho(T_1, T^*)\varepsilon(T^*)\sigma_{\ln S_a(T_1)} \\ \mu_{\ln S_a(T_2)} + \rho(T_2, T^*)\varepsilon(T^*)\sigma_{\ln S_a(T_2)} \\ . \\ . \\ \mu_{\ln S_a(T_n)} + \rho(T_n, T^*)\varepsilon(T^*)\sigma_{\ln S_a(T_n)} \end{bmatrix} \quad (6)$$

where $\rho(T_j, T^*)$ is the correlation between $\varepsilon(T_j)$ and $\varepsilon(T^*)$ [see, e.g., Baker and Jayaram (2008)].

- Step 4: Compute the covariance of $\left(\ln S_a(T_1), \ln S_a(T_2), ..., \ln S_a(T_n)\right)$ conditioned on $\varepsilon(T^*)$. This covariance matrix (denoted Σ) is estimated as follows:

  Let $\boldsymbol{\Sigma}_0$ denote the (unconditional) covariance matrix of the vector $\left(\ln S_a(T_1), \ln S_a(T_2), ..., \ln S_a(T_n)\right)$.

$$\boldsymbol{\Sigma}_0 = \begin{bmatrix} \sigma^2_{\ln S_a(T_1)} & \rho(T_1, T_2)\sigma_{\ln S_a(T_1)}\sigma_{\ln S_a(T_2)} & \cdots & \rho(T_1, T_n)\sigma_{\ln S_a(T_1)}\sigma_{\ln S_a(T_n)} \\ \rho(T_2, T_1)\sigma_{\ln S_a(T_2)}\sigma_{\ln S_a(T_1)} & \sigma^2_{\ln S_a(T_2)} & \cdots & \rho(T_2, T_n)\sigma_{\ln S_a(T_2)}\sigma_{\ln S_a(T_n)} \\ . & . & \cdots & . \\ . & . & \cdots & . \\ \rho(T_n, T_1)\sigma_{\ln S_a(T_n)}\sigma_{\ln S_a(T_1)} & \rho(T_n, T_2)\sigma_{\ln S_a(T_n)}\sigma_{\ln S_a(T_2)} & \cdots & \sigma^2_{\ln S_a(T_n)} \end{bmatrix} \quad (7)$$

  Let $\boldsymbol{\Sigma}_1$ denote the covariance between $\left(\ln S_a(T_1), \ln S_a(T_2), ..., \ln S_a(T_n)\right)$ and $\ln S_a(T^*)$, defined as follows:

$$\boldsymbol{\Sigma}_1 = \begin{bmatrix} \rho(T_1, T^*)\sigma_{\ln S_a(T_1)}\sigma_{\ln S_a(T^*)} \\ \rho(T_2, T^*)\sigma_{\ln S_a(T_2)}\sigma_{\ln S_a(T^*)} \\ . \\ . \\ \rho(T_n, T^*)\sigma_{\ln S_a(T_n)}\sigma_{\ln S_a(T^*)} \end{bmatrix} \quad (8)$$

  The covariance matrix of $\left(\ln S_a(T_1), \ln S_a(T_2), ..., \ln S_a(T_n)\right)$ conditioned on $\ln S_a(T^*)$ can be computed as follows (e.g., Johnson and Wichern 2007):

$$\boldsymbol{\Sigma} = \boldsymbol{\Sigma}_0 - \frac{1}{\sigma^2_{\ln S_a(T^*)}} \boldsymbol{\Sigma}_1 \boldsymbol{\Sigma}_1' \quad (9)$$

where $\boldsymbol{\Sigma}_1^{'}$ denotes the transpose of $\boldsymbol{\Sigma}_1$. The conditional standard deviation of the lnS_a's is the square root of the diagonals of $\boldsymbol{\Sigma}$, also given by Equation 10.

$$\sigma_{\ln S_a(T)|\ln S_a(T^*)} = \sigma_{\ln S_a(T)}\sqrt{1-\rho\left(T,T^*\right)^2} \tag{10}$$

Figure 2.1 shows the target conditional response spectrum mean and standard deviation obtained corresponding to magnitude = 7, distance to the rupture = 10 km, T^* = 2.63 sec, and $\varepsilon(T^*)$ = 2.0. These values have been chosen to be compatible with ground-motion studies carried out by Haselton et al. (2009). The unconditional lnS_a means and standard deviations corresponding to this scenario, $\mu_{\ln S_a(T_j)}$ and $\sigma_{\ln S_a(T_j)}$, are obtained from the Campbell and Bozorgnia (2008) ground-motion model. (Since lnS_a's at multiple periods follow a multivariate normal distribution, the exponential of the mean lnS_a equals the median spectral acceleration. This is why the axis of Figure 2.1 is labeled as 'Median S_a'.)

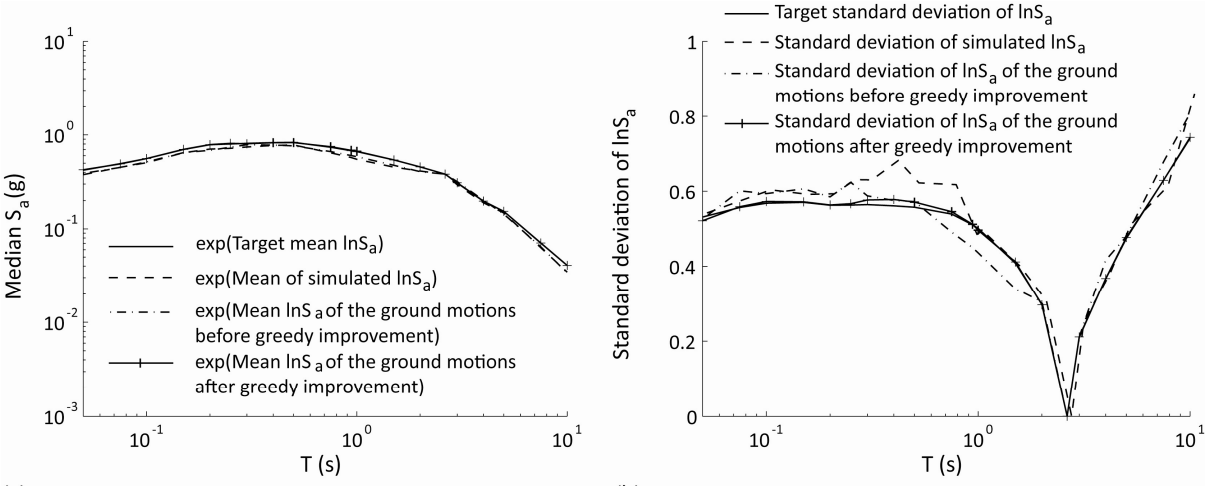

(a) (b)

Figure 2.1 (a) Response spectrum mean and (b) response spectrum standard deviation.

2.3.2 Response Spectrum Simulation

Using a Monte Carlo simulation, 40 response spectra were simulated by sampling from a multivariate normal distribution with the mean and covariance matrices defined by Equations 6 and 9 for the target scenario described above. The response spectra were simulated at 20 periods logarithmically spaced between 0.05 and 10.0 sec and are shown in Figure 2.2a. A large period range was used to ensure a good match in the entire response spectrum that covers regions of higher modes and nonlinearity. Because individual spectra may vary while still achieving a target mean and variance of the overall set, there is often little penalty in considering a broad period range in this step.

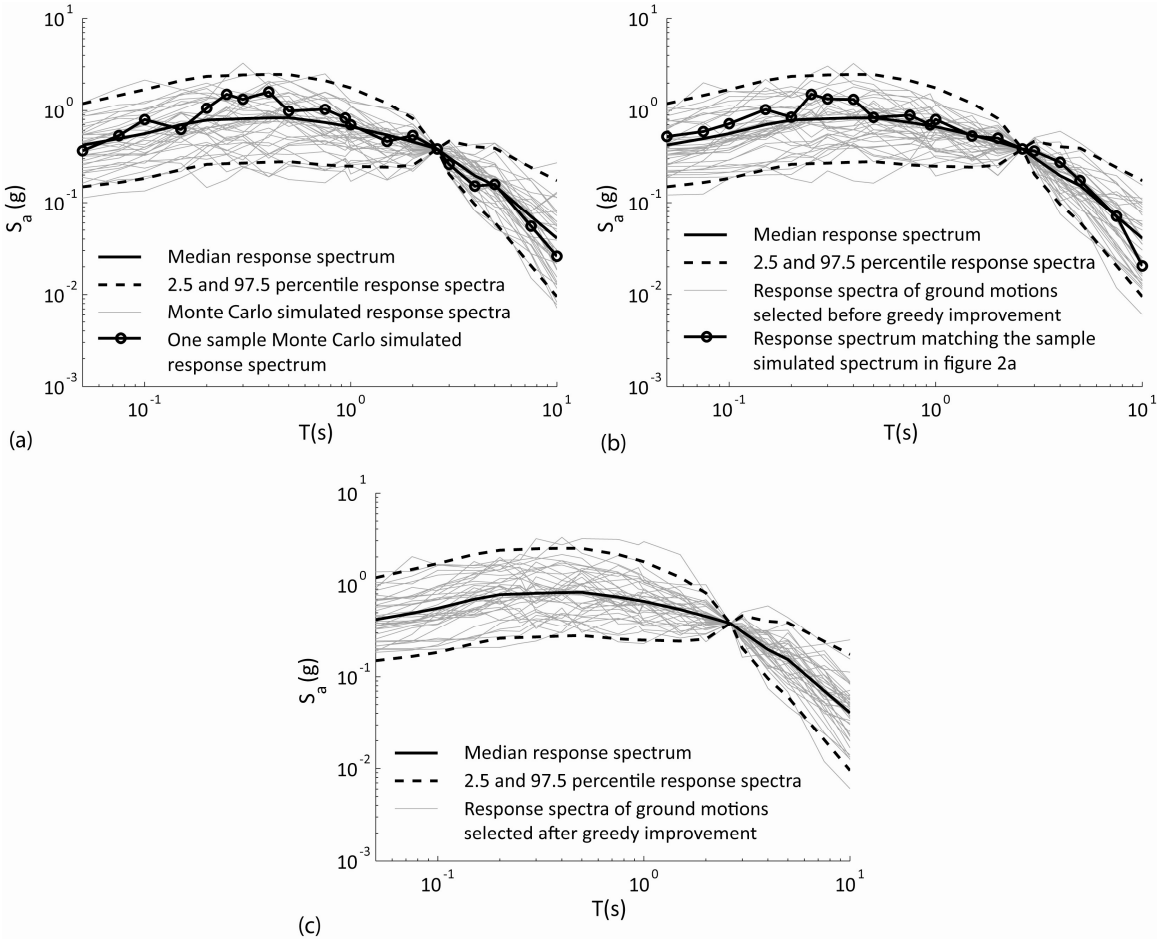

Figure 2.2 (a) Simulated response spectra; (b) response spectra of ground motions selected before greedy optimization; and (c) response spectra of ground motions selected after greedy optimization.

Figure 2.1a compares the mean of the Monte Carlo simulated response spectra to the target mean; obviously, the mean values agree reasonably well. Figure 2.1b shows a reasonable agreement between the standard deviation of the simulated lnS_a values and the target standard deviation. The small deviation seen in these figures is because the sample mean and standard deviation for moderately small sample sizes do not necessarily match the target mean and standard deviation.

2.3.3 Selection of Ground Motions to Match Simulated Spectra

Forty ground motions were selected from the NGA database (Chiou et al. 2008) that individually match the 40 response spectra simulated in the previous step. For two-dimensional structural models, a single ground motion component was required as an input for every time history analysis. [For three-dimensional structural models, two ground motion components may be selected by considering their geometric mean response spectrum, as described in Jayaram and Baker (2010).] Here, each horizontal component of a recording from the same station in the NGA database was treated separately as an individual ground motion. No constraints on the magnitudes and distances of the selected recordings were used, but such constraints are easily accommodated by simply restricting the set of ground motions considered for selection. Prior to selection, each of the available 7102 ground motions in the NGA database was scaled so that its $S_a(T^*)$ matches the target $S_a(T^*)$ from the target mean spectrum (seen in Figure 2.1a) when T^* is equal to 2.63 sec. Figure 2.2b shows the response spectra of the selected ground motions. The sample and the target means and standard deviations are shown in Figure 2.1, where it can be seen that the sample and the target response spectrum mean and variance match reasonably well. Additionally, the selected ground motion spectra also match the specified target correlation structure (specified by the non-diagonal terms of the covariance matrix in Equation 9) reasonably well, as indicated by a mean absolute error between the sample and the target correlations of 0.12.

The computational time required for selecting the set of 40 ground motions is 10 sec using a MATLAB implementation on an 8GB RAM 2.33GHz quad core processor. This computational efficiency allows for the algorithm to be optionally applied multiple times if considering several candidate sets to choose from. While selecting the ground motions shown in

Figure 2.2, we applied the algorithm twenty times to obtain multiple candidate ground-motion sets and chose the set with the minimum value of SSE. This approach is beneficial in situations where recorded ground motion spectra that adequately match one or more of the simulated spectra are not available.

2.3.4 Greedy Optimization Technique

The greedy optimization technique was used to modify the ground-motion suite selected in the previous step. The spectra of the selected ground motions are shown in Figure 2.2c. The means and the standard deviations of the set, shown in Figure 2.1, have a near perfect match with the target means and standard deviations. The mean absolute error between the sample and the target correlations is 0.15.

In total, the computational time required to select the set of 40 ground motions from the 7102 available ground motions was about 180 sec using a MATLAB implementation on an 8GB RAM 2.33GHz quad core processor. A MATLAB implementation of the proposed ground-motion selection algorithm can be downloaded from *http://www.stanford.edu/~bakerjw/gm_selection.html*.

2.3.5 Selection of a Smaller Number of Ground Motions

To test the effectiveness of the algorithm in sampling smaller ground motion sets, it is repeated to select a set of 10 ground motions for the scenario described earlier (magnitude = 7, distance to rupture = 10 km, $T^* = 2.63$ sec and $\varepsilon(T^*) = 2$). The response spectra of the selected records are shown in Figure 2.3a. The set means and standard deviations were compared to the target means and standard deviations in Figure 2.3b-c. The matches are good, illustrating the effectiveness of the algorithm in selecting small sets of ground motions. The mean absolute error between the sample and the target correlations is 0.17. The computational time required to select the set of 10 ground motions is about 25 sec using a MATLAB implementation on an 8GB RAM 2.33GHz quad core processor. The computational time required for selecting the set of 10 ground motions without using the greedy optimization technique is 4 sec.

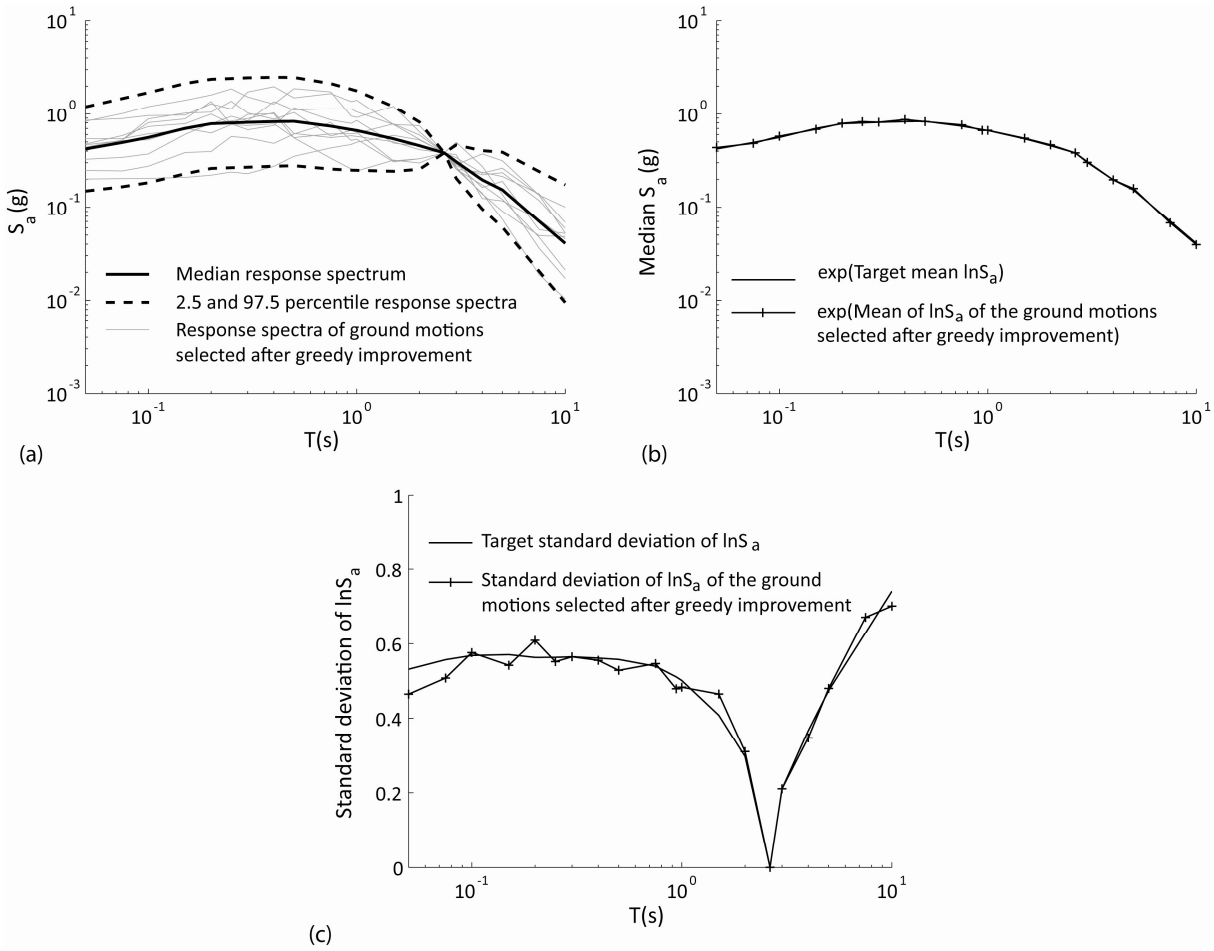

Figure 2.3 (a) Response spectra of 10 selected ground motions; (b) response spectrum mean; and (c) response spectrum standard deviation.

2.4 Impact of Matching Spectrum Variance on Structural Response

Code-based structural design and PBEE applications require statistics such as the mean (e.g., American Society of Civil Engineers 2005) or the median and the dispersion (e.g., Applied Technology Council 2009a) of the structural response. This next section evaluates the impact of ground-motion selection considering a target response spectrum mean and variance (as compared to considering only a target mean) on these statistics.

2.4.1 Ground-Motion Selection

The ground motions used for evaluating structural response were selected using the method described in the previous section for a target scenario with magnitude = 7, distance to rupture = 10 km, V_{s30} = 400 m/sec, and a strike-slip mechanism. The Campbell and Bozorgnia (2008) ground-motion model was used to estimate the mean and variance of the response spectrum. The values of ε and period T^* were varied to obtain multiple test scenarios. Three typical ε values of 0, 1, and 2 were considered. The structures considered in this work have periods (T^*) ranging between 0.5 sec and 2.63 sec.

In order to investigate the impact of matching response spectrum variance (Equation 9) on the structural response statistics, sets of 40 ground motions were selected using two methods: 'Method 1' matched only the target mean [a common approach in current practice, e.g., Baker and Cornell, 2006 and Method 300 in Haselton et al. (2009)]; 'Method 2' matched both the target mean and the target variance using the approach proposed here. The target response spectrum mean and covariance matrices were evaluated using Equations 6 and 9 for each combination of ε and T^*. Figure 2.4 shows example response spectra of ground motions selected using these two methods (for ε = 2 and T^* = 2.63 sec).

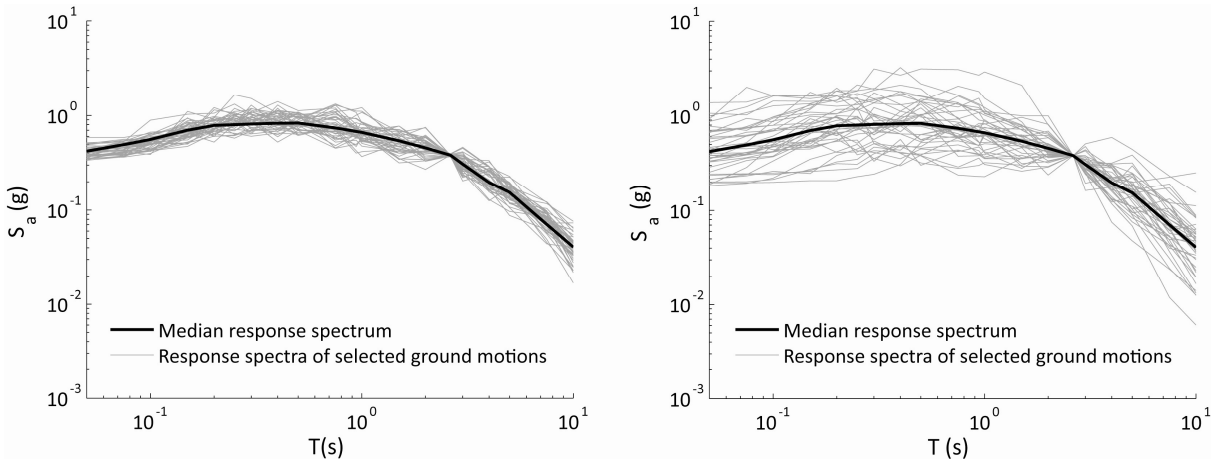

Figure 2.4 Response spectra of 40 selected ground motions for ε = 2 and T^* = 2.63 sec; (a) Method 1 matched target response spectrum mean, and (b) Method 2 matched target response spectrum mean and variance.

2.4.2 Structural Response

This section describes the response of sample nonlinear SDOF structures and MDOF buildings designed according to modern building codes. Herein, we consider only maximum displacement for the SDOF structures and maximum interstory drift ratio (MIDR) for the MDOF structures.

2.4.2.1 Description of Structural Systems

The SDOF structures considered in this work follow a non-deteriorating, bilinear force-displacement relationship (Chopra 2001). They have T^* = 0.5 sec, 5% damping, and post-yielding stiffness equal to 10% of elastic stiffness. Single-degree-of-freedom structures with '*R* factors' (the ratio of the target spectral acceleration at the period of the structure, $S_a(T^*)$, to the yield spectral acceleration = ω^2 * yield displacement, where ω is the structure's fundamental circular frequency) of 1, 4 and 8 were considered to study varying levels of nonlinear behavior. The *R* factor is controlled by varying the yield displacements of the SDOF structures relative to the $S_a(T^*)$ value obtained from the target spectrum. The SDOF structures are non-deteriorating systems, so structural collapse is not considered.

The MDOF structures used in this study were designed per modern building codes and modeled utilizing the Open System for Earthquake Engineering Simulation (OpenSEES) (McKenna et al. 2007) by Haselton and Deierlein (2007). The structural models consider strength and stiffness deterioration (Ibarra et al. 2005) unlike in the SDOF case. The designs for these buildings were checked by practicing engineers as part of the Applied Technology Council Project ATC-63 (2009b). They have also been used for previous extensive ground-motion studies (Haselton et al., 2009). The two buildings used in the current study are a 4-story reinforced concrete moment frame structure with T^* = 0.94 sec, and a 20-story reinforced concrete moment frame structure with T^* = 2.63 sec. The buildings show deterioration, and collapse is said to occur if dynamic instability (large increases in the drift for small increases in the ground-motion intensity) is reached in the model (Haselton and Deierlein 2007).

2.4.2.2 Response of SDOF Systems

Table 2.1 shows the mean, median and dispersion (dispersion refers to logarithmic standard deviation) of ductility ratios (spectral displacement divided by the yield displacement) of the SDOF structures under the different ground-motion scenarios described earlier. The ductility statistics were estimated using the two sets of 40 ground motions selected using Method 1 (ground motions selected by matching only the target response spectrum mean) and Method 2 (ground motions selected by matching the target response spectrum mean and variance). As shown in Table 2.1, the median ductilities are similar across the two ground-motion selection methods, while the mean and the dispersion of the response are higher in Method 2, when the ground-motion variance is considered. The higher dispersion of the response seen when using Method 2 is because of the uncertainty in the response spectra, which is ignored in Method 1. As expected, the increase in dispersion is particularly significant at large R values when the structure behaves in a nonlinear manner. Note that there are no differences between the methods when $R = 1$, because the response is dependent only on $S_a(T^*)$, which is identical in both cases.

Table 2.1 Ductility ratios of example SDOF structures.

ε	R	Median Ductility		Dispersion of Ductility		Mean Ductility	
		Method 1	Method 2	Method 1	Method 2	Method 1	Method 2
0	1	1.00	1.00	0	0	1.00	1.00
	4	3.93	3.76	0.24	0.31	4.21	4.18
	8	10.76	9.97	0.28	0.42	10.82	10.74
1	1	1.00	1.00	0	0	1.00	1.00
	4	3.55	3.35	0.22	0.33	3.79	3.93
	8	8.04	8.16	0.28	0.46	8.57	9.46
2	1	1.00	1.00	0	0	1.00	1.00
	4	3.27	3.04	0.19	0.28	3.39	3.34
	8	6.90	7.44	0.24	0.41	7.34	7.98

Figure 2.5 shows the fraction of response analyses that result in a ductility less than a specified value for the SDOF structure with $R = 8$ in the $\varepsilon = 1$ scenario, estimated using Methods 1 and 2. This type of plot is referred to as an empirical cumulative distribution function, or CDF. The CDFs intersect at a value of approximately 0.5 due to the similarity in the median response in both cases. The CDF obtained using Method 2 is flatter, with heavier tails as a result of the larger dispersion observed in this case. As seen in Figure 2.5a, the upper tails of the CDFs are heavier than the lower tails. Since the mean response is the area above the CDF (the mean of a random variable is the area under the complementary CDF, which equals 1 - CDF), it can be visually observed that the difference in the heaviness of the upper tails results in a larger mean value of the response in case of Method 2 as compared to Method 1. This is a graphical evidence of the larger mean values reported earlier in Table 2.1. Analytically, if the responses were to follow a lognormal distribution (a common assumption in PBEE), the properties of the lognormal distribution imply that a larger dispersion results in a larger mean for a fixed median, which also explains the larger means observed in Method 2.

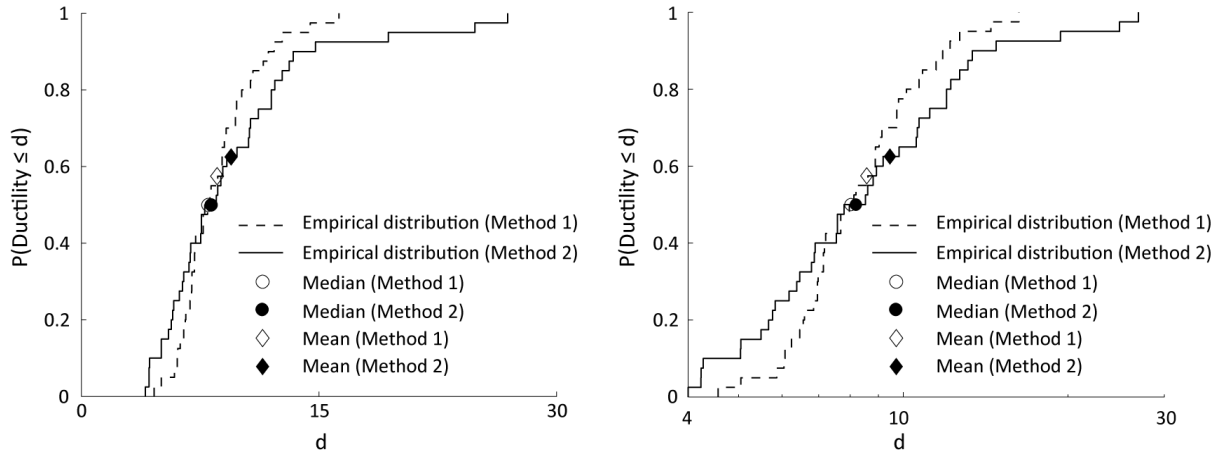

Figure 2.5 Distribution of the structural response of the SDOF structure corresponding to $R = 8$ and $\varepsilon\left(T^*\right) = 1$: (a) Linear scale and (b) logarithmic scale.

2.4.2.3 Response of MDOF Systems

Table 2.2 summarizes the MIDR estimates for the MDOF structures considered in this study under various ground-motion scenarios, estimated using Methods 1 and 2. The distributions of responses are summarized using the probability of collapse (i.e., counted fraction of responses indicating collapse) and the median and the dispersion of the non-collapse responses.

As shown in Table 2.2 as observed in the SDOF case, the medians are similar regardless of whether Method 1 or 2 was used in all considered scenarios. The dispersions are larger, however, when the ground-motion variance is considered in Method 2. The increase in the dispersion also results in an increased probability of observing large values of structural response. This can result in an increased probability of structural collapse while using Method 2, as evidenced, for example, when $\varepsilon = 2$ in Table 2.2.

Figure 2.6 shows the empirical CDF of the MIDR of the 20-story frame corresponding to the $\varepsilon = 2$ ground-motion scenario. As seen in the SDOF case, the CDF obtained using Method 2 is flatter and has heavier tails on account of larger dispersion. The maximum plotted values of the CDFs differ from one, and the difference equals the probability of collapse.

Table 2.2 Maximum interstory drift ratio of 20-story and 4-story moment frames.

Building	ε	Median MIDR		Dispersion of MIDR		Collapse Probability	
		Method 1	Method 2	Method 1	Method 2	Method 1	Method 2
20-story moment frame	0	0.0044	0.0043	0.18	0.32	0	0
	1	0.0096	0.0086	0.24	0.29	0	0
	2	0.0186	0.0196	0.25	0.43	0	0.05
4-story moment frame	0	0.0072	0.0072	0.09	0.09	0	0
	1	0.0137	0.0139	0.26	0.29	0	
	2	0.0279	0.0237	0.28	0.46	0.10	

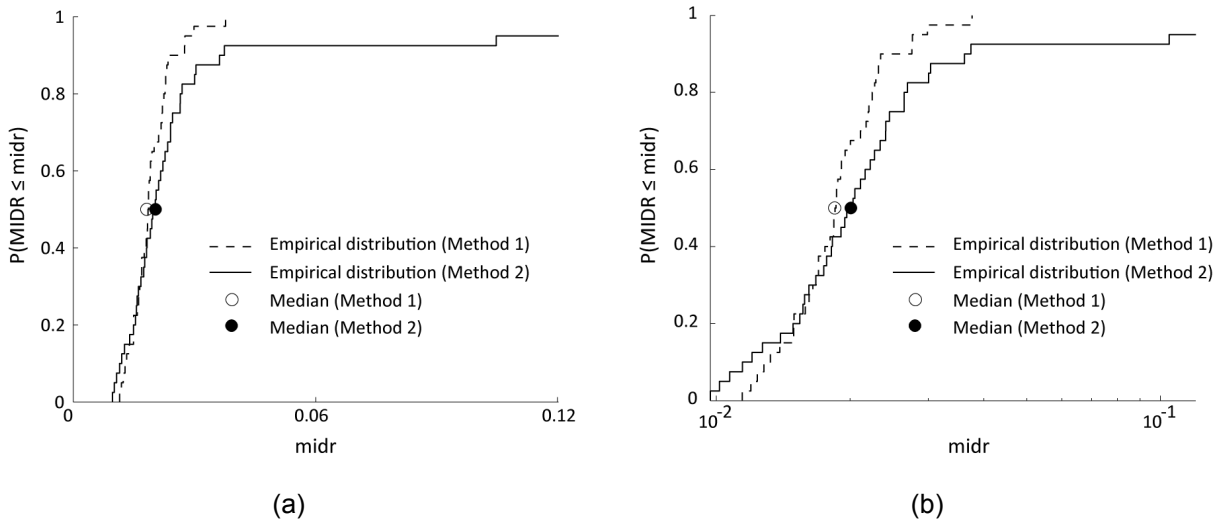

Figure 2.6 Distribution of the structural response of the 20-story moment frame building corresponding to $\varepsilon\left(T^*\right)=2$: (a) linear scale and (b) logarithmic scale.

In summary, the response estimates for the SDOF and the MDOF structures across several ground-motion scenarios show that the consideration of the response spectrum variance while selecting ground motions does not significantly impact the median structural response, but tends to increase the mean response and the dispersion in the response. The increased dispersion can result in more extreme responses, which can lead to a larger probability of structural collapse. These example analysis cases serve to illustrate the potential importance of matching response spectrum variance, calling for more detailed investigations in the future.

2.5 IMPLICATIONS

Code-based design is often concerned with the average response of the structure (e.g., ASCE 2005). The average response is typically interpreted as the mean response, although sometimes it is interpreted as the median. If median structural response is of interest, the consideration of the response spectrum variance while selecting ground motions does not have a significant impact in the limited investigation performed here. On the other hand, if mean structural response is of interest, the consideration of the response spectrum variance appears to increase the mean structural response and may thus impact code-based design calculations.

In contrast, PBEE often requires knowledge about the full distribution of structural response (ATC-58 2009). Matching target response spectrum variance increases the dispersion of structural response, thereby affecting the distribution of structural response and, consequently, the damage state and loss estimation computations in PBEE. The increase in the dispersion leads to higher and lower extremes of structural response and the associated damage states and losses. Because this increased dispersion can also lead to a larger probability of structural collapse, PBEE calculations will thus almost certainly be affected by this issue.

In summary, the example analyses presented above and engineering intuition suggest that the target response spectrum variance used when selecting ground motions has an impact on the distribution of structural responses obtained from resulting dynamic analysis for both code-based design checks and PBEE analysis. Further study is needed to quantify the magnitude of these impacts, and this new algorithm will facilitate such studies.

3 SELECTED GROUND MOTIONS

Using the approach outlined in Section 2, two sets of 'broad-band' ground motions were selected that have the distribution of response spectra associated with moderately large earthquakes at small distances. A third set of ground motions was selected to have strong velocity pulses that might be expected at sites experiencing near-fault directivity. A fourth set of ground motions is provided to match a Uniform Hazard Spectrum for a site in Oakland, California, and is comparable to ground motions that would be used to satisfy a code-type analysis. Details regarding the selection of these sets of ground motions are provided in this section.

3.1 SET #1A: BROAD-BAND GROUND MOTIONS (M = 7, R = 10 KM, SOIL SITE)

This ground motion set consists of 40 unscaled three-component ground motions selected so that their horizontal response spectra match the median and log standard deviations predicted for a magnitude 7 strike-slip earthquake at a distance of 10 km. The site V_{s30} (average shear wave velocity in the top 30 m) was assumed to be 250 m/sec. The means and standard deviations of resulting response spectra were computed from Boore and Atkinson (2008), and correlations of response spectra among periods were computed from Baker and Jayaram (2008). The ground motions were selected to match this target at periods between 0 and 5 sec, as this was identified as the period range of interest for the systems being studied in the Transportation Research Program. Figure 3.1 illustrates the distribution of response spectra expected for this earthquake scenario (where the median response spectrum is computed by taking the exponential of $\overline{\ln S_a(T_i)}$, and the 2.5 and 97.5 percentiles of the distribution are the exponentials of $\overline{\ln S_a(T_i)} \pm 1.96\sigma(T_i)$).

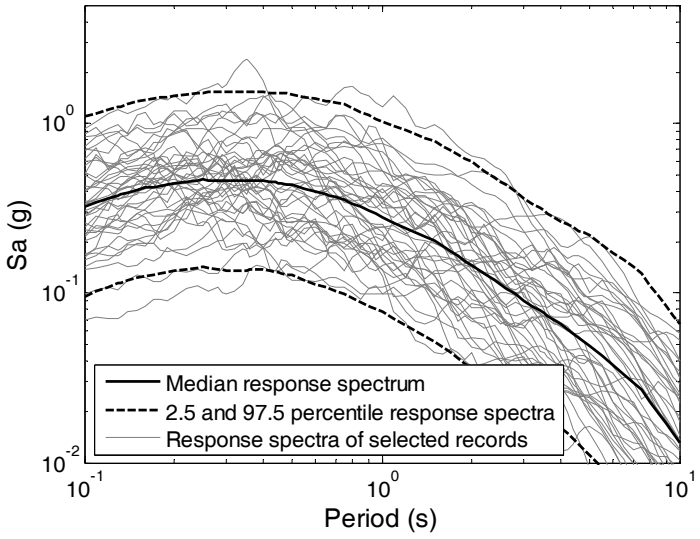

(a)

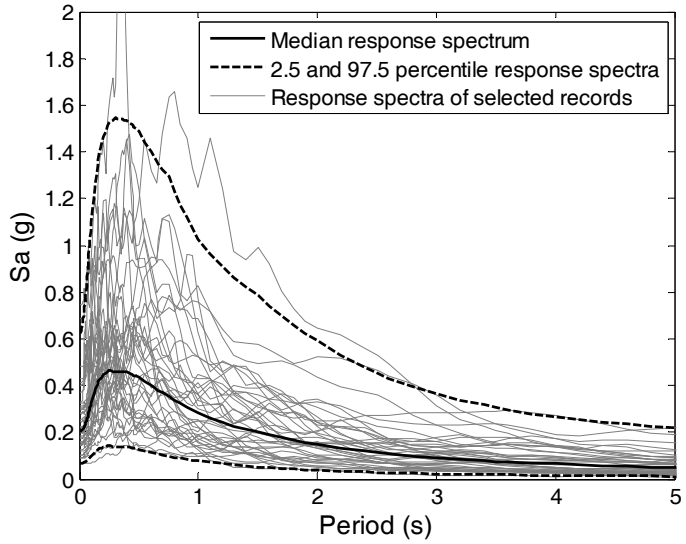

(b)

Figure 3.1 Response spectra of the selected ground motions[3] for soil sites, compared to the target response spectra predicted by the ground motion model (Boore and Atkinson 2008): (a) plot with log-log of the axes and (b) plot with linear scaling of the axes.

[3] Throughout this chapter, plots of response spectra show the geometric mean spectra of the horizontal ground motion components after they have been rotated to their fault-normal and fault-parallel orientations. This is only one way of defining spectral acceleration for multi-component ground motions, but was deemed suitable for these graphical comparisons. The project website at *http://peer.berkeley.edu/transportation/publications_data.html* contains the complete documentation of the ground motions and spectra, and includes tables of these geometric mean spectra as well as GMRotI50 spectra (Boore et al. 2006) (which are generally very similar to the geometric mean values), vertical response spectra and individual-component response spectra.

When using the procedure of Section 2 to search for ground motions matching the target means and standard deviations, ground motions of any magnitude and with distance < 50 km were considered. This decision is justified because ground motion response spectra are often more important to structural response than the ground motion magnitude and distance (Shome et al. 1998), so using a wide magnitude and distance range would increase the number of potential usable ground motions without significantly compromising the accuracy of resulting structural analysis results obtained using the ground motions. Further, having ground motions with variability in their magnitude and distance values allows researchers to examine whether there are trends in computed structural or geotechnical response parameters that correlate with variation in the ground motion properties (such as magnitude and distance). Such studies are not possible when all of the selected ground motions have a narrow range of magnitudes and distances. Comparison of the ground motion magnitudes and distances obtained in this manner, relative to the case when one attempts to match a narrow magnitude and distance target, are provided in Section 3.6.

Because the selected ground motions in this set are intended specifically for use at soil sites, only recorded ground motions with site V_{s30} values between 200 and 400 m/sec were considered for selection.

The response spectra of the selected ground motions are shown in Figure 3.1, and they visually match the target means and standard deviations of the logarithmic response spectrum predicted for this scenario. This match is further illustrated in Figure 3.2, which compares of the means and standard deviations of $\ln S_a$ for the recorded ground motions to the associated targets. Table A.1 in Appendix A provides further summary data for the selected ground motions.

3.2 SET #1B: BROAD-BAND GROUND MOTIONS (M = 6, R = 25 KM, SOIL SITE)

This ground motion set was selected using the same procedures as Set #1A, except the ground motions were selected so that their response spectra match the median and log standard deviations predicted for a magnitude 6 strike-slip earthquake at a distance of 25 km. The site V_{s30} (average shear wave velocity in the top 30 m) was again assumed to be 250 m/sec. The response spectra of the selected ground motions are shown in Figure 3.3 with the target spectra superimposed, and Comparison of the means and standard deviations of the selected spectra are

compared to their corresponding targets in Figure 3.4. Selected summary data for these ground motions is provided in Table A.2 of Appendix A.

Figure 3.5 shows the response spectra from Set #1A and #1B of the ground motions superimposed in a single plot to illustrate the broad range of spectral amplitudes represented by the union of these two sets. Another way to view this variability is as a histogram of spectral values at a single period, as shown in Figure 3.6 for a period of 1 sec. As evident in Figure 3.5 and Figure 3.6, the elastic spectral values across the union of these two sets can vary by up to two orders of magnitude, and that the sets overlap at intermediate spectral values. Recalling that these ground motions are all unscaled, the union of these sets provides a set of as-recorded ground motions that cover a broad range of intensities of interest at sites located near active crustal earthquake sources.

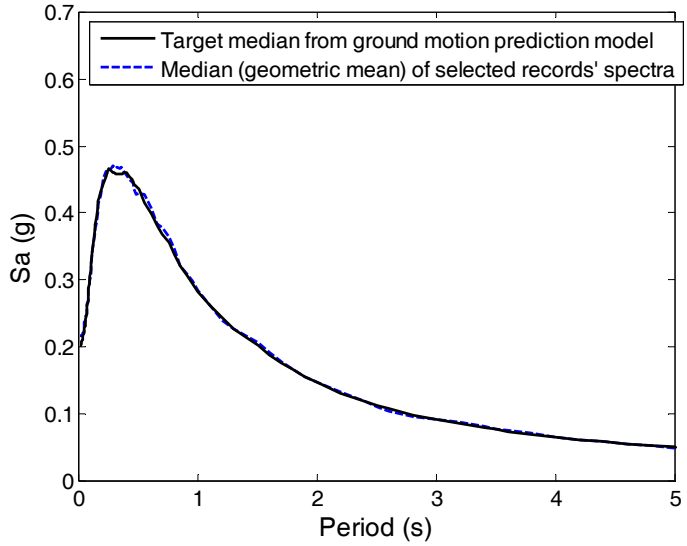

(a)

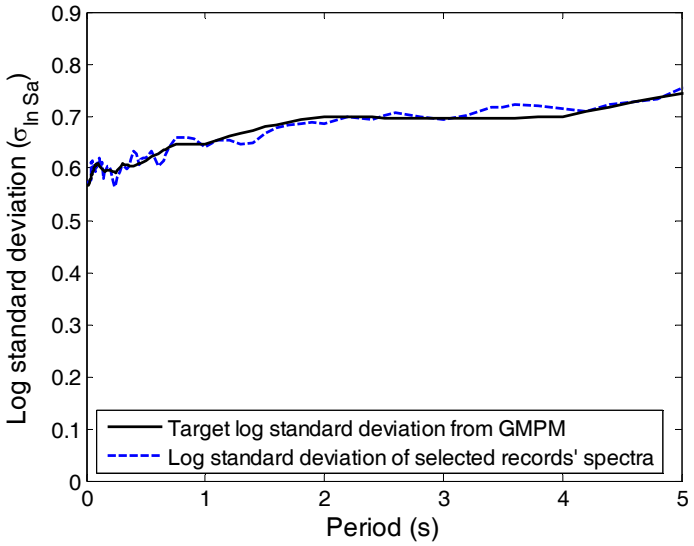

(b)

Figure 3.2 **(a) Target median response spectra and the median response spectra of the selected ground motions for soil sites (medians are computed as the exponentials of mean lnS_a values); and (b) target standard deviations of lnS_a, and standard deviations of the lnS_a values of the selected ground motions.**

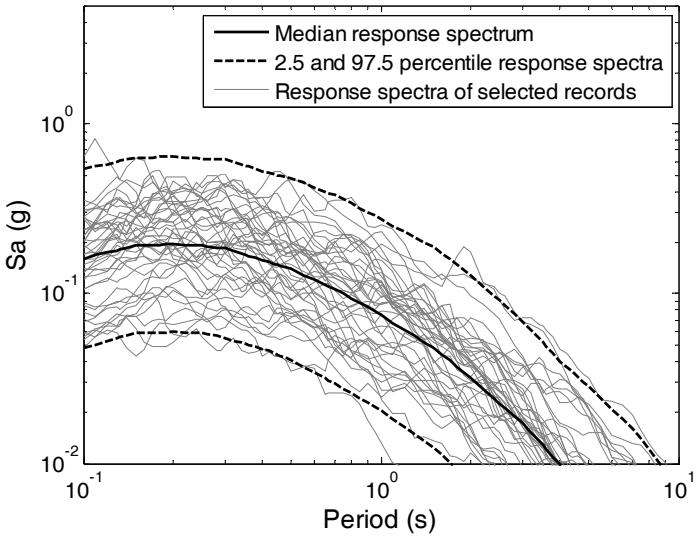

(a)

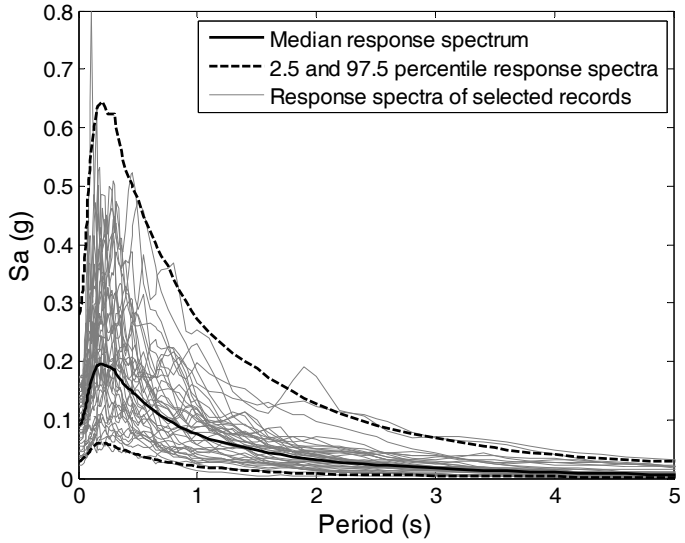

(b)

Figure 3.3 Response spectra of the selected ground motions for soil sites, compared to the target response spectra predicted by the ground motion model (Boore and Atkinson 2008): (a) plot with log-log of the axes and (b) plot with linear scaling of the axes.

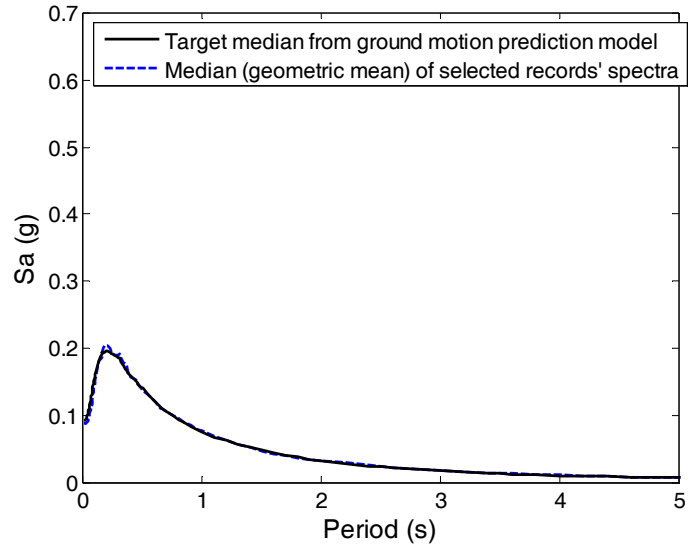

(a)

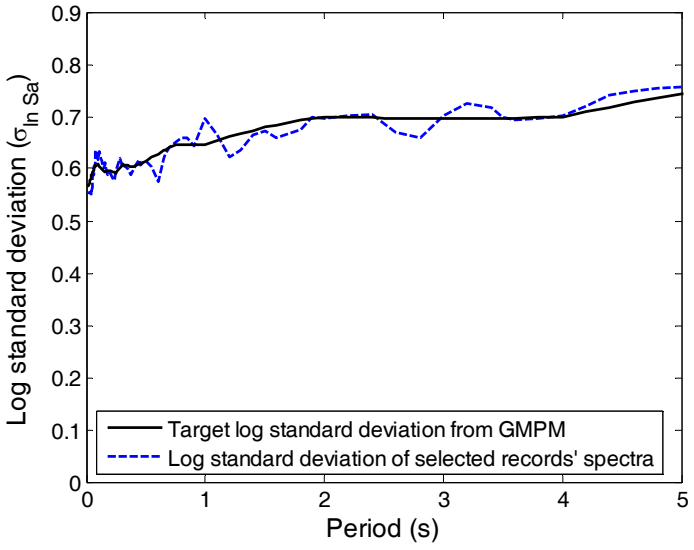

(b)

Figure 3.4 **(a) Target median response spectra and the median response spectra of the selected ground motions for soil sites (medians are computed as the exponentials of mean lnS_a values); and (b) Target standard deviations of lnS_a, and standard deviations of the lnS_a values of the selected ground motions.**

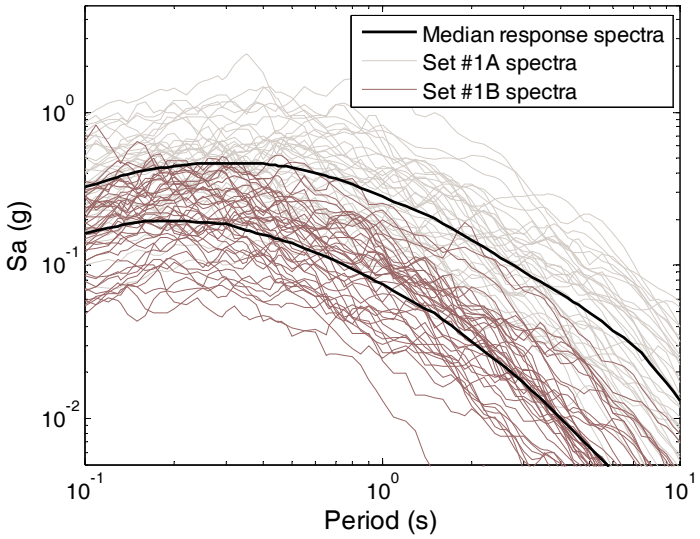

Figure 3.5 Spectra ground motions selected for Set #1A and #1B.

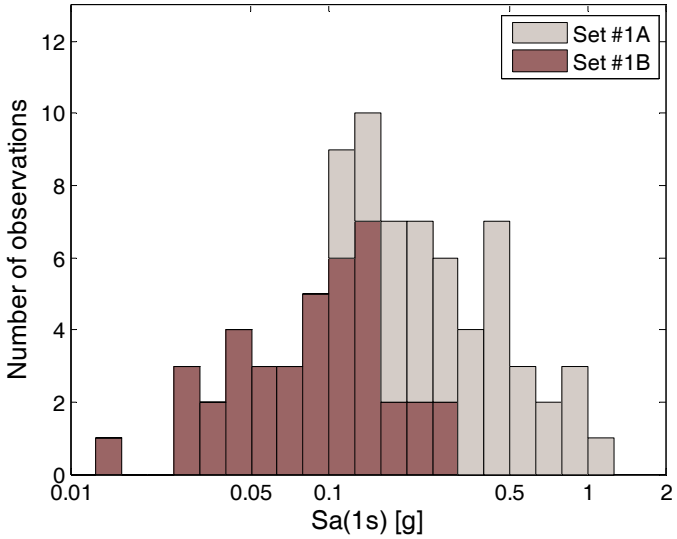

Figure 3.6 Histogram of spectral acceleration values at a period of 1 sec from the ground motions in Set #1A and #1B.

3.3 SET #2: BROAD-BAND GROUND MOTIONS (M = 7, R = 10 KM, ROCK SITE)

This ground motion set consists of 40 unscaled three-component ground motions selected so that their response spectra match the median and log standard deviations predicted for a magnitude 7 strike slip earthquake at a distance of 10 km. The site V_{s30} was assumed to be 760 m/sec; this shear wave velocity is the only value that differs from the target scenario for Set #1. The larger

V_{s30} value was chosen because ground motions are intended to be representative of those observed at rock sites or to be used as bedrock level ground motions for site response analyses. The distribution of response spectra associated with this event was computed as for Set #1A and #1B. All ground motions in the database with $V_{s30} > 625$ m/sec were considered for inclusion in the set (this was the narrowest range for which there were sufficient ground motions to ensure a good match to the target response spectrum distribution).

The response spectra of the selected ground motions are shown in Figure 3.7, and as with Set #1 they visually match the target means and standard deviations of the logarithmic response spectra predicted for this scenario. This match is also illustrated in Figure 3.8, which compares the means and standard deviations of $\ln S_a$ for the recorded ground motions to the associated targets. Table A.3 in the appendix provides further summary data for the selected ground motions.

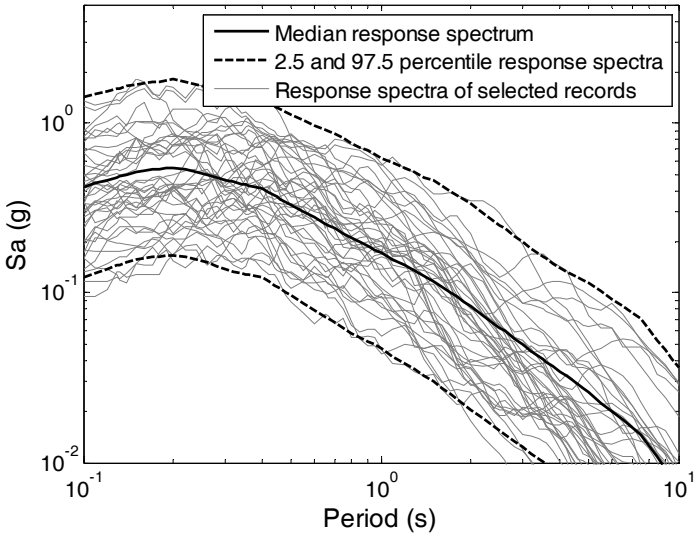

(a)

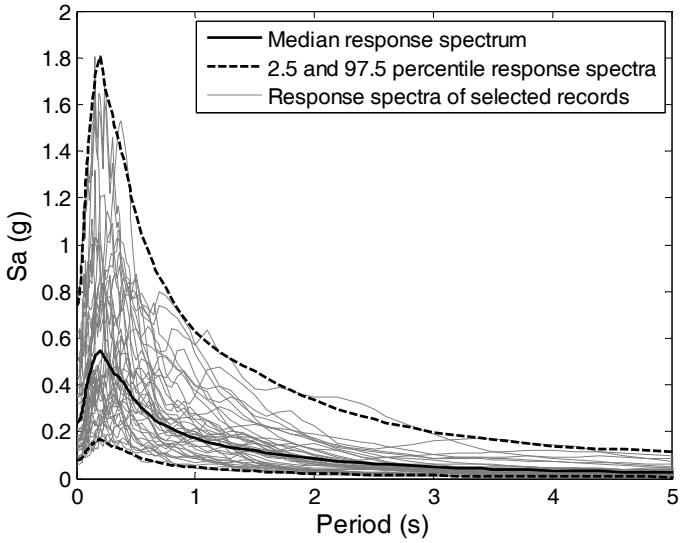

(b)

Figure 3.7 Response spectra of the selected ground motions for rock sites, compared to the target response spectra predicted by the ground motion model (Boore and Atkinson 2008): (a) plot with log-log scaling of the axes, and (b) plot with linear scaling of the axes

.

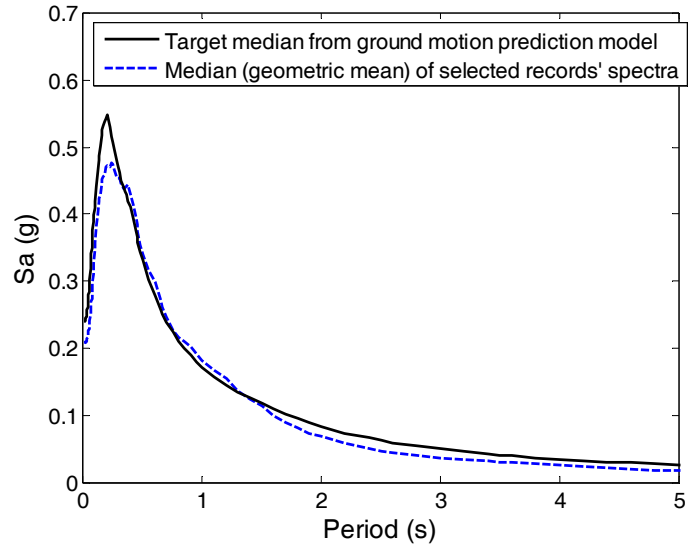

(a)

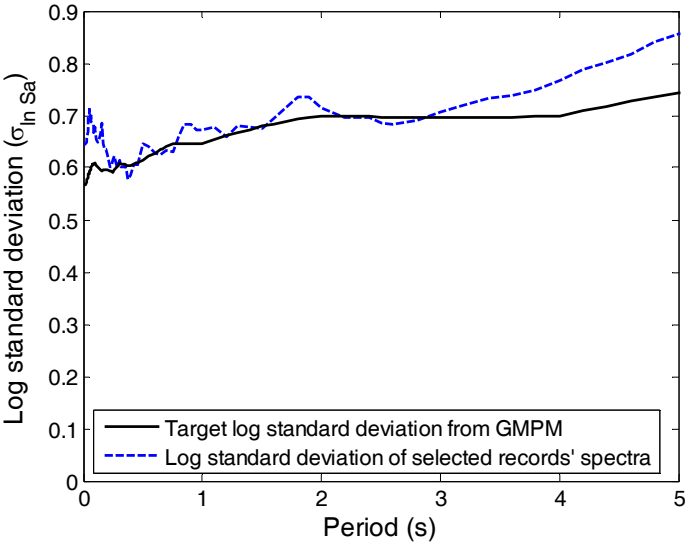

(b)

Figure 3.8 **(a) Target median response spectra and the median response spectra of the selected ground motions for rock sites (medians are computed as the exponentials of mean lnS_a values); and (b) Target standard deviations of lnS_a, and standard deviations of the lnS_a values of the selected ground motions.**

3.4 SET #3: PULSE-LIKE GROUND MOTIONS

This ground motion set consists of 40 unscaled three-component ground motions containing strong velocity pulses of varying periods in their strike-normal components. These velocity pulses are expected to occur in some ground motions observed near fault ruptures due to directivity effects. Example velocity time histories of these motions are shown in Figure 3.9.

The ground motions in this set were all selected because they have a strong velocity pulse in the strike-normal direction, as determined using the method described by Baker (2007). Strong velocity pulses are also apparent in a range of other orientations in these ground motions, but the strike-normal component was the one studied carefully during the selection process. The method used here to identify velocity pulses has previously been used in the PEER Design Ground Motion Library (Youngs et al. 2006) and the ATC-63 project (Applied Technology Council 2009b). The near-fault ground motions used in the ATC-63 project are similar to those here—slight differences will be discussed below. For this set, no attempt was made to match any target response spectrum, so the selection procedure of Section 2 was not used.

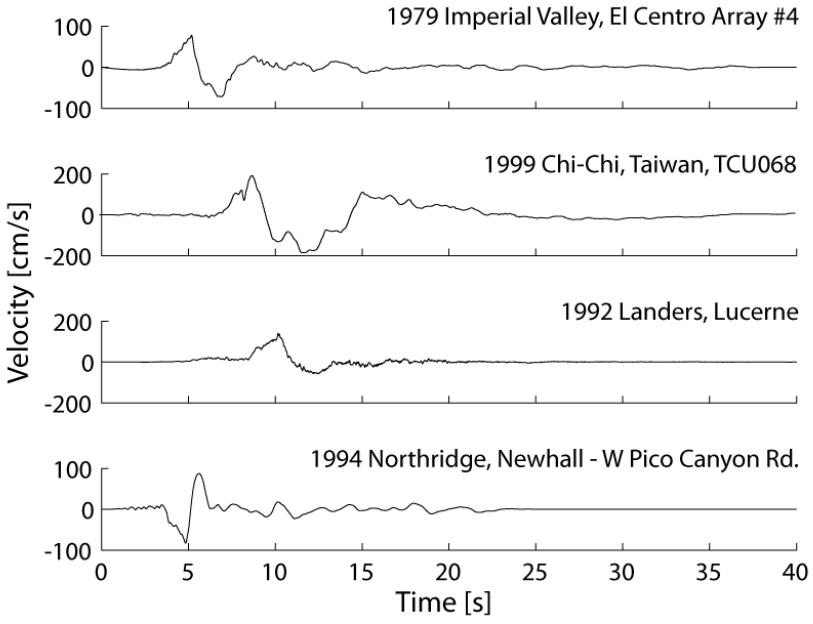

Figure 3.9 Strike-normal velocity time histories of four ground motions from Set #3.

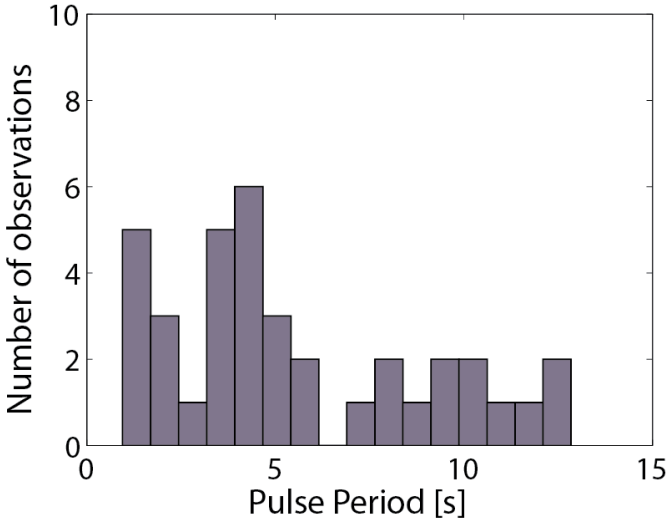

Figure 3.10 Histogram of pulse periods in ground motion Set #3.

These 40 ground motions were chosen to have a variety of pulse periods. This was done because the pulse period, relative to the period(s) of oscillation a structure, is known to be an important factor affecting structural response. The histogram of pulse periods present in this set is shown in

. Pulse periods range between 1.0 seconds and 12.9 sec, with a mean of 5.5 sec. Pulse periods were determined as part of the analysis technique used to identify the pulses (Baker 2007), and pulse periods for the selected ground motions were tabulated along with other data in Table A.4 of Appendix A.

Histograms of peak ground velocities of the selected ground motions are shown in Figure 3.11, indicating that these ground motions are generally very intense. Strike-normal peak ground velocities ranged from 30 to 185 cm/sec, with a mean of 85 cm/sec. Strike parallel peak ground velocities were generally somewhat smaller (17 to 115 cm/sec, with a mean of 61 cm/sec), with the exception of the Chi-Chi TCU068 motion having a strike parallel PGV of 250 cm/sec. Distances from the fault rupture are shown in Figure 3.12. All but one ground motion was observed within 11 km of the fault rupture, and the mean distance was 5 km. The selected ground motions come from earthquakes with a variety of rupture mechanisms.

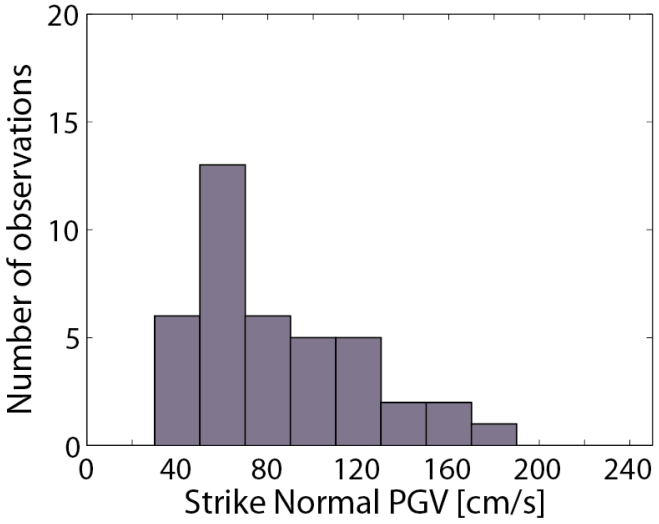

Figure 3.11 Histogram of strike-normal peak ground velocities in ground motion Set #3.

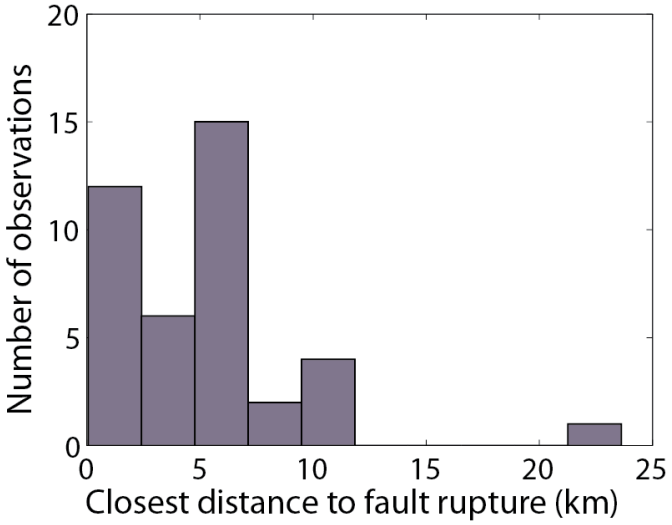

Figure 3.12 Histogram of closest distances to the fault ruptures for the ground motions in Set #3.

One benefit of the technique used to identify velocity pulses is that it also extracts the pulse portion of the ground motion from the overall ground motion. Example output from this extraction analysis is shown in Figure 3.13. Separate sets of time histories for the original motion, the extracted pulse and the residual ground motion are provided at *http://peer.berkeley.edu/transportation/publications_data.html*, to facilitate any studies of the effects of the pulse and non-pulse components of the motions separately.

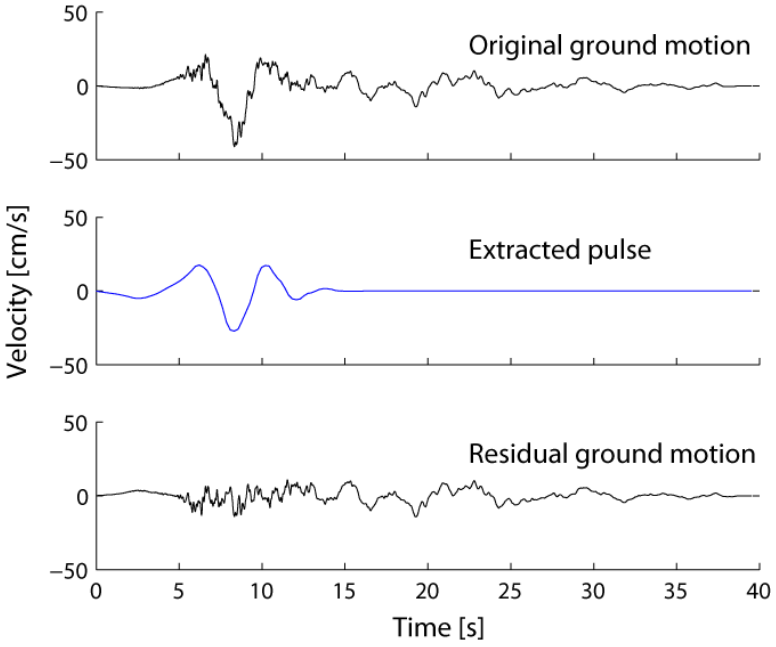

Figure 3.13 Original ground motion, extracted pulse, and residual ground motion for the 1979 Imperial Valley El Centro Array #3 ground motion.

3.5 SET #4: SITE-SPECIFIC GROUND MOTIONS FOR OAKLAND

These site-specific ground motions were selected to be representative of the hazard at the site of the I-880 viaduct in Oakland, California, which runs from near the intersection of Center and 3rd Streets to Market and 5th Streets. Those locations are noted in Figure 3.14. For the hazard analysis used here, a location of 37.803N x 122.287W was used; this location is labeled 'Oakland site' in Figure 3.14.

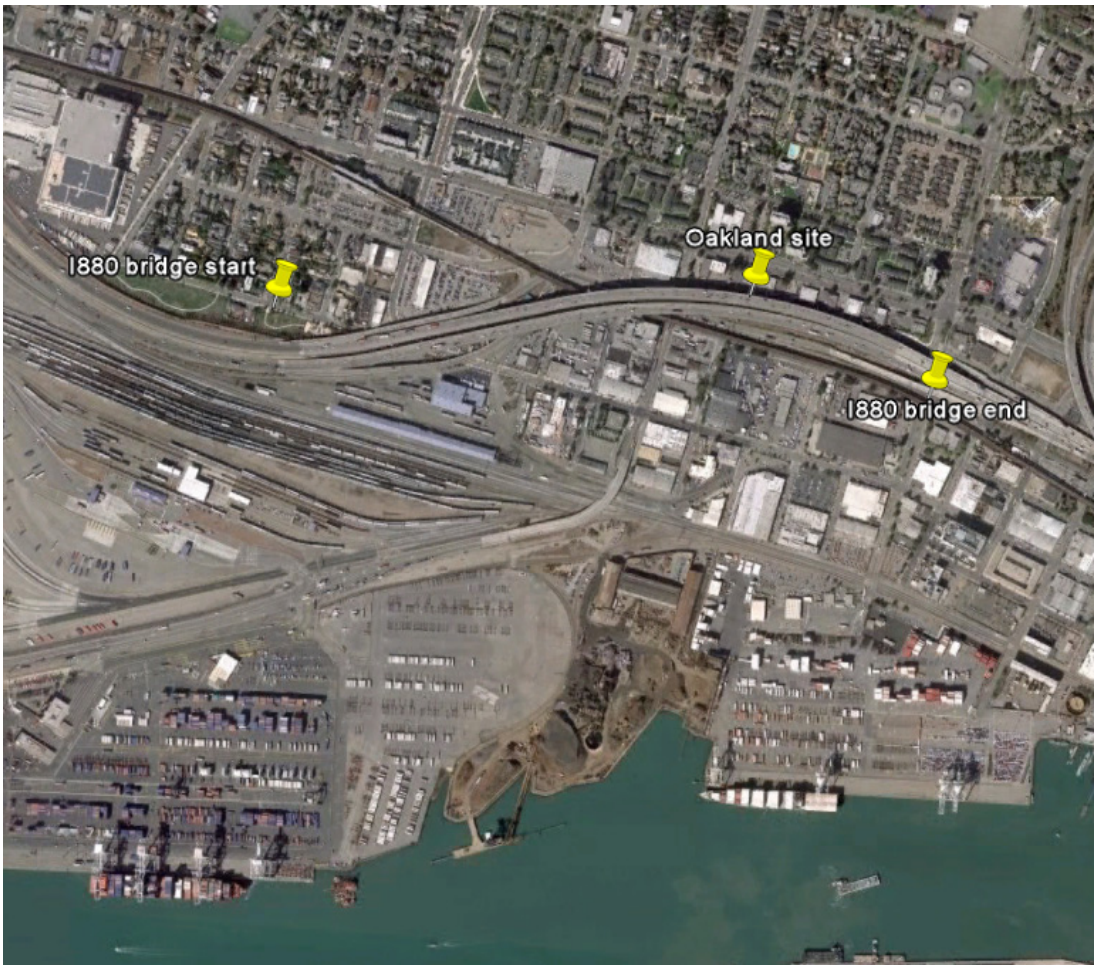

Figure 3.14 Location of I-880 bridge viaduct. Aerial imagery from Google Earth (*http://earth.google.com*).

3.5.1 Information from Previous Ground Motion Selection for this Site

Ground motions were previously selected for this site as part of the 2002 PEER Testbeds effort (2002). Information from that effort was thus utilized to determine site conditions and initial selection parameters. Key information from this 2002 report is summarized here. The bridge is located on soil classified as *Sc* ('soft rock') by the Uniform Building Code. Ground motions were selected under the assumption that the NEHRP side class is *C* or *D*. The 2002 report hazard analysis calculations showed that spectral accelerations at 1 sec were caused primarily by earthquakes with magnitudes of 6.6 to 7 on the nearby Hayward fault (these observations are confirmed in the new hazard analysis below). The ground motions selected in 2002 were chosen to have distances of less than 10 km, and magnitudes from 5.5 to 6.2 (for the '50% in 50 years'

case) and magnitudes greater than 6.6 (for the '10% in 50 years' and '2% in 50 years' cases). The ground motions were taken exclusively from strike-slip earthquake recordings. As stated: "Some of the selected recordings contain strong forward rupture directivity pulses, but others do not." All ground motions were rotated to the strike-normal and strike-parallel orientations. Ten ground motions were provided at each hazard level.

The report states that "The ground motion time histories have not been scaled, because a unique period for use in scaling has not been identified. Once a period has been identified, a scaling factor should be found for the strike-normal component using the strike-normal response spectral value." Uniform hazard spectra were provided for each of the three exceedance probabilities of interest, which are used as the targets for ground motion scaling.

3.5.2 Hazard Analysis

To characterize seismic hazard at the site (37.803N, 122.287W), the 2008 USGS hazard maps and interactive deaggregations tools were used (Petersen et al. 2008; USGS 2008). The assumed site conditions were V_{s30} = 360 m/s (i.e., the NEHRP site class C/D boundary). Uniform hazard spectra were obtained, along with the mean magnitude/ distance/ε values associated with occurrence of each spectral value. This information is summarized in Table 3.1, Table 3.2, and Table 3.3 for probabilities of exceedance of 2%, 10%, and 50% in 50 years. These uniform hazard spectra are plotted in Figure 3.15.

Table 3.1 Uniform hazard spectrum and mean deaggregation values of distance, magnitude and ε for the Oakland site, with a 2% probability of exceedance in 50 years.

Period (sec)	S_a (g)	R (km)	M	ε
0.0	0.94	8.8	6.78	1.70
0.1	1.78	8.4	6.73	1.76
0.2	2.20	8.4	6.77	1.74
0.3	2.13	8.5	6.81	1.73
1.0	1.14	9.9	7.00	1.74
2.0	0.60	13.4	7.20	1.74
5.0	0.22	16.0	7.43	1.64

Table 3.2 Uniform hazard spectrum and mean deaggregation values of distance, magnitude and ε for the Oakland site, with a 10% probability of exceedance in 50 years.

Period (sec)	S_a (g)	R (km)	M	ε
0.0	0.60	10.1	6.80	1.05
0.1	1.11	10.0	6.75	1.10
0.2	1.38	10.0	6.78	1.10
0.3	1.32	10.2	6.82	1.09
1.0	0.67	11.8	7.00	1.09
2.0	0.34	15.6	7.15	1.09
5.0	0.12	16.9	7.31	1.01

Table 3.3 Uniform hazard spectrum and mean deaggregation values of distance, magnitude and ε for the Oakland site, with a 50% probability of exceedance in 50 years.

Period (s)	Sa (g)	R (km)	M	ε
0.0	0.27	15.1	6.79	0.00
0.1	0.48	15.0	6.73	0.10
0.2	0.60	15.7	6.76	0.11
0.3	0.56	16.2	6.80	0.10
1.0	0.26	19.3	6.96	0.04
2.0	0.12	24.2	7.06	0.02
5.0	0.04	24.2	7.13	-0.02

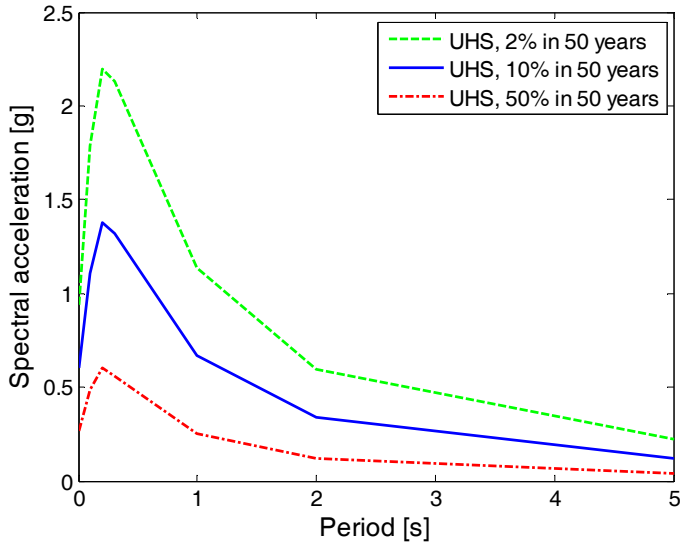

Figure 3.15 Uniform hazard spectra for the Oakland site.

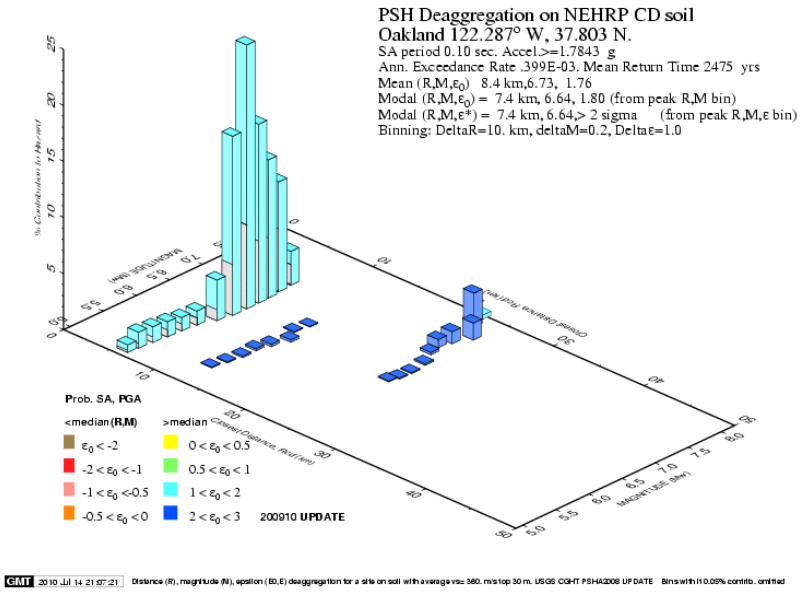

Figure 3.16 Deaggregation plot for S_a(0.1 sec) exceeded with 2% probability in 50 years The largest contribution is from the Hayward fault at 7 km, with a small contribution from M>7 earthquakes on the San Andreas fault (figure from USGS 2008).

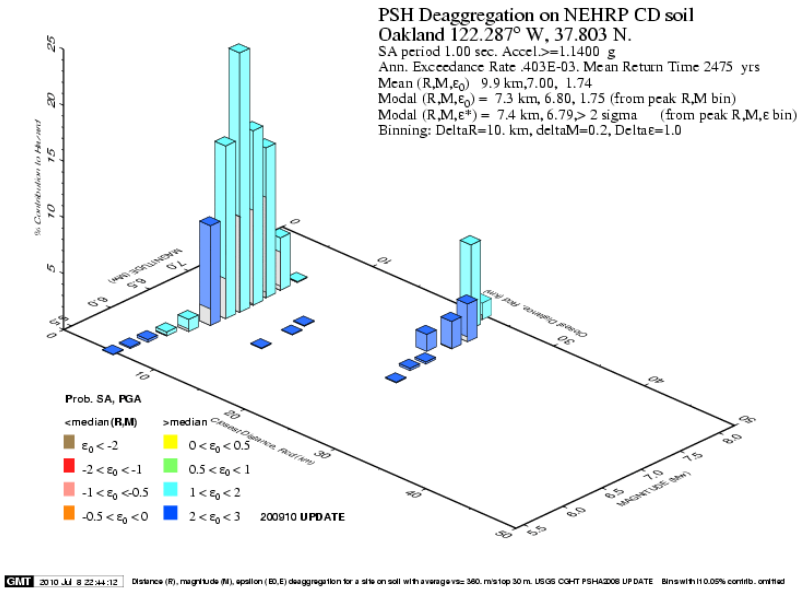

Figure 3.17 Deaggregation plot for S_a (0.1 sec) exceeded with 2% probability in 50 years. The largest contribution is from the Hayward fault at 7 km, with some contribution from M>7 earthquakes on the San Andreas fault (figure from USGS 2008).

The mean deaggregation values in Table 3.1, Table 3.2, and Table 3.3 provide some idea as to the causal earthquakes causing occurrence of these spectral values. More complete information is only available, however, by looking at a complete deaggregation plot for a given period and spectral amplitude. Figure 3.16 and Figure 3.17 show the deaggregation plots for S_a values exceeded with 2% probability in 50 years at periods of 0.1 and 1 sec, respectively. We see that at 0.1 sec almost all occurrences of $S_a(0.1 \text{ sec}) = 1.78g$ are caused by earthquakes on the Hayward fault at 7 km, having magnitudes of approximately 7. For reference, a map of the Oakland site is shown in Figure 3.19, noting the Hayward fault approximately 7 km away. Looking back to Table 3.1, the mean magnitude of 6.73 corresponds to these large Hayward fault events, and the mean distance of 8.4 km corresponds to the Hayward fault distance (it is larger than 7 km because some ground motions are caused on portions of the Hayward fault not occurring on this closest segment, and also because this is the mean distance of all events, and includes some events on the more distant San Andreas fault). At a period of 1 sec, shown in

Figure 3.17, the contribution from the San Andreas Fault has increased. That contribution continues to grow as the period gets larger (as seen in the increasing mean magnitude values with increasing period in Table 3.1). Another noteworthy feature in Table 3.1, Table 3.2, and Table 3.3 is that the deaggregation results for S_a with 50% probability of exceedance in 50 years all have mean ε values of approximately zero, corresponding to median S_a values for the given magnitude and distance; at lower exceedance probabilities, the ε values are positive, corresponding to stronger-than-median ground motions. This is also verified in Figure 3.18, where the median predicted spectrum for a magnitude 7 strike-slip earthquake at 10 km is compared to the Uniform Hazard Spectra, and is seen to match the UHS for 50% probability of exceedance in 50 years.

Studying the other hazard levels reveals that the mean distances increase and mean magnitudes and ε's decrease as the probability of exceedance increases from 2% to 10% and 50% in 50 years. This is expected; at these lower ground motion intensity levels one does not need such an extreme event (i.e., close distance, large magnitude, and large ε) to achieve the given S_a level. At the 50% in 50-year level especially, larger-distance events contribute significantly to the hazard.

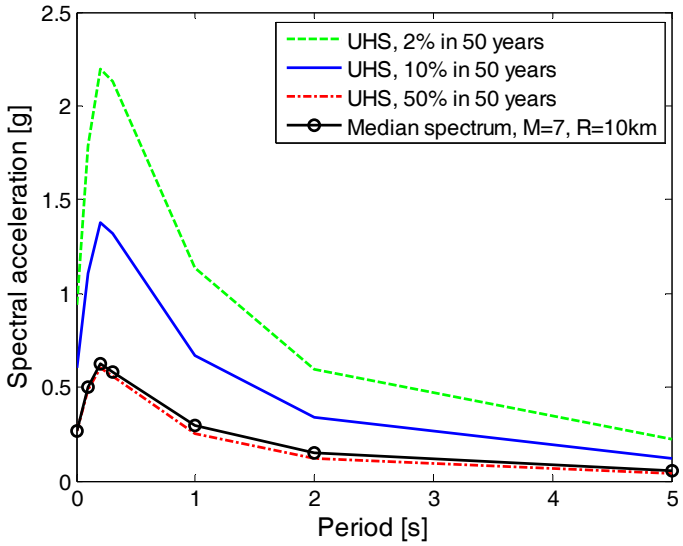

Figure 3.18 Uniform hazard spectra for the Oakland site, compared to the median predicted spectrum for an M = 7, R = 10 km event [as predicted by Campbell and Bozorgnia (2008)].

Figure 3.19 Oakland site. The pushpin marks the site location; the Hayward fault is shown in the upper right portion of the map, approximately 7 km from the site.

This variation in causal sources with period is one reason why the uniform hazard spectrum cannot be interpreted as the response spectrum associated with any single ground motion (Reiter 1990; Beyer and Bommer 2007). Also, note that the mean ε values in Table 3.1 are typically about 1.7, indicating that these spectral values are associated with ground motions having spectra 1.7 standard deviations larger than the mean predicted (logarithmic) spectra associated with the causal earthquake. Any single ground motion is unlikely to be this much larger than mean at all periods, providing a second reason why these uniform hazard spectra should not be interpreted as the spectra of individual ground motions that might be seen at this Oakland site (Baker and Cornell 2006). To help illustrate this, the uniform hazard spectra are re-plotted in Figure 3.15, along with median predicted spectrum (i.e., the exponential of the mean predicted logarithmic spectrum) for a magnitude 7 earthquake at a distance of 10 km. This is the dominant causal earthquake for occurrence of S_a (1 sec) = 1.14g, the 2% in 50-year hazard value

from Table 3.1, but the amplitude of this spectrum is dramatically lower than the 2% in 50-year spectrum. In fact, it is only slightly larger than the 50% in 50-year spectrum.

Despite the limitations of uniform hazard spectra discussed above, ground motions selected and scaled to approximately match these uniform hazard spectra have the advantage that their amplitude at any given period has approximately the same probability of exceedance; this is a useful property when wanting to use a single set of ground motions to analyze structures sensitive to excitation at differing periods with ground motions that are comparably 'intense' in their excitation of each building. These uniform hazard spectra will thus be used as target spectra for the selection of site-specific ground motions.

3.5.3 Ground Motion Selection

With the above hazard and site information, ground motions were selected to represent the hazard at the site. The following criteria and procedures were used for selection:

- Forty three-component ground motions were selected at each hazard level.
- The selected ground motions were rotated from their as-recorded orientations to strike-normal and strike-parallel orientations.
- Ground motions were selected based on their close match to the target spectrum over a range of periods between 0 and 5 sec.
- The ground motions were amplitude scaled to match their target spectrum as closely as possible. (In the selection and scaling operation, mismatch was computed as the sum of squared differences between the logarithm of the scaled ground motion's geometric mean spectrum and the logarithm of the target spectrum.) All three components of the ground motion were scaled by the same factor. No ground motions were scaled by more than a factor of 8. The mean scale factors of the selected ground motions were 3.8, 2.5, and 1.5 at the 2%, 10%, and 50% in 50 years hazard levels, respectively.
- Ground motions were selected to have magnitudes between 5.9 and 7.3, to approximately match the magnitudes of causal earthquakes identified in the hazard calculations above.

- Ground motions were selected to have closest distances to the fault rupture of between 0 and 20 km for the 2% and 10% in 50 years hazard levels. At the 50% in 50 years hazard level, ground motions were selected to have closest distances to the fault rupture of between 0 and 30 km. These limits were chosen to be approximately consistent with the hazard deaggregation results above.
- Ground motions were selected to have V_{s30} values less than 550 m/sec, to approximately represent the site conditions at the location of interest.
- No ground motions were selected from dam abutments or from instruments located above the first floor of a structure.
- No restriction was put on the mechanism of the earthquake associated with the ground motion.
- No restriction was put on the number of ground motions selected from a single earthquake, although some ground motions were omitted manually if the initial selection identified two ground motions in close proximity to each other.
- The site of interest was close enough to the Hayward fault to potentially experience directivity effects, so some selected ground motions have velocity pulses in the fault-normal component of the recording. The selected sets for the 2%, 10%, and 50% in 50 years hazard levels have 19, 16, and 7 pulses, respectively. The pulses were identified using the procedure of Baker (2007) and have a variety of pulse periods between 1 and 7 sec. The fraction of pulse-like motions is approximately consistent with what might be expected at a site of this type (Shahi and Baker 2011), but an exact comparison is not possible because hazard analysis used here does not explicitly account for directivity effects (even if it did the fraction of pulses expected would vary with the period of interest). This characterization nonetheless provides an approximate representation of potential directivity effects at the site.

The above criteria are a compromise between the desire to have ground motions whose properties closely matched the target properties identified above, and the limitations of the finite number of recorded strong ground motions available for use. The restrictions above result in 172

ground motions being available at the 2% and 10% in 50 years hazard levels, out of 3551 total ground motions in the NGA library. At the 50% in 50 years hazard level, there are 303 available ground motions because of the increased range of acceptable distances used in that case.

Response spectra of the selected ground motions are shown Figure 3.20, Figure 3.21, and Figure 3.22, and the three sets are all shown in a single plot in Figure 3.23. In general, the selected motions closely match the target, but there is variability around the target spectra due to the inherent 'bumpiness' of real ground motions. The geometric means of the selected spectra generally closely match the target spectra. An exception is at periods greater than 2.5 sec for the 2% in 50 years hazard level, where the selected motions are slightly lower on average than the target spectrum; this is in part because those spectral values are partially driven by different events than the spectral values at shorter periods, as discussed above, so recorded ground motions tend not to have the shape of this enveloped uniform hazard spectrum. The discrepancy in this case is unavoidable given the currently available ground motion library, unless one is willing to relax the selection criteria listed above.

Additional summary data, as well as the time histories of the ground motions, are provided online at *http://peer.berkeley.edu/transportation/gm_peer_transportation.html*.

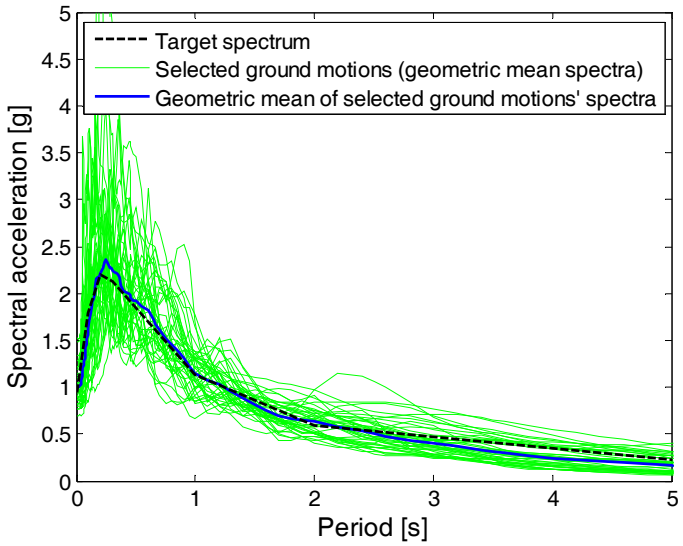

Figure 3.20 Target uniform hazard spectrum at the 2% in 50 years hazard level, and the response spectra of the selected ground motions.

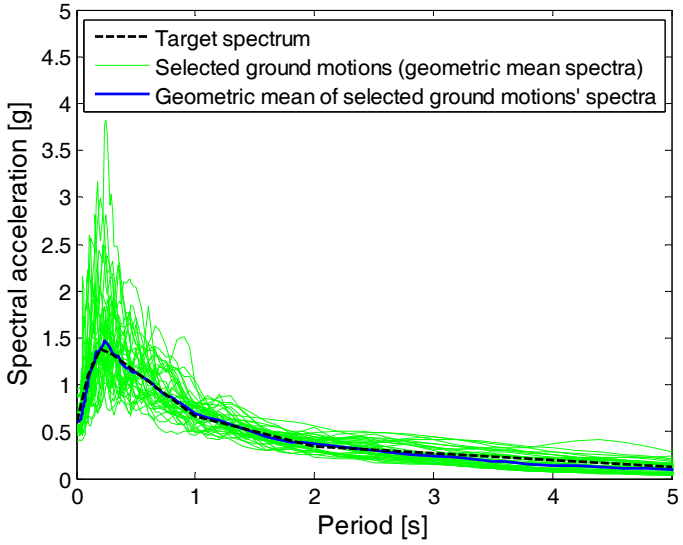

Figure 3.21 Target uniform hazard spectrum at the 10% in 50 years hazard level, and the response spectra of the selected ground motions.

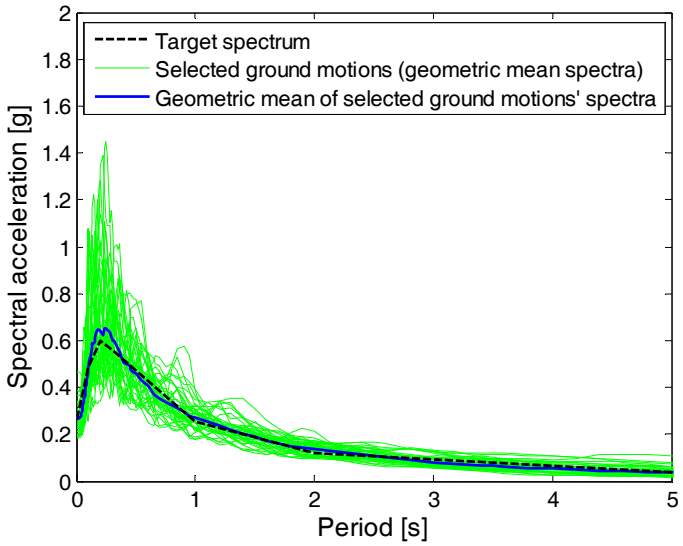

Figure 3.22 Target uniform hazard spectrum at the 50% in 50 years hazard level, and the response spectra of the selected ground motions.

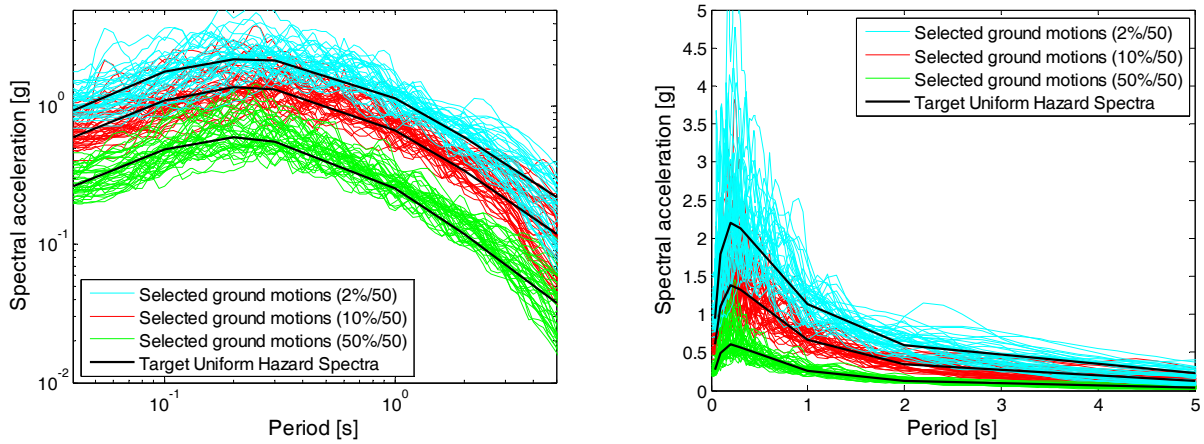

Figure 3.23 Target uniform hazard spectrum at all three hazard levels, and the response spectra of the selected ground motions. (a) Log scale plot, and (b) linear scale plot.

3.6 ADDITIONAL COMPARISONS BETWEEN SELECTED GROUND MOTION SETS

Sets #1 and #2 were termed 'broadband' sets as they aimed to capture a specified variability in response spectra and also have a range of associated magnitude and distance values. In contrast, the ground motions in Set #4 aimed to match a specific response spectrum and specific magnitude and distance value. To illustrate the differences in resulting selected ground motions, a few comparisons between these sets are made.

Figure 3.24 shows the spectra from Set #1A (top row) and Set #4 at the 50% in 50 years level (bottom row) in both log scale (left column) and linear scale (right column) to aid comparison of similar plots that were shown above. Clearly Set #1A has more variability in its response spectra than Set #4. Looking at the example individual spectra shown in these subfigures in blue, the individual spectra tend to be 'bumpier' in Set #1A than Set #4. The bumpy Set #1 spectra are more representative of spectra from typical ground motions, as they have been selected to match the variability and period-to-period correlations in response spectra from real ground motions, while the Set #4 spectra tend to be smoother than typical spectra, as they were preferentially selected due to their match to a smooth target spectrum. The Set #1B and #2 spectra are comparable to the Set #1A spectra plotted here, and the Set #4 spectra at the other two amplitudes are similar to the #4 spectra shown here.

To illustrate some differences between the broadband sets and the site-specific sets, Figure 3.25 shows the magnitudes and distances of the selected ground motions for two sets of ground motions. Some important characteristics of the broadband set are that they have wider variability in the magnitude and distance values of the selected ground motions, the ground motions are not scaled, and there was no attempt made to include or exclude velocity pulses from the set. Some important properties of the site-specific set are that they come from a relatively narrower range of magnitude and distance values (as only ground motions from that narrower range were considered for selection), the ground motions were amplitude scaled to match their associated target spectrum, and velocity pulses were included in the sets, to represent the expected fraction of ground motions at that site and hazard level that are expected to contain a velocity pulse.

The other broadband sets are qualitatively similar to Figure 3.25a in that they have a broader range of magnitude and distance values, and the site-specific sets at the other two hazard levels are similar to Figure 3.25b in that they have a narrow range of magnitudes and distances.

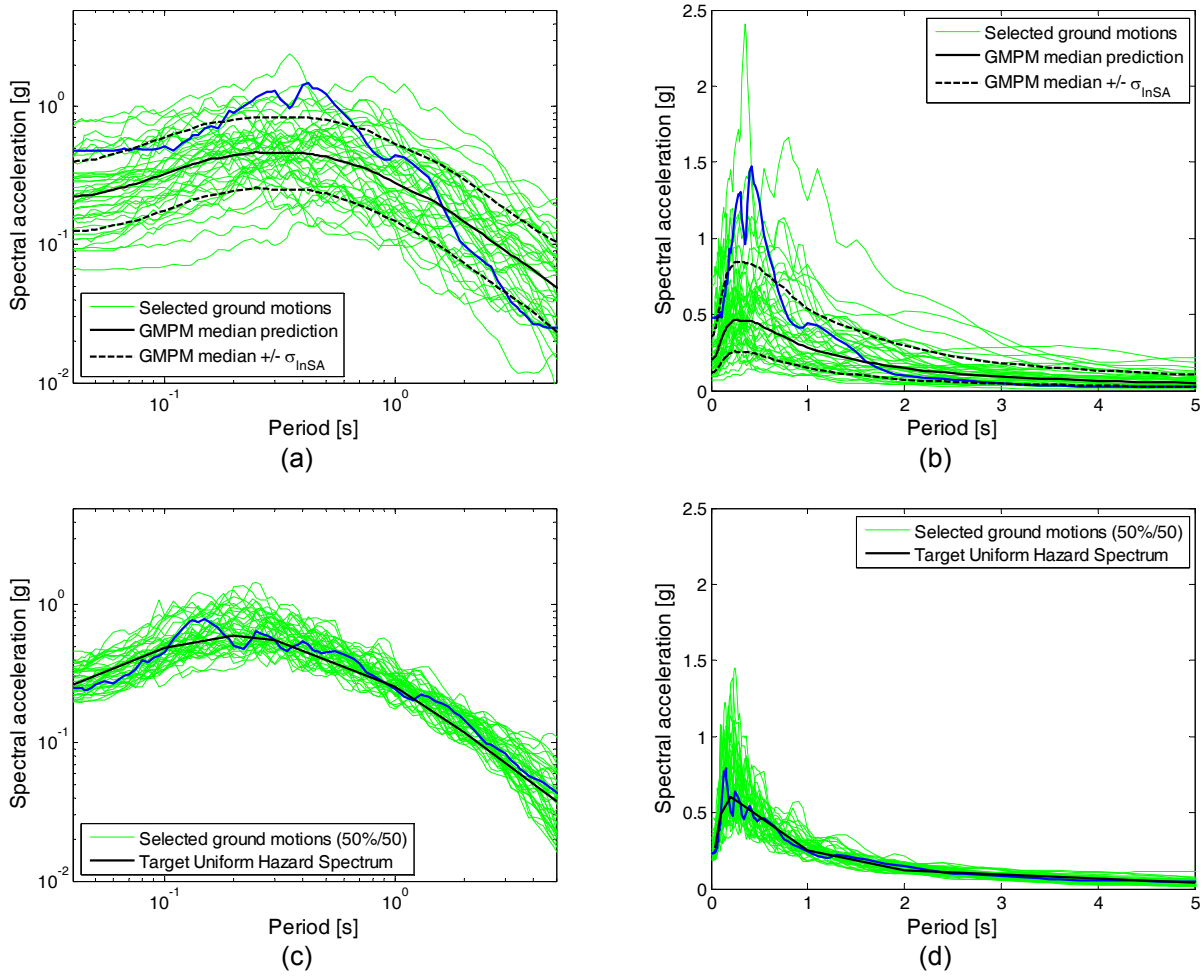

Figure 3.24 **(a) Set #1A (broadband soil) ground motions, plotted in log scale; (b) Set #1A (broadband soil) ground motions, plotted in linear scale; (c) Set #4 (site specific) ground motions for the 50% in 50 years hazard level, plotted in log scale; and (d) Set #4 (site specific) ground motions for the 50% in 50 years hazard level, plotted in linear scale.**

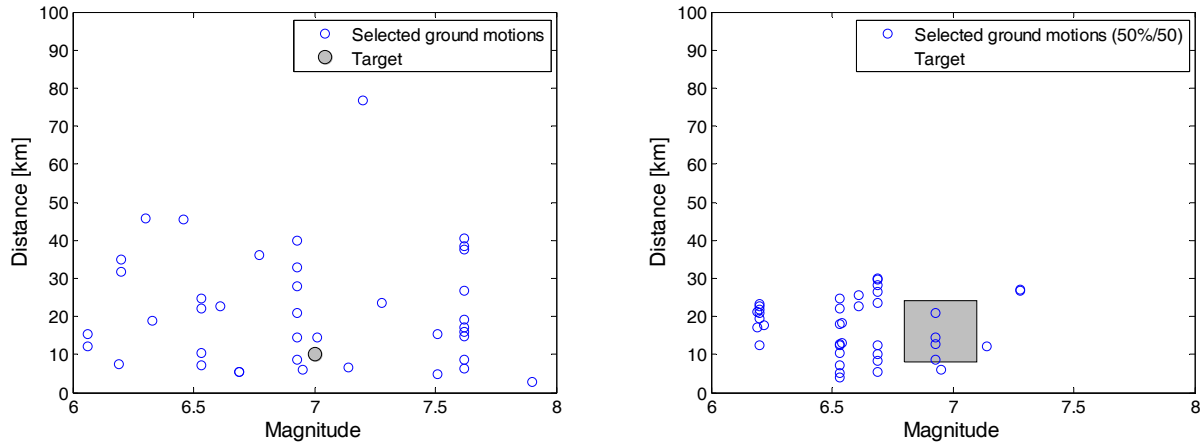

Figure 3.25 Magnitude and distance of target ground motion scenario, and magnitudes and distances of selected ground motions. (a) Set #1A (broadband soil) ground motions plotted in log scale; and (b) Set #4 (site specific) ground motions for the 50% in 50 years hazard level.

Finally, it is worth emphasizing again two other differences between the broadband and site-specific sets. The broadband sets have not been scaled, and there was no attempt to include or exclude velocity pulses from the selected motions. The site-specific sets, on the other hand, consist of ground motions that have been scaled so their spectra closely match the target, and velocity pulses have been included in proportion to the expected likelihood of seeing velocity pulses for that particular site and ground motion intensity level (so the number of velocity pulses in each set increases as the target spectrum increases). With these differences in mind, it will hopefully be apparent which set is most appropriate for a given analysis situation.

4 COMPARISON TO OTHER GROUND MOTION SETS

Several other efforts have provided standardized sets of ground motions for purposes similar to the goals here. A brief description of three similar popular sets is provided here for the purpose of comparison with the ground motions selected above, and to aid readers in choosing which set of motions might be most appropriate for their particular application.

4.1 SAC GROUND MOTIONS

Somerville et al. (1997) (*nisee.berkeley.edu/data/strong_motion/sacsteel/ground_motions.html*) selected sets of ten two-component ground motions selected to match NEHRP design response spectra for firm soil sites in Los Angeles, Seattle, and Boston at multiple hazard levels (2% and 10% probabilities of exceedance in 50 years for all three sites, plus 50% probability of exceedance in 50 years at Los Angeles). Some of these ground motions were then used as inputs to site response analysis using SHAKE91 (Idriss and Sun 1992) to generate ground motions to be used for soft soil sites in each of the three cities of interest.

The recorded ground motions were selected to have magnitudes and distances that matched the approximate deaggregation results for hazard calculations at the specific sites considered. Recorded ground motions were supplemented by simulations when sufficient appropriate recordings were not available. Processing of the recorded ground motions (filtering and baseline correcting) was performed by the authors. The ground motions were scaled to best match their corresponding target design spectra. These objectives are very similar to those used to select Set #4 above, and some the Set #4 selection criteria were patterned directly after the criteria used here.

In addition to the above site-specific ground motions, a set of twenty three-component ground motions were selected to represent near-fault sites (ten recorded motions and ten simulated motions). These ground motions were selected because they were observed near earthquakes of relatively large magnitude. As with Set #3 above, which has similar goals, no target spectrum was considered when selecting these motions and no scaling of these motions was performed.

Some differences between the SAC motions and the above ground motions are:

- The SAC ground motions were selected in 1997, when available databases of recorded ground motions were much more limited compared to 2010. Therefore, the recorded ground motions used in the SAC set come from a much more limited set of earthquakes than the sets provided in this report.
- A greater number of motions are provided in the sets provided in this report, reflecting the greater availability of recorded ground motions and greater willingness of analysts to perform more dynamic analyses.
- The SAC ground motions were developed for specific locations, allowing seismic hazard information for those locations to be considered when selecting ground motions. Sets #1-3 above have no specific associated site and thus could not utilize seismic hazard information. Set #4 above was selected under objectives similar to those of the SAC ground motion selection effort, although only a single site was considered for Set #4 while three sites were considered by Somerville et al.
- The SAC ground motions have been pre-scaled. Sets #1-3 above (the 'broadband' sets) are not pre-scaled, while the site-specific Set #4 has been pre-scaled.
- The SAC ground motions were selected to satisfy NEHRP building code requirements, specifically with respect to design response spectra. The above ground motions are intended for more general use, and thus do not use the NEHRP design spectra as a target spectrum (recognizing that this type of spectrum is often not appropriate for performance-based assessments).
- While the SAC near-fault ground motions were selected with similar objectives to the above Set #3, the SAC authors did not ensure that all ground motions in the set contained

velocity pulses and did not report any properties of velocity pulses that are present in the selected ground motions. Research progress since 1997 has enabled the Set #3 above to include such additional information.

4.2 LMSR GROUND MOTIONS

Krawinkler et al. (Krawinkler et al. 2003; Medina and Krawinkler 2003) selected four sets of ground motions, of which the Large-Magnitude Small-Distance (LMSR) set in particular has been widely used. This set consists of 20 two-component ground motions with magnitudes between 6.5 and 7, and distances between 13 and 30 km. No further effort was made to select the ground motions based on their response spectra. Three other sets provided by these authors had smaller magnitudes and/or larger distances, and were deemed less useful due to their lower ground motion intensity (although, after being scaled up to comparable response spectral values, these other sets were observed to produce similar structural responses to the LMSR set). These ground motions are similar in nature to Set #1 and Set #2 above, with the following minor differences:

- A greater number of motions are provided in the above sets, reflecting the greater availability of recorded ground motions and greater willingness of analysts to perform more dynamic analyses.
- The above sets provide two sets of motions, representing rock and soil site conditions.
- The above sets pay explicit attention to the response spectra of the selected motions. The LMSR set has similar variability in response spectra to the above broadband sets—this was achieved implicitly by limiting the magnitude and distance values of the selected ground motions to be comparable to a single event within the limitations of the finite ground motion library.
- The LMSR set has a much narrower range of magnitudes and distances than the above broadband sets.

4.3 FEMA P695 GROUND MOTIONS

Kircher et al. (Applied Technology Council 2009b, Appendix A) selected two ground motion sets for the FEMA P695 project that are intended to be structure independent and site independent, as is the objective of Sets #1 and #2 in this project. They provided a 'Far Field' set of 22 ground motions recorded at distances greater than 10 km, and a 'Near Field' set of 28 ground motions recorded at distances less than 10 km. One half of the ground motions in the Near Field set contained velocity pulses; these pulses were identified using the same wavelet-based technique used in the current project (Baker 2007). Two component ground motions were provided. Only those ground motions with peak ground acceleration greater than 0.2*g* and peak ground velocity greater than 15 cm/sec were selected, and the sets were then 'normalized' (pre-scaled) to manipulate the variability in ground motion intensities seen in the scaled ground motions. After normalization, the authors note that the Far Field set of ground motions has a median spectrum comparable to that of a magnitude 7 earthquake at a distance of 15 km. The median spectrum of the Near-Field set was said to be comparable to a magnitude 7 earthquake at a distance of 5 km. The ground motions were selected specifically for assessing the collapse capacity of buildings using the FEMA P695 assessment procedure, so the suggested normalization and scaling procedure provided by the authors may or may not be appropriate for other types of analysis objectives.

Some differences between the FEMA P695 motions and the above ground motions are:

- A greater number of motions are provided in the above sets.
- The FEMA P695 ground motions have been pre-scaled, while the above Sets #1-3 are provided unscaled. The above Set #4 has been pre-scaled, but does not retain the spectral variability of the FEMA P695 set.
- While both the P695 sets and the above sets of ground motions can be further scaled or modified by users, the FEMA P695 guidelines provide a specific set of recommended scaling instructions tailored for the purposes of assessing median collapse capacity of a structure.

- The 14 pulse-like ground motions in the FEMA P695 set (some of which match the ground motions provided in Set #3 here) are mixed with non-pulse-like ground motions, while here they are provided in an explicitly separate set.

5 CONCLUSIONS

This report summarizes an effort to select several sets of standardized ground motions for use by the PEER Transportation Research Program. The motions utilized the existing high-quality NGA database of recorded ground motions, and selectively searched that database for motions deemed appropriate for use in a variety of instances. Recent ground motion selection research at PEER has focused primarily on situations where the structure and location of interest are known, so that ground motions can be selected and modified with specific structural properties and seismic hazard information in mind. This project, in contrast, considered a wide variety of structural and geotechnical systems at a wide range of locations, requiring standardized sets of ground motions to facilitate comparative evaluations in this research. Even in situations where a specific location is of interest, the Transportation Research Program sometimes evaluates alternative structural systems (with differing periods of vibration) for potential use at a given location. Therefore, ground motion selection techniques that depend upon knowledge of structural periods are not applicable, and other techniques were thus needed to choose appropriate ground motion sets.

To facilitate this work, a new computationally efficient, theoretically consistent ground-motion selection algorithm was proposed in Section 2 to enable selection of a suite of ground motions whose response spectra have a target mean and a target variance. The algorithm first uses Monte Carlo simulation to probabilistically generate multiple realizations of response spectra from a target distribution, and then selects recorded ground motions whose response spectra individually match the simulated response spectra. A greedy optimization technique then further improves the match between the target and the sample means and variances by replacing one previously selected ground motion at a time with a record from the ground-motion database that causes the best improvement in the match. It was shown empirically that this algorithm selects ground motions whose response spectra have the target mean and variance.

The proposed algorithm was first used to select ground motions for estimating the seismic response of sample single-degree-of-freedom (SDOF) and multiple-degree-of-freedom (MDOF) structures, in order to assess the impact of considering response spectrum variance on the structural response estimates. SDOF structures with different levels of non-linearity (as indicated by their R factors) were analyzed using the selected ground motions. It was seen that considering the response spectrum variance does not significantly affect the resulting median response, but slightly increases the mean response and considerably increases the dispersion (logarithmic standard deviation) of the response. The increase in the mean and the dispersion is larger for more non-linear SDOF structures. Two code-compliant MDOF structures with heights of 4 and 20 stories were also analyzed using the selected ground motions. As with the SDOF structures, it was seen that considering the response spectrum variance does not significantly affect the median response but increases the dispersion of the response and the probability of observing collapse. These observations have implications for applications where the dispersion of the response is an important consideration, such as in many performance-based engineering evaluations. In addition to facilitating selection of ground motions for this project, the algorithm will likely be useful for a broad range of other applications. A MATLAB implementation of the proposed ground-motion selection algorithm can be downloaded from *http://www.stanford.edu/~bakerjw/gm_selection.html.*

Once this new selection procedure was introduced, several sets of standardized ground motions were selected in Section 3. The selected sets included three 'broadband' sets (Sets #1A, 1B, and 2) that capture spectral variability associated with a scenario earthquake magnitude and distance; sets were selected for two earthquake scenarios on both rock and soil site conditions. Ground motion Set #3 was selected to consist entirely of ground motions with strong velocity pulses for analysts interested in the effect of such pulses on their structural or geotechnical system. Finally, 'site-specific' sets of ground motions were selected (Set #4), so that their response spectra closely matched a target Uniform Hazard Spectrum for a site in Oakland, California, at 2%, 10%, and 50% probabilities of exceedance in 50 years. The assumed range of periods of interest was 0 to 5 sec for all ground motion sets. These sets of ground motions vary in the procedures used to select them, the degree of heterogeneity of the ground motions within the set, and the analysis objectives that they might be suited for. For that reason, comparisons of the

properties of the various sets were provided, as well as comparisons to other popular ground motion sets in use today.

This report includes selected summary data for the ground motion sets, but the most detailed information is available in the form of the ground motion time histories themselves, and their metadata such as associated magnitudes, distances, and response spectra. A brief summary of the ground motion properties is provided in Appendix, A which provides a few metadata fields for each selected ground motion. A much more complete set of information is available from the project website (*http://peer.berkeley.edu/transportation/publications_data.html*), including complete time histories and response spectra for all three components of each ground motion. The Appendix A tables and project website spreadsheets all include the NGA Number for each ground motion, which matches the corresponding field in the NGA Flatfile (*http://peer.berkeley.edu/nga/documentation.html*). Some data not in the current NGA Flatfile, such as directivity pulse periods, scale factors (when applicable), and ε values, are included in the Appendix A tables or in spreadsheets posted at the project website.

REFERENCES

AMEC Geomatrix Inc. (2009). *Design ground motion library*. Oakland, CA, 42 pgs.

American Society of Civil Engineers. (2005). *Minimum design loads for buildings and other structures*. ASCE 7-05, American Society of Civil Engineers/Structural Engineering Institute, Reston, VA.

Applied Technology Council. (2009a). *ATC-58, Guidelines for Seismic Performance Assessment of Buildings, 50% Draft*. Applied Technology Council, Redwood City, California, 260 pgs.

Applied Technology Council. (2009b). *Quantification of Building Seismic Performance Factors (FEMA P695, ATC-63)*. FEMA P695, 421 pgs.

Baker, J. W. (2007). Quantitative classification of near-fault ground motions using wavelet analysis, *Bull. Seismo. Soc. Am.*, 97(5):1486-1501.

Baker, J. W. (2011). The Conditional Mean Spectrum: a tool for ground motion selection, *J. Struct. Engrg.*, 137(1), in press.

Baker, J. W., and Cornell, C. A. (2006). Spectral shape, epsilon and record selection, *Earthq. Engrg. Struct. Dyn.*, 35(9):1077–1095.

Baker, J. W., and Jayaram, N. (2008). Correlation of spectral acceleration values from NGA ground motion models, *Earthq. Spectra*, 24(1):299-317.

Bazzurro, P., Cornell, C. A., Shome, N., and Carballo, J. E. (1998). Three proposals for characterizing MDOF nonlinear seismic response, *J. Struct. Engrg.*, 124(11):1281-1289.

Beyer, K., and Bommer, J. J. (2007). Selection and scaling of real accelerograms for bi-directional loading: A review of current practice and code provisions, *J. Struct. Engrg.*, 11:13-45.

Boore, D. M., and Atkinson, G. M. (2008). Ground-motion prediction equations for the average horizontal component of PGA, PGV, and 5%-Damped PSA at spectral periods between 0.01 s and 10.0 s, *Earthq. Spectra*, 24(1):99-138.

Boore, D. M., Watson-Lamprey, J., and Abrahamson, N. A. (2006). Orientation-independent measures of ground motion, *Bull. Seismo. Soc. Am.*, 96(4A):1502-1511.

Buratti, N., Stafford, P. J., and Bommer, J. J. (2011). Earthquake accelerogram selection and scaling procedures for estimating the distribution of drift response, *J. Struct. Engrg.*, (in press).

Campbell, K. W., and Bozorgnia, Y. (2008). NGA ground motion model for the geometric mean horizontal component of PGA, PGV, PGD and 5% damped linear elastic response spectra for periods ranging from 0.01 to 10 s." *Earthq. Spectra*, 24(1):139-171.

Chiou, B., Darragh, R., Gregor, N., and Silva, W. (2008). NGA Project Strong-Motion Database, *Earthq. Spectra*, 24(1):23-44.

Chopra, A. K. (2001). *Dynamics of Structures: Theory and Applications to Earthquake Engineering*. Prentice Hall, Upper Saddle River, NJ.

Haselton, C. B., and Deierlein, G. G. (2007). *Assessing seismic collapse safety of modern reinforced concrete moment frame buildings*. Pacific Earthquake Engineering Research Center, Berkeley, CA.

Haselton, C. B., Baker, J. W., Bozorgnia, Y., Goulet, C. A., Kalkan, E., Luco, N., Shantz, T., Shome, N., Stewart, J. P., Tothong, P., Watson-Lamprey, J., and Zareian, F. (2009). *Evaluation of Ground Motion Selection and Modification Methods: Predicting Median Interstory Drift Response of Buildings*. PEER Technical Report 2009/01, Berkeley, California, 288 pgs.

Ibarra, L. F., Medina, R. A., and Krawinkler, H. (2005). Hysteretic models that incorporate strength and stiffness deterioration, *Earthq. Engrg. Struct. Dyn.*, 34(12):1489-1511.

Idriss, I. M., and Sun, J. I. (1992). "User's Manual for SHAKE91: A computer program for conducting equivalent linear seismic response analyses of horizontally layered soil deposits, *Center for Geotechnical Modeling,* Department of Civil Engineering, University of California, Davis, CA.

Jayaram, N., and Baker, J. W. (2008). Statistical tests of the joint distribution of spectral acceleration values, *Bull. Seismo. Soc. Am.*, 98(5):2231-2243.

Jayaram, N., and Baker, J. W. (2010). Ground-motion selection for PEER Transportation Research Program, *Proc., 7th Internl. Conf. Urban Earthq. Engrg. (7CUEE) & 5th Internl. Conf. Earthq. Engrg. (5ICEE)*, Tokyo, Japan, 9 pgs.

Jayaram, N., Lin, T., and Baker, J. W. (2011). A computationally efficient ground-motion selection algorithm for matching a target response spectrum mean and variance, *Earthq. Spectra*, in press.

Kennedy, R., Short, S., Merz, K., Tokarz, F., Idriss, I., Power, M., and Sadigh, K. (1984). *Engineering characterization of ground motion - Task I: effects of characteristics of free-field motion on structural response*. U.S. Nuclear Regulatory Commision, Washington, D.C.

Kottke, A., and Rathje, E. M. (2008). A semi-automated procedure for selecting and scaling recorded earthquake motions for dynamic analysis, *Earthq. Spectra*, 24(4):911-932.

Kramer, S. L., and Mitchell, R. A. (2006). Ground motion intensity measures for liquefaction hazard evaluation, *Earthq. Spectra,* 22(2):413-438.

Krawinkler, H., Medina, R., and Alavi, B. (2003). Seismic drift and ductility demands and their dependence on ground motions, *Engrg. Struct.*, 25(5):637-653.

Mavroeidis, G. P., Dong, G., and Papageorgiou, A. S. (2004). Near-fault ground motions, and the response of elastic and inelastic single-degree-of-freedom (SDOF) systems, *Earthq. Engrg. Struct. Dyn.*, 33(9):1023-1049.

McKenna, F., Fenves, G. L., and Scott, M. H. (2007). "Open system for earthquake engineering simulation (OpenSees)." *Pacific Earthquake Engineering Research Center*, http://opensees.berkeley.edu/.

Medina, R. A., and Krawinkler, H. (2003). *Seismic Demands for Nondeteriorating Frame Structures and Their Dependence on Ground Motions*, Stanford University, Stanford, CA.

Naeim, F., Alimoradi, A., and Pezeshk, S. (2004). Selection and scaling of ground motion time histories for structural design using genetic algorithms, *Earthq. Spectra*, 20(2):413-426.

Petersen, M. D., Frankel, A. D., Harmsen, S. C., Mueller, C. S., Haller, K. M., Wheeler, R. L., Wesson, R. L., Zeng, Y., Boyd, O. S., Perkins, D. M., Luco, N., Field, E. H., Wills, C. J., and Rukstales, K. S. (2008). Documentation for the 2008 update of the United States national seismic hazard maps, *U.S. Geological Survey Open-File Report 2008–1128*, Open-File Report 2008–1128, 1128, 61 pgs.

Reiter, L. (1990). *Earthquake Hazard Analysis: Issues and Insights*. Columbia University Press, New York.

Rodriguez-Marek, A., and Bray, J. D. (2006). Seismic site response for near-fault forward directivity ground motions, *J. Geotech. Geoenviro. Engrg.*, 132(12):1611-1620.

Shahi, S., and Baker, J. W. (2011). An empirically calibrated framework for including the effects of near-fault directivity in probabilistic seismic hazard analysis, *Bull. Seismo. Soc. Am.*, 101(2), in press.

Shantz, T. (2006). Selection and scaling of earthquake records for nonlinear dynamic analysis of first model dominated bridge structures, *Proc., 8th Natl. Conf. Earthq. Engrg.*, San Francisco, California, 10 pgs.

Shome, N., Cornell, C. A., Bazzurro, P., and Carballo, J. E. (1998). Earthquakes, records, and nonlinear responses, *Earthq. Spectra*, 14(3):469-500.

Somerville, P. G. (2002). *PEER Testbeds Project Report: Ground motion time histories for the I880 Bridge, Oakland*, http://peer.berkeley.edu/ research/peertestbeds/i-880.htm.

Somerville, P., Smith, N., Punyamurthula, S., and Sun, J. (1997). *Development of Ground Motion Time Histories for Phase 2 of the FEMA/SAC Steel Project*, SAC Joint Venture, Richmond, California.

Stewart, J. P., Chiou, S. J., Bray, J. D., Graves, R. W., Somerville, P. G., and Abrahamson, N. A. (2002). Ground motion evaluation procedures for performance-based design, *Soil Dyn. Earthq. Engrg.*, 22(9-12):765-772.

USGS (2008). “Interactive Deaggregation Tools.” http://eqint.cr.usgs.gov/deaggint/2008/.

Watson-Lamprey, J., and Abrahamson, N. A. (2006). Selection of ground motion time series and limits on scaling, *Soil Dyn. Earthq. Engrg.*, 26(5):477-482.

Youngs, R., Power, M., and Chin, C. (2006). Design ground motion library, *Proc., 8th Natl. Conf. Earthq. Engrg.*, San Francisco, CA, 10 pgs.

Appendix A: Tables of Selected Ground Motions

The following tables provide basic summary data for the selected ground motions. A significant amount of additional summary data, including response spectra and time history files for these ground motions, are available on the accompanying project website (*http://peer.berkeley.edu/transportation/publications_data.html*).

Table A.1 Set #1A ground motions: Broad-band ground motions (M = 7, R = 10 km, soil site).

Record number	NGA Record Sequence Number	Earthquake Name	Year	Station	Magnitude	Closest Distance	Preferred Vs30 (m/s)
1	231	Mammoth Lakes-01	1980	Long Valley Dam (Upr L Abut)	6.1	15.5	345
2	1203	Chi-Chi, Taiwan	1999	CHY036	7.6	16.1	233
3	829	Cape Mendocino	1992	Rio Dell Overpass – FF	7.0	14.3	312
4	169	Imperial Valley-06	1979	Delta	6.5	22.0	275
5	1176	Kocaeli, Turkey	1999	Yarimca	7.5	4.8	297
6	163	Imperial Valley-06	1979	Calipatria Fire Station	6.5	24.6	206
7	1201	Chi-Chi, Taiwan	1999	CHY034	7.6	14.8	379
8	1402	Chi-Chi, Taiwan	1999	NST	7.6	38.4	375
9	1158	Kocaeli, Turkey	1999	Duzce	7.5	15.4	276
10	281	Trinidad	1980	Rio Dell Overpass, E Ground	7.2	-	312
11	730	Spitak, Armenia	1988	Gukasian	6.8	-	275
12	768	Loma Prieta	1989	Gilroy Array #4	6.9	14.3	222
13	1499	Chi-Chi, Taiwan	1999	TCU060	7.6	8.5	273
14	266	Victoria, Mexico	1980	Chihuahua	6.3	19.0	275
15	761	Loma Prieta	1989	Fremont - Emerson Court	6.9	39.9	285
16	558	Chalfant Valley-02	1986	Zack Brothers Ranch	6.2	7.6	271
17	1543	Chi-Chi, Taiwan	1999	TCU118	7.6	26.8	215
18	2114	Denali, Alaska	2002	TAPS Pump Station #10	7.9	2.7	329
19	179	Imperial Valley-06	1979	El Centro Array #4	6.5	7.1	209
20	931	Big Bear-01	1992	San Bernardino - E & Hospitality	6.5	-	271
21	900	Landers	1992	Yermo Fire Station	7.3	23.6	354
22	1084	Northridge-01	1994	Sylmar - Converter Sta	6.7	5.4	251
23	68	San Fernando	1971	LA - Hollywood Stor FF	6.6	22.8	317
24	527	N. Palm Springs	1986	Morongo Valley	6.1	12.1	345
25	776	Loma Prieta	1989	Hollister - South & Pine	6.9	27.9	371
26	1495	Chi-Chi, Taiwan	1999	TCU055	7.6	6.4	273
27	1194	Chi-Chi, Taiwan	1999	CHY025	7.6	19.1	278
28	161	Imperial Valley-06	1979	Brawley Airport	6.5	10.4	209
29	1236	Chi-Chi, Taiwan	1999	CHY088	7.6	37.5	273
30	1605	Duzce, Turkey	1999	Duzce	7.1	6.6	276
31	1500	Chi-Chi, Taiwan	1999	TCU061	7.6	17.2	273
32	802	Loma Prieta	1989	Saratoga - Aloha Ave	6.9	8.5	371
33	6	Imperial Valley-02	1940	El Centro Array #9	7.0	6.1	213
34	2656	Chi-Chi, Taiwan-03	1999	TCU123	6.2	31.8	273
35	982	Northridge-01	1994	Jensen Filter Plant	6.7	5.4	373
36	2509	Chi-Chi, Taiwan-03	1999	CHY104	6.2	35.1	223
37	800	Loma Prieta	1989	Salinas - John & Work	6.9	32.8	271
38	754	Loma Prieta	1989	Coyote Lake Dam (Downst)	6.9	20.8	295
39	1183	Chi-Chi, Taiwan	1999	CHY008	7.6	40.4	211
40	3512	Chi-Chi, Taiwan-06	1999	TCU141	6.3	45.7	215

Table A.2 Set #1B ground motions: Broad-band ground motions (M = 6, R = 25 km, soil site).

Record number	NGA Record Sequence Number	Earthquake Name	Year	Station	Magnitude	Closest Distance	Preferred Vs30 (m/s)
1	915	'Big Bear-01'	1992	'Lake Cachulla'	6.5	-	345
2	935	'Big Bear-01'	1992	'Snow Creek'	6.5	-	345
3	761	'Loma Prieta'	1989	'Fremont - Emerson Court'	6.9	39.9	285
4	190	'Imperial Valley-06'	1979	'Superstition Mtn Camera'	6.5	24.6	362
5	2008	'CA/Baja Border Area'	2002	'El Centro Array #7'	5.3	-	211
6	552	'Chalfant Valley-02'	1986	'Lake Crowley - Shehorn Res.'	6.2	24.5	339
7	971	'Northridge-01'	1994	'Elizabeth Lake'	6.7	36.6	235
8	1750	'Northwest China-02'	1997	'Jiashi'	5.9	-	275
9	268	'Victoria, Mexico'	1980	'SAHOP Casa Flores'	6.3	39.3	339
10	2003	'CA/Baja Border Area'	2002	'Calexico Fire Station'	5.3	-	231
11	668	'Whittier Narrows-01'	1987	'Norwalk - Imp Hwy, S Grnd'	6.0	20.4	270
12	88	'San Fernando'	1971	'Santa Felita Dam (Outlet)'	6.6	24.9	376
13	357	'Coalinga-01'	1983	'Parkfield - Stone Corral 3E'	6.4	34.0	376
14	188	'Imperial Valley-06'	1979	'Plaster City'	6.5	30.3	345
15	22	'El Alamo'	1956	'El Centro Array #9'	6.8	-	213
16	762	'Loma Prieta'	1989	'Fremont - Mission San Jose'	6.9	39.5	368
17	535	'N. Palm Springs'	1986	'San Jacinto - Valley Cemetary'	6.1	31.0	339
18	951	'Northridge-01'	1994	'Bell Gardens - Jaboneria'	6.7	44.1	309
19	2465	'Chi-Chi, Taiwan-03'	1999	'CHY034'	6.2	37.0	379
20	456	'Morgan Hill'	1984	'Gilroy Array #2'	6.2	13.7	271
21	2009	'CA/Baja Border Area'	2002	'Holtville Post Office'	5.3	0.0	203
22	470	'Morgan Hill'	1984	'San Juan Bautista, 24 Polk St'	6.2	27.2	371
23	216	'Livermore-01'	1980	'Tracy - Sewage Treatm Plant'	5.8	-	271
24	2664	'Chi-Chi, Taiwan-03'	1999	'TCU145'	6.2	48.5	215
25	522	'N. Palm Springs'	1986	'Indio'	6.1	35.6	207
26	131	'Friuli, Italy-02'	1976	'Codroipo'	5.9	41.4	275
27	964	'Northridge-01'	1994	'Compton - Castlegate St'	6.7	47.0	309
28	460	'Morgan Hill'	1984	'Gilroy Array #7'	6.2	12.1	334
29	920	'Big Bear-01'	1992	'North Shore - Salton Sea Pk HQ'	6.5	-	265
30	933	'Big Bear-01'	1992	'Seal Beach - Office Bldg'	6.5	-	371
31	214	'Livermore-01'	1980	'San Ramon - Eastman Kodak'	5.8	-	271
32	328	'Coalinga-01'	1983	'Parkfield - Cholame 3W'	6.4	45.7	339
33	122	'Friuli, Italy-01'	1976	'Codroipo'	6.5	33.4	275
34	2473	'Chi-Chi, Taiwan-03'	1999	'CHY047'	6.2	46.2	273
35	757	'Loma Prieta'	1989	'Dumbarton Bridge West End FF'	6.9	35.5	275
36	705	'Whittier Narrows-01'	1987	'West Covina - S Orange Ave'	6.0	16.3	309
37	247	'Mammoth Lakes-06'	1980	'Bishop - Paradise Lodge'	5.9	-	345
38	340	'Coalinga-01'	1983	'Parkfield - Fault Zone 16'	6.4	27.7	339
39	3275	'Chi-Chi, Taiwan-06'	1999	'CHY036'	6.3	46.2	233
40	604	'Whittier Narrows-01'	1987	'Canoga Park - Topanga Can'	6.0	49.0	267

Table A.3 Set #2 ground motions: Broad-band ground motions (M = 7, R = 10 km, rock site).

Record number	NGA Record Sequence Number	Earthquake Name	Year	Station	Magnitude	Closest Distance	Preferred Vs30 (m/s)
1	72	San Fernando	1971	Lake Hughes #4	6.6	25.1	822
2	769	Loma Prieta	1989	Gilroy Array #6	6.9	18.3	663
3	1165	Kocaeli, Turkey	1999	Izmit	7.5	7.2	811
4	1011	Northridge-01	1994	LA - Wonderland Ave	6.7	20.3	1223
5	164	Imperial Valley-06	1979	Cerro Prieto	6.5	15.2	660
6	1787	Hector Mine	1999	Hector	7.1	11.7	685
7	80	San Fernando	1971	Pasadena - Old Seismo Lab	6.6	21.5	969
8	1618	Duzce, Turkey	1999	Lamont 531	7.1	8.0	660
9	1786	Hector Mine	1999	Heart Bar State Park	7.1	61.2	685
10	1551	Chi-Chi, Taiwan	1999	TCU138	7.6	9.8	653
11	3507	Chi-Chi, Taiwan-06	1999	TCU129	6.3	24.8	664
12	150	Coyote Lake	1979	Gilroy Array #6	5.7	3.1	663
13	572	Taiwan SMART1(45)	1986	SMART1 E02	7.3	-	660
14	285	Irpinia, Italy-01	1980	Bagnoli Irpinio	6.9	8.2	1000
15	801	Loma Prieta	1989	San Jose - Santa Teresa Hills	6.9	14.7	672
16	286	Irpinia, Italy-01	1980	Bisaccia	6.9	21.3	1000
17	1485	Chi-Chi, Taiwan	1999	TCU045	7.6	26.0	705
18	1161	Kocaeli, Turkey	1999	Gebze	7.5	10.9	792
19	1050	Northridge-01	1994	Pacoima Dam (downstr)	6.7	7.0	2016
20	2107	Denali, Alaska	2002	Carlo (temp)	7.9	50.9	964
21	1	Helena, Montana-01	1935	Carroll College	6.0	-	660
22	1091	Northridge-01	1994	Vasquez Rocks Park	6.7	23.6	996
23	1596	Chi-Chi, Taiwan	1999	WNT	7.6	1.8	664
24	771	Loma Prieta	1989	Golden Gate Bridge	6.9	79.8	642
25	809	Loma Prieta	1989	UCSC	6.9	18.5	714
26	265	Victoria, Mexico	1980	Cerro Prieto	6.3	14.4	660
27	1078	Northridge-01	1994	Santa Susana Ground	6.7	16.7	715
28	763	Loma Prieta	1989	Gilroy - Gavilan Coll.	6.9	10.0	730
29	1619	Duzce, Turkey	1999	Mudurnu	7.1	34.3	660
30	957	Northridge-01	1994	Burbank - Howard Rd.	6.7	16.9	822
31	2661	Chi-Chi, Taiwan-03	1999	TCU138	6.2	22.2	653
32	3509	Chi-Chi, Taiwan-06	1999	TCU138	6.3	33.6	653
33	810	Loma Prieta	1989	UCSC Lick Observatory	6.9	18.4	714
34	765	Loma Prieta	1989	Gilroy Array #1	6.9	9.6	1428
35	1013	Northridge-01	1994	LA Dam	6.7	5.9	629
36	1012	Northridge-01	1994	LA 00	6.7	19.1	706
37	1626	Sitka, Alaska	1972	Sitka Observatory	7.7	34.6	660
38	989	Northridge-01	1994	LA - Chalon Rd	6.7	20.5	740
39	748	Loma Prieta	1989	Belmont – Envirotech	6.9	44.1	628
40	1549	Chi-Chi, Taiwan	1999	TCU129	7.6	1.8	664

Table A.4 Set #3 ground motions: Pulse-like ground motions.

Record number	NGA Record Sequence Number	Earthquake Name	Year	Station Name	Magnitude	Closest Distance (km)	Pulse Period (s)	Preferred Vs30 (m/s)
1	170	Imperial Valley-06	1979	EC County Center FF	6.5	7.3	4.5	192
2	171	Imperial Valley-06	1979	EC Meloland Overpass FF	6.5	0.1	3.3	186
3	179	Imperial Valley-06	1979	El Centro Array #4	6.5	7.1	4.6	209
4	180	Imperial Valley-06	1979	El Centro Array #5	6.5	4.0	4.0	206
5	181	Imperial Valley-06	1979	El Centro Array #6	6.5	1.4	3.8	203
6	182	Imperial Valley-06	1979	El Centro Array #7	6.5	0.6	4.2	211
7	183	Imperial Valley-06	1979	El Centro Array #8	6.5	3.9	5.4	206
8	184	Imperial Valley-06	1979	El Centro Differential Array	6.5	5.1	5.9	202
9	451	Morgan Hill	1984	Coyote Lake Dam (SW Abut)	6.2	0.5	1.0	597
10	763	Loma Prieta	1989	Gilroy - Gavilan Coll.	6.9	10.0	1.8	730
11	779	Loma Prieta	1989	LGPC	6.9	3.9	4.4	478
12	879	Landers	1992	Lucerne	7.3	2.2	5.1	685
13	900	Landers	1992	Yermo Fire Station	7.3	23.6	7.5	354
14	982	Northridge-01	1994	Jensen Filter Plant	6.7	5.4	3.5	373
15	983	Northridge-01	1994	Jensen Filter Plant Generator	6.7	5.4	3.5	526
16	1044	Northridge-01	1994	Newhall - Fire Sta	6.7	5.9	1.0	269
17	1045	Northridge-01	1994	Newhall - W Pico Canyon Rd.	6.7	5.5	2.4	286
18	1063	Northridge-01	1994	Rinaldi Receiving Sta	6.7	6.5	1.2	282
19	1084	Northridge-01	1994	Sylmar - Converter Sta	6.7	5.4	3.5	251
20	1085	Northridge-01	1994	Sylmar - Converter Sta East	6.7	5.2	3.5	371
21	1086	Northridge-01	1994	Sylmar - Olive View Med FF	6.7	5.3	3.1	441
22	1106	Kobe, Japan	1995	KJMA	6.9	1.0	1.0	312
23	1119	Kobe, Japan	1995	Takarazuka	6.9	0.3	1.4	312
24	1161	Kocaeli, Turkey	1999	Gebze	7.5	10.9	5.8	792
25	1197	Chi-Chi, Taiwan	1999	CHY028	7.6	3.1	2.2	543
26	1244	Chi-Chi, Taiwan	1999	CHY101	7.6	10.0	4.6	259
27	1489	Chi-Chi, Taiwan	1999	TCU049	7.6	3.8	11.7	487
28	1492	Chi-Chi, Taiwan	1999	TCU052	7.6	0.7	8.4	579
29	1493	Chi-Chi, Taiwan	1999	TCU053	7.6	6.0	12.8	455
30	1494	Chi-Chi, Taiwan	1999	TCU054	7.6	5.3	10.5	461
31	1505	Chi-Chi, Taiwan	1999	TCU068	7.6	0.3	12.2	487
32	1510	Chi-Chi, Taiwan	1999	TCU075	7.6	0.9	5.2	573
33	1511	Chi-Chi, Taiwan	1999	TCU076	7.6	2.8	4.0	615
34	1515	Chi-Chi, Taiwan	1999	TCU082	7.6	5.2	9.0	473
35	1519	Chi-Chi, Taiwan	1999	TCU087	7.6	7.0	9.4	474
36	1528	Chi-Chi, Taiwan	1999	TCU101	7.6	2.1	10.0	273
37	1529	Chi-Chi, Taiwan	1999	TCU102	7.6	1.5	9.7	714
38	1530	Chi-Chi, Taiwan	1999	TCU103	7.6	6.1	8.2	494
39	1546	Chi-Chi, Taiwan	1999	TCU122	7.6	9.4	10.9	475
40	1595	Chi-Chi, Taiwan	1999	WGK	7.6	10.0	4.4	259

Table A.5 Set #4 ground motions selected for the 2% in 50 years hazard level.

Record number	NGA Record Sequence Number	Earthquake Name	Year	Station	Magnitude	Hypocentral Distance (km)	Closest Distance (km)	Preferred Vs30 (m/s)	FN Pulse	Pulse Period (s)
1	6	Imperial Valley-02	1940	El Centro Array #9	7.0	13.0	6.1	213	0	
2	159	Imperial Valley-06	1979	Agrarias	6.5	2.6	0.7	275	1	2.30
3	161	Imperial Valley-06	1979	Brawley Airport	6.5	43.2	10.4	209	1	4.03
4	165	Imperial Valley-06	1979	Chihuahua	6.5	18.9	7.3	275	0	
5	171	Imperial Valley-06	1979	EC Meloland Overpass FF	6.5	19.4	0.1	186	1	3.35
6	173	Imperial Valley-06	1979	El Centro Array #10	6.5	26.3	6.2	203	1	4.49
7	174	Imperial Valley-06	1979	El Centro Array #11	6.5	29.4	12.5	196	1	7.36
8	175	Imperial Valley-06	1979	El Centro Array #12	6.5	32.0	17.9	197	0	
9	178	Imperial Valley-06	1979	El Centro Array #3	6.5	28.7	12.9	163	1	5.24
10	179	Imperial Valley-06	1979	El Centro Array #4	6.5	27.1	7.1	209	1	4.61
11	180	Imperial Valley-06	1979	El Centro Array #5	6.5	27.8	4.0	206	1	4.05
12	181	Imperial Valley-06	1979	El Centro Array #6	6.5	27.5	1.4	203	1	3.84
13	183	Imperial Valley-06	1979	El Centro Array #8	6.5	28.1	3.9	206	1	5.39
14	184	Imperial Valley-06	1979	El Centro Differential Array	6.5	27.2	5.1	202	1	5.86
15	185	Imperial Valley-06	1979	Holtville Post Office	6.5	19.8	7.7	203	1	4.80
16	187	Imperial Valley-06	1979	Parachute Test Site	6.5	48.6	12.7	349	0	
17	266	Victoria, Mexico	1980	Chihuahua	6.3	36.7	19.0	275	0	
18	316	Westmorland	1981	Parachute Test Site	5.9	20.5	16.7	349	1	3.58
19	549	Chalfant Valley-02	1986	Bishop - LADWP South St	6.2	20.3	17.2	271	0	
20	718	Superstition Hills-01	1987	Wildlife Liquef. Array	6.2	24.8	17.6	207	0	
21	721	Superstition Hills-02	1987	El Centro Imp. Co. Cent	6.5	35.8	18.2	192	0	
22	728	Superstition Hills-02	1987	Westmorland Fire Sta	6.5	19.5	13.0	194	0	
23	768	Loma Prieta	1989	Gilroy Array #4	6.9	32.4	14.3	222	0	
24	802	Loma Prieta	1989	Saratoga - Aloha Ave	6.9	27.2	8.5	371	1	4.47
25	821	Erzican, Turkey	1992	Erzincan	6.7	9.0	4.4	275	1	2.65
26	949	Northridge-01	1994	Arleta - Nordhoff Fire Sta	6.7	11.1	8.7	298	0	
27	959	Northridge-01	1994	Canoga Park - Topanga Can	6.7	4.9	14.7	267	0	
28	982	Northridge-01	1994	Jensen Filter Plant	6.7	13.0	5.4	373	1	3.53
29	1042	Northridge-01	1994	N Hollywood - Coldwater Can	6.7	13.1	12.5	446	0	
30	1044	Northridge-01	1994	Newhall - Fire Sta	6.7	20.3	5.9	269	0	
31	1052	Northridge-01	1994	Pacoima Kagel Canyon	6.7	19.3	7.3	508	0	
32	1063	Northridge-01	1994	Rinaldi Receiving Sta	6.7	10.9	6.5	282	1	1.23
33	1082	Northridge-01	1994	Sun Valley - Roscoe Blvd	6.7	12.4	10.1	309	0	
34	1085	Northridge-01	1994	Sylmar - Converter Sta East	6.7	13.6	5.2	371	1	3.49
35	1116	Kobe, Japan	1995	Shin-Osaka	6.9	46.0	19.2	256	0	
36	1602	Duzce, Turkey	1999	Bolu	7.1	41.3	12.0	326	0	
37	1605	Duzce, Turkey	1999	Duzce	7.1	1.6	6.6	276	0	
38	2457	Chi-Chi, Taiwan-03	1999	CHY024	6.2	25.5	19.7	428	1	3.19
39	2734	Chi-Chi, Taiwan-04	1999	CHY074	6.2	10.1	6.2	553	0	
40	2739	Chi-Chi, Taiwan-04	1999	CHY080	6.2	14.5	12.5	553	0	

Table A.6 Set #4 ground motions selected for the 10% in 50 years hazard level.

Record number	NGA Record Sequence Number	Earthquake Name	Year	Station	Magnitude	Hypocentral Distance (km)	Closest Distance (km)	Preferred Vs30 (m/s)	FN Pulse	Pulse Period (s)
1	6	Imperial Valley-02	1940	El Centro Array #9	7.0	13.0	6.1	213	0	
2	159	Imperial Valley-06	1979	Agrarias	6.5	2.6	0.7	275	1	2.30
3	161	Imperial Valley-06	1979	Brawley Airport	6.5	43.2	10.4	209	1	4.03
4	165	Imperial Valley-06	1979	Chihuahua	6.5	18.9	7.3	275	0	
5	173	Imperial Valley-06	1979	El Centro Array #10	6.5	26.3	6.2	203	1	4.49
6	174	Imperial Valley-06	1979	El Centro Array #11	6.5	29.4	12.5	196	1	7.36
7	175	Imperial Valley-06	1979	El Centro Array #12	6.5	32.0	17.9	197	0	
8	178	Imperial Valley-06	1979	El Centro Array #3	6.5	28.7	12.9	163	1	5.24
9	179	Imperial Valley-06	1979	El Centro Array #4	6.5	27.1	7.1	209	1	4.61
10	180	Imperial Valley-06	1979	El Centro Array #5	6.5	27.8	4.0	206	1	4.05
11	181	Imperial Valley-06	1979	El Centro Array #6	6.5	27.5	1.4	203	1	3.84
12	183	Imperial Valley-06	1979	El Centro Array #8	6.5	28.1	3.9	206	1	5.39
13	184	Imperial Valley-06	1979	El Centro Differential Array	6.5	27.2	5.1	202	1	5.86
14	185	Imperial Valley-06	1979	Holtville Post Office	6.5	19.8	7.7	203	1	4.80
15	187	Imperial Valley-06	1979	Parachute Test Site	6.5	48.6	12.7	349	0	
16	192	Imperial Valley-06	1979	Westmorland Fire Sta	6.5	52.8	15.3	194	0	
17	266	Victoria, Mexico	1980	Chihuahua	6.3	36.7	19.0	275	0	
18	316	Westmorland	1981	Parachute Test Site	5.9	20.5	16.7	349	1	3.58
19	549	Chalfant Valley-02	1986	Bishop - LADWP South St	6.2	20.3	17.2	271	0	
20	718	Superstition Hills-01	1987	Wildlife Liquef. Array	6.2	24.8	17.6	207	0	
21	721	Superstition Hills-02	1987	El Centro Imp. Co. Cent	6.5	35.8	18.2	192	0	
22	728	Superstition Hills-02	1987	Westmorland Fire Sta	6.5	19.5	13.0	194	0	
23	767	Loma Prieta	1989	Gilroy Array #3	6.9	31.4	12.8	350	0	
24	768	Loma Prieta	1989	Gilroy Array #4	6.9	32.4	14.3	222	0	
25	802	Loma Prieta	1989	Saratoga - Aloha Ave	6.9	27.2	8.5	371	1	4.47
26	949	Northridge-01	1994	Arleta - Nordhoff Fire Sta	6.7	11.1	8.7	298	0	
27	959	Northridge-01	1994	Canoga Park - Topanga Can	6.7	4.9	14.7	267	0	
28	982	Northridge-01	1994	Jensen Filter Plant	6.7	13.0	5.4	373	1	3.53
29	1004	Northridge-01	1994	LA - Sepulveda VA Hospital	6.7	8.5	8.4	380	0	
30	1042	Northridge-01	1994	N Hollywood - Coldwater Can	6.7	13.1	12.5	446	0	
31	1044	Northridge-01	1994	Newhall - Fire Sta	6.7	20.3	5.9	269	0	
32	1063	Northridge-01	1994	Rinaldi Receiving Sta	6.7	10.9	6.5	282	1	1.23
33	1082	Northridge-01	1994	Sun Valley - Roscoe Blvd	6.7	12.4	10.1	309	0	
34	1085	Northridge-01	1994	Sylmar - Converter Sta East	6.7	13.6	5.2	371	1	3.49
35	1602	Duzce, Turkey	1999	Bolu	7.1	41.3	12.0	326	0	
36	1605	Duzce, Turkey	1999	Duzce	7.1	1.6	6.6	276	0	
37	1611	Duzce, Turkey	1999	Lamont 1058	7.1	13.4	0.2	425	0	
38	2699	Chi-Chi, Taiwan-04	1999	CHY024	6.2	27.9	19.7	428	0	
39	2734	Chi-Chi, Taiwan-04	1999	CHY074	6.2	10.1	6.2	553	0	
40	2739	Chi-Chi, Taiwan-04	1999	CHY080	6.2	14.5	12.5	553	0	

Table A.7 Set #4 ground motions selected for the 50% in 50 years hazard level.

Record number	NGA Record Sequence Number	Earthquake Name	Year	Station	Magnitude	Hypocentral Distance (km)	Closest Distance (km)	Preferred Vs30 (m/s)	FN Pulse	Pulse Period (s)
1	6	Imperial Valley-02	1940	El Centro Array #9	7.0	13.0	6.1	213	0	
2	68	San Fernando	1971	LA - Hollywood Stor FF	6.6	39.5	22.8	316	0	
3	79	San Fernando	1971	Pasadena - CIT Athenaeum	6.6	42.8	25.5	415	0	
4	161	Imperial Valley-06	1979	Brawley Airport	6.5	43.2	10.4	209	1	4.03
5	162	Imperial Valley-06	1979	Calexico Fire Station	6.5	17.7	10.5	231	0	
6	163	Imperial Valley-06	1979	Calipatria Fire Station	6.5	57.1	24.6	206	0	
7	169	Imperial Valley-06	1979	Delta	6.5	33.7	22.0	275	0	
8	174	Imperial Valley-06	1979	El Centro Array #11	6.5	29.4	12.5	196	1	7.36
9	175	Imperial Valley-06	1979	El Centro Array #12	6.5	32.0	17.9	197	0	
10	179	Imperial Valley-06	1979	El Centro Array #4	6.5	27.1	7.1	209	1	4.61
11	183	Imperial Valley-06	1979	El Centro Array #8	6.5	28.1	3.9	206	1	5.39
12	184	Imperial Valley-06	1979	El Centro Differential Array	6.5	27.2	5.1	202	1	5.86
13	187	Imperial Valley-06	1979	Parachute Test Site	6.5	48.6	12.7	349	0	
14	302	Irpinia, Italy-02	1980	Rionero In Vulture	6.2	29.8	22.7	530	0	
15	549	Chalfant Valley-02	1986	Bishop - LADWP South St	6.2	20.3	17.2	271	0	
16	553	Chalfant Valley-02	1986	Long Valley Dam (Downst)	6.2	23.8	21.1	345	0	
17	718	Superstition Hills-01	1987	Wildlife Liquef. Array	6.2	24.8	17.6	207	0	
18	721	Superstition Hills-02	1987	El Centro Imp. Co. Cent	6.5	35.8	18.2	192	0	
19	728	Superstition Hills-02	1987	Westmorland Fire Sta	6.5	19.5	13.0	194	0	
20	754	Loma Prieta	1989	Coyote Lake Dam (Downst)	6.9	30.9	20.8	295	0	
21	767	Loma Prieta	1989	Gilroy Array #3	6.9	31.4	12.8	350	0	
22	768	Loma Prieta	1989	Gilroy Array #4	6.9	32.4	14.3	222	0	
23	802	Loma Prieta	1989	Saratoga - Aloha Ave	6.9	27.2	8.5	371	1	4.47
24	880	Landers	1992	Mission Creek Fault	7.3	32.9	27.0	345	0	
25	882	Landers	1992	North Palm Springs	7.3	32.3	26.8	345	0	
26	982	Northridge-01	1994	Jensen Filter Plant	6.7	13.0	5.4	373	1	3.53
27	985	Northridge-01	1994	LA - Baldwin Hills	6.7	28.2	29.9	297	0	
28	987	Northridge-01	1994	LA - Centinela St	6.7	25.4	28.3	235	0	
29	1004	Northridge-01	1994	LA - Sepulveda VA Hospital	6.7	8.5	8.4	380	0	
30	1008	Northridge-01	1994	LA - W 15th St	6.7	29.6	29.7	405	0	
31	1010	Northridge-01	1994	LA- Wadsworth VA Hospital S	6.7	19.6	23.6	414	0	
32	1042	Northridge-01	1994	N Hollywood - Coldwater Can	6.7	13.1	12.5	446	0	
33	1077	Northridge-01	1994	Santa Monica City Hall	6.7	22.5	26.5	336	0	
34	1082	Northridge-01	1994	Sun Valley - Roscoe Blvd	6.7	12.4	10.1	309	0	
35	1602	Duzce, Turkey	1999	Bolu	7.1	41.3	12.0	326	0	
36	2624	Chi-Chi, Taiwan-03	1999	TCU073	6.2	24.8	20.9	273	0	
37	2655	Chi-Chi, Taiwan-03	1999	TCU122	6.2	24.5	19.3	475	0	
38	2739	Chi-Chi, Taiwan-04	1999	CHY080	6.2	14.5	12.5	553	0	
39	2752	Chi-Chi, Taiwan-04	1999	CHY101	6.2	28.0	21.7	259	0	
40	2893	Chi-Chi, Taiwan-04	1999	TCU122	6.2	31.9	23.2	475	0	

Appendix B: An Alternative Ground-Motion Selection Technique

The ground-motion selection algorithm described in the body of this manuscript selects an initial set of ground motions whose response spectra match a set of simulated response spectra. These simulations are obtained from a multivariate normal distribution parameterized by the target mean and covariance matrices. A greedy optimization technique then further improves the match between the target and the sample means and variances and obtains the final set of ground motions.

Sometimes, it may not be possible to completely parameterize the distribution of the response spectra using the mean and covariance information. This includes situations where ground motions are selected to match the UHS (where only the mean spectrum needs to be considered) or where the mean and the variance information, but not the correlation information, are available. There may also be situations where the response spectrum does not follow a multivariate normal distribution. For such situations, the authors propose the following technique for selecting the initial ground-motion set that can be subsequently improved by the greedy optimization technique. The steps involved in the technique are summarized below.

- Step 1: Initialize the algorithm with an empty ground-motion set.
- Step 2: Set $i = 1$.
- Step 3: If the ith database ground motion (G_i) is not already present in the ground-motion set, include it in the set and compute $SSE_{s,i}$ (i.e., the SSE_s of the set after G_i is included, where SSE_s is defined in Equation 2).
- Step 4: Delete G_i from the set, if included in Step 3. Increment i by 1.

- Step 5: If i is less than or equal to the size of the ground-motion database, go to Step 3. Otherwise, identify the ground motion $\tilde{i}$ that results in the minimum value of $SSE_{s,i}$.

  Add the $\tilde{i}$ th ground motion in the database to the ground-motion set.

- Step 5: If the size of the set equals the desired number of ground motions, terminate the algorithm. Otherwise, go to Step 2.

This selection technique will provide a reasonable starting set of ground motions that can be subsequently improved using the greedy optimization technique described earlier in the manuscript. This selection technique does not take advantage of the knowledge of the response spectrum distribution or the correlation structure, but is therefore more general in its application. It is also empirically seen to produce sets of ground motions with response spectrum mean and variance closely matching the corresponding target values.

To test the effectiveness of the technique, it is used to select a set of 40 ground motions for the scenario described earlier (magnitude = 7, distance to rupture = 10km, T^* = 2.63s and $\varepsilon(T^*)$ = 2). The response spectra of the selected records are shown in Figure B.1a. The ground-motion set means and standard deviations are compared to the target means and standard deviations in FigureFigureb-c. It can be seen that the matches are good, illustrating the effectiveness of the technique. Incidentally, despite the fact that the technique does not use the correlation information, it is seen that the mean absolute error between the sample and the target correlations (Equation 7) is only 0.15.

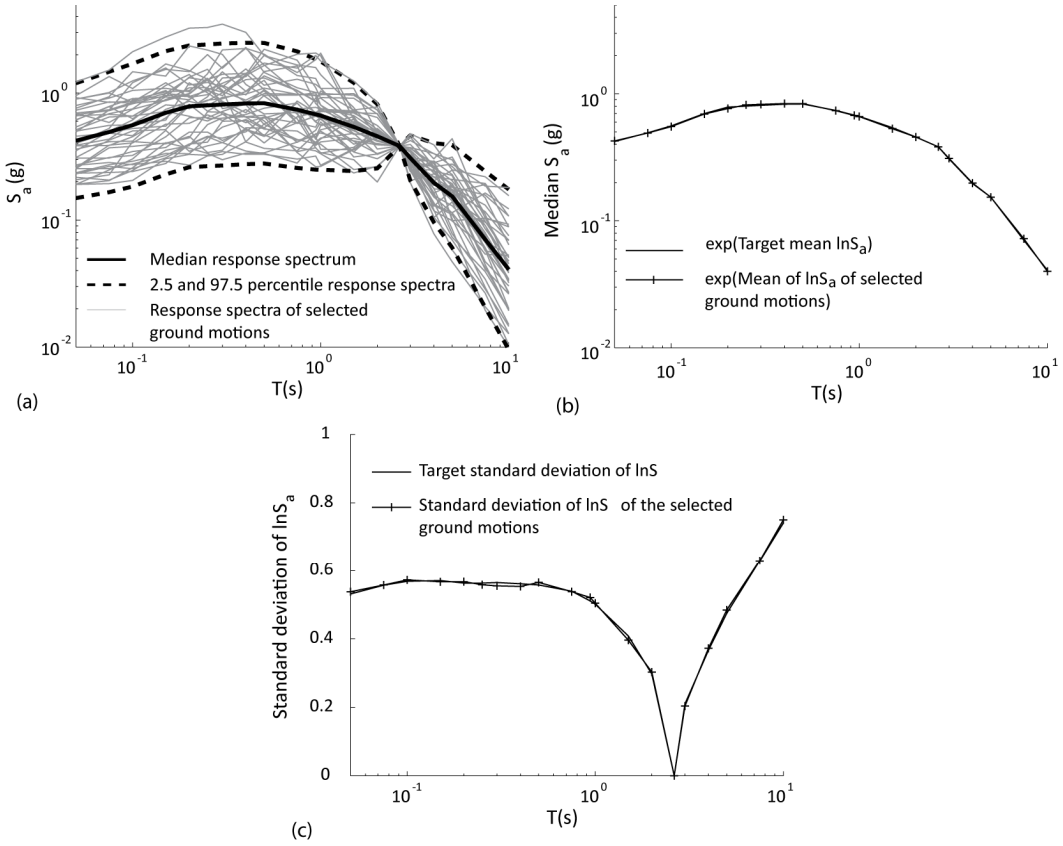

Figure B.1: (a) Response spectra of 40 ground motions selected using the greedy selection and optimization techniques; (b) response spectrum mean; and (c) response spectrum standard deviation.

PEER REPORTS

PEER reports are available individually or by yearly subscription. PEER reports can be ordered at http://peer.berkeley.edu/publications/peer_reports.html or by contacting the Pacific Earthquake Engineering Research Center, 325 Davis Hall mail code 1792, Berkeley, CA 94720. Tel.: (510) 642-3437; Fax: (510) 665-1655; Email: peer_editor@berkeley.edu

PEER 2011/03 *New Ground Motion Selection Procedures and Selected Motions for the PEER Transportation Research Program.* Jack W. Baker, Ting Lin, Shrey K. Shahi, and Nirmal Jayaram. March 2011.

PEER 2011/02 *A Bayesian Network Methodology for Infrastructure Seismic Risk Assessment and Decision Support.* Michelle T. Bensi, Armen Der Kiureghian, and Daniel Straub. March 2011.

PEER 2011/01 *Demand Fragility Surfaces for Bridges in Liquefied and Laterally Spreading Ground.* Scott J. Brandenberg, Jian Zhang, Pirooz Kashighandi, Yili Huo, and Minxing Zhao. March 2011.

PEER 2010/05 *Guidelines for Performance-Based Seismic Design of Tall Buildings.* Developed by the Tall Buildings Initiative. November 2010.

PEER 2010/04 *Application Guide for the Design of Flexible and Rigid Bus Connections between Substation Equipment Subjected to Earthquakes.* Jean-Bernard Dastous and Armen Der Kiureghian. September 2010.

PEER 2010/03 *Shear Wave Velocity as a Statistical Function of Standard Penetration Test Resistance and Vertical Effective Stress at Caltrans Bridge Sites.* Scott J. Brandenberg, Naresh Bellana, and Thomas Shantz. June 2010.

PEER 2010/02 *Stochastic Modeling and Simulation of Ground Motions for Performance-Based Earthquake Engineering.* Sanaz Rezaeian and Armen Der Kiureghian. June 2010.

PEER 2010/01 *Structural Response and Cost Characterization of Bridge Construction Using Seismic Performance Enhancement Strategies.* Ady Aviram, Božidar Stojadinović, Gustavo J. Parra-Montesinos, and Kevin R. Mackie. March 2010.

PEER 2009/03 *The Integration of Experimental and Simulation Data in the Study of Reinforced Concrete Bridge Systems Including Soil-Foundation-Structure Interaction.* Matthew Dryden and Gregory L. Fenves. November 2009.

PEER 2009/02 *Improving Earthquake Mitigation through Innovations and Applications in Seismic Science, Engineering, Communication, and Response. Proceedings of a U.S.-Iran Seismic Workshop.* October 2009.

PEER 2009/01 *Evaluation of Ground Motion Selection and Modification Methods: Predicting Median Interstory Drift Response of Buildings.* Curt B. Haselton, Ed. June 2009.

PEER 2008/10 *Technical Manual for Strata.* Albert R. Kottke and Ellen M. Rathje. February 2009.

PEER 2008/09 *NGA Model for Average Horizontal Component of Peak Ground Motion and Response Spectra.* Brian S.-J. Chiou and Robert R. Youngs. November 2008.

PEER 2008/08 *Toward Earthquake-Resistant Design of Concentrically Braced Steel Structures.* Patxi Uriz and Stephen A. Mahin. November 2008.

PEER 2008/07 *Using OpenSees for Performance-Based Evaluation of Bridges on Liquefiable Soils.* Stephen L. Kramer, Pedro Arduino, and HyungSuk Shin. November 2008.

PEER 2008/06 *Shaking Table Tests and Numerical Investigation of Self-Centering Reinforced Concrete Bridge Columns.* Hyung IL Jeong, Junichi Sakai, and Stephen A. Mahin. September 2008.

PEER 2008/05 *Performance-Based Earthquake Engineering Design Evaluation Procedure for Bridge Foundations Undergoing Liquefaction-Induced Lateral Ground Displacement.* Christian A. Ledezma and Jonathan D. Bray. August 2008.

PEER 2008/04 *Benchmarking of Nonlinear Geotechnical Ground Response Analysis Procedures.* Jonathan P. Stewart, Annie On-Lei Kwok, Yousseff M. A. Hashash, Neven Matasovic, Robert Pyke, Zhiliang Wang, and Zhaohui Yang. August 2008.

PEER 2008/03 *Guidelines for Nonlinear Analysis of Bridge Structures in California.* Ady Aviram, Kevin R. Mackie, and Božidar Stojadinović. August 2008.

PEER 2008/02 *Treatment of Uncertainties in Seismic-Risk Analysis of Transportation Systems.* Evangelos Stergiou and Anne S. Kiremidjian. July 2008.

PEER 2008/01 *Seismic Performance Objectives for Tall Buildings.* William T. Holmes, Charles Kircher, William Petak, and Nabih Youssef. August 2008.

PEER 2007/12 *An Assessment to Benchmark the Seismic Performance of a Code-Conforming Reinforced Concrete Moment-Frame Building.* Curt Haselton, Christine A. Goulet, Judith Mitrani-Reiser, James L. Beck, Gregory G. Deierlein, Keith A. Porter, Jonathan P. Stewart, and Ertugrul Taciroglu. August 2008.

PEER 2007/11 *Bar Buckling in Reinforced Concrete Bridge Columns.* Wayne A. Brown, Dawn E. Lehman, and John F. Stanton. February 2008.

PEER 2007/10 *Computational Modeling of Progressive Collapse in Reinforced Concrete Frame Structures.* Mohamed M. Talaat and Khalid M. Mosalam. May 2008.

PEER 2007/09 *Integrated Probabilistic Performance-Based Evaluation of Benchmark Reinforced Concrete Bridges.* Kevin R. Mackie, John-Michael Wong, and Božidar Stojadinović. January 2008.

PEER 2007/08 *Assessing Seismic Collapse Safety of Modern Reinforced Concrete Moment-Frame Buildings.* Curt B. Haselton and Gregory G. Deierlein. February 2008.

PEER 2007/07 *Performance Modeling Strategies for Modern Reinforced Concrete Bridge Columns.* Michael P. Berry and Marc O. Eberhard. April 2008.

PEER 2007/06 *Development of Improved Procedures for Seismic Design of Buried and Partially Buried Structures.* Linda Al Atik and Nicholas Sitar. June 2007.

PEER 2007/05 *Uncertainty and Correlation in Seismic Risk Assessment of Transportation Systems.* Renee G. Lee and Anne S. Kiremidjian. July 2007.

PEER 2007/04 *Numerical Models for Analysis and Performance-Based Design of Shallow Foundations Subjected to Seismic Loading.* Sivapalan Gajan, Tara C. Hutchinson, Bruce L. Kutter, Prishati Raychowdhury, José A. Ugalde, and Jonathan P. Stewart. May 2008.

PEER 2007/03 *Beam-Column Element Model Calibrated for Predicting Flexural Response Leading to Global Collapse of RC Frame Buildings.* Curt B. Haselton, Abbie B. Liel, Sarah Taylor Lange, and Gregory G. Deierlein. May 2008.

PEER 2007/02 *Campbell-Bozorgnia NGA Ground Motion Relations for the Geometric Mean Horizontal Component of Peak and Spectral Ground Motion Parameters.* Kenneth W. Campbell and Yousef Bozorgnia. May 2007.

PEER 2007/01 *Boore-Atkinson NGA Ground Motion Relations for the Geometric Mean Horizontal Component of Peak and Spectral Ground Motion Parameters.* David M. Boore and Gail M. Atkinson. May. May 2007.

PEER 2006/12 *Societal Implications of Performance-Based Earthquake Engineering.* Peter J. May. May 2007.

PEER 2006/11 *Probabilistic Seismic Demand Analysis Using Advanced Ground Motion Intensity Measures, Attenuation Relationships, and Near-Fault Effects.* Polsak Tothong and C. Allin Cornell. March 2007.

PEER 2006/10 *Application of the PEER PBEE Methodology to the I-880 Viaduct.* Sashi Kunnath. February 2007.

PEER 2006/09 *Quantifying Economic Losses from Travel Forgone Following a Large Metropolitan Earthquake.* James Moore, Sungbin Cho, Yue Yue Fan, and Stuart Werner. November 2006.

PEER 2006/08 *Vector-Valued Ground Motion Intensity Measures for Probabilistic Seismic Demand Analysis.* Jack W. Baker and C. Allin Cornell. October 2006.

PEER 2006/07 *Analytical Modeling of Reinforced Concrete Walls for Predicting Flexural and Coupled–Shear-Flexural Responses.* Kutay Orakcal, Leonardo M. Massone, and John W. Wallace. October 2006.

PEER 2006/06 *Nonlinear Analysis of a Soil-Drilled Pier System under Static and Dynamic Axial Loading.* Gang Wang and Nicholas Sitar. November 2006.

PEER 2006/05 *Advanced Seismic Assessment Guidelines.* Paolo Bazzurro, C. Allin Cornell, Charles Menun, Maziar Motahari, and Nicolas Luco. September 2006.

PEER 2006/04 *Probabilistic Seismic Evaluation of Reinforced Concrete Structural Components and Systems.* Tae Hyung Lee and Khalid M. Mosalam. August 2006.

PEER 2006/03 *Performance of Lifelines Subjected to Lateral Spreading.* Scott A. Ashford and Teerawut Juirnarongrit. July 2006.

PEER 2006/02 *Pacific Earthquake Engineering Research Center Highway Demonstration Project.* Anne Kiremidjian, James Moore, Yue Yue Fan, Nesrin Basoz, Ozgur Yazali, and Meredith Williams. April 2006.

PEER 2006/01 *Bracing Berkeley. A Guide to Seismic Safety on the UC Berkeley Campus.* Mary C. Comerio, Stephen Tobriner, and Ariane Fehrenkamp. January 2006.

PEER 2005/16 *Seismic Response and Reliability of Electrical Substation Equipment and Systems.* Junho Song, Armen Der Kiureghian, and Jerome L. Sackman. April 2006.

PEER 2005/15 *CPT-Based Probabilistic Assessment of Seismic Soil Liquefaction Initiation.* R. E. S. Moss, R. B. Seed, R. E. Kayen, J. P. Stewart, and A. Der Kiureghian. April 2006.

PEER 2005/14 *Workshop on Modeling of Nonlinear Cyclic Load-Deformation Behavior of Shallow Foundations.* Bruce L. Kutter, Geoffrey Martin, Tara Hutchinson, Chad Harden, Sivapalan Gajan, and Justin Phalen. March 2006.

PEER 2005/13 *Stochastic Characterization and Decision Bases under Time-Dependent Aftershock Risk in Performance-Based Earthquake Engineering.* Gee Liek Yeo and C. Allin Cornell. July 2005.

PEER 2005/12 *PEER Testbed Study on a Laboratory Building: Exercising Seismic Performance Assessment.* Mary C. Comerio, editor. November 2005.

PEER 2005/11 *Van Nuys Hotel Building Testbed Report: Exercising Seismic Performance Assessment.* Helmut Krawinkler, editor. October 2005.

PEER 2005/10 *First NEES/E-Defense Workshop on Collapse Simulation of Reinforced Concrete Building Structures.* September 2005.

PEER 2005/09 *Test Applications of Advanced Seismic Assessment Guidelines.* Joe Maffei, Karl Telleen, Danya Mohr, William Holmes, and Yuki Nakayama. August 2006.

PEER 2005/08 *Damage Accumulation in Lightly Confined Reinforced Concrete Bridge Columns.* R. Tyler Ranf, Jared M. Nelson, Zach Price, Marc O. Eberhard, and John F. Stanton. April 2006.

PEER 2005/07 *Experimental and Analytical Studies on the Seismic Response of Freestanding and Anchored Laboratory Equipment.* Dimitrios Konstantinidis and Nicos Makris. January 2005.

PEER 2005/06 *Global Collapse of Frame Structures under Seismic Excitations*. Luis F. Ibarra and Helmut Krawinkler. September 2005.

PEER 2005//05 *Performance Characterization of Bench- and Shelf-Mounted Equipment.* Samit Ray Chaudhuri and Tara C. Hutchinson. May 2006.

PEER 2005/04 *Numerical Modeling of the Nonlinear Cyclic Response of Shallow Foundations.* Chad Harden, Tara Hutchinson, Geoffrey R. Martin, and Bruce L. Kutter. August 2005.

PEER 2005/03 *A Taxonomy of Building Components for Performance-Based Earthquake Engineering.* Keith A. Porter. September 2005.

PEER 2005/02 *Fragility Basis for California Highway Overpass Bridge Seismic Decision Making*. Kevin R. Mackie and Božidar Stojadinović. June 2005.

PEER 2005/01 *Empirical Characterization of Site Conditions on Strong Ground Motion.* Jonathan P. Stewart, Yoojoong Choi, and Robert W. Graves. June 2005.

PEER 2004/09 *Electrical Substation Equipment Interaction: Experimental Rigid Conductor Studies.* Christopher Stearns and André Filiatrault. February 2005.

PEER 2004/08 *Seismic Qualification and Fragility Testing of Line Break 550-kV Disconnect Switches.* Shakhzod M. Takhirov, Gregory L. Fenves, and Eric Fujisaki. January 2005.

PEER 2004/07 *Ground Motions for Earthquake Simulator Qualification of Electrical Substation Equipment.* Shakhzod M. Takhirov, Gregory L. Fenves, Eric Fujisaki, and Don Clyde. January 2005.

PEER 2004/06 *Performance-Based Regulation and Regulatory Regimes.* Peter J. May and Chris Koski. September 2004.

PEER 2004/05 *Performance-Based Seismic Design Concepts and Implementation: Proceedings of an International Workshop.* Peter Fajfar and Helmut Krawinkler, editors. September 2004.

PEER 2004/04 *Seismic Performance of an Instrumented Tilt-up Wall Building.* James C. Anderson and Vitelmo V. Bertero. July 2004.

PEER 2004/03 *Evaluation and Application of Concrete Tilt-up Assessment Methodologies.* Timothy Graf and James O. Malley. October 2004.

PEER 2004/02 *Analytical Investigations of New Methods for Reducing Residual Displacements of Reinforced Concrete Bridge Columns.* Junichi Sakai and Stephen A. Mahin. August 2004.

PEER 2004/01 *Seismic Performance of Masonry Buildings and Design Implications.* Kerri Anne Taeko Tokoro, James C. Anderson, and Vitelmo V. Bertero. February 2004.

PEER 2003/18 *Performance Models for Flexural Damage in Reinforced Concrete Columns.* Michael Berry and Marc Eberhard. August 2003.

PEER 2003/17 *Predicting Earthquake Damage in Older Reinforced Concrete Beam-Column Joints.* Catherine Pagni and Laura Lowes. October 2004.

PEER 2003/16 *Seismic Demands for Performance-Based Design of Bridges.* Kevin Mackie and Božidar Stojadinović. August 2003.

PEER 2003/15 *Seismic Demands for Nondeteriorating Frame Structures and Their Dependence on Ground Motions.* Ricardo Antonio Medina and Helmut Krawinkler. May 2004.

PEER 2003/14 *Finite Element Reliability and Sensitivity Methods for Performance-Based Earthquake Engineering.* Terje Haukaas and Armen Der Kiureghian. April 2004.

PEER 2003/13 *Effects of Connection Hysteretic Degradation on the Seismic Behavior of Steel Moment-Resisting Frames.* Janise E. Rodgers and Stephen A. Mahin. March 2004.

PEER 2003/12 *Implementation Manual for the Seismic Protection of Laboratory Contents: Format and Case Studies.* William T. Holmes and Mary C. Comerio. October 2003.

PEER 2003/11 *Fifth U.S.-Japan Workshop on Performance-Based Earthquake Engineering Methodology for Reinforced Concrete Building Structures.* February 2004.

PEER 2003/10 *A Beam-Column Joint Model for Simulating the Earthquake Response of Reinforced Concrete Frames.* Laura N. Lowes, Nilanjan Mitra, and Arash Altoontash. February 2004.

PEER 2003/09 *Sequencing Repairs after an Earthquake: An Economic Approach.* Marco Casari and Simon J. Wilkie. April 2004.

PEER 2003/08 *A Technical Framework for Probability-Based Demand and Capacity Factor Design (DCFD) Seismic Formats*. Fatemeh Jalayer and C. Allin Cornell. November 2003.

PEER 2003/07 *Uncertainty Specification and Propagation for Loss Estimation Using FOSM Methods.* Jack W. Baker and C. Allin Cornell. September 2003.

PEER 2003/06 *Performance of Circular Reinforced Concrete Bridge Columns under Bidirectional Earthquake Loading*. Mahmoud M. Hachem, Stephen A. Mahin, and Jack P. Moehle. February 2003.

PEER 2003/05 *Response Assessment for Building-Specific Loss Estimation.* Eduardo Miranda and Shahram Taghavi. September 2003.

PEER 2003/04 *Experimental Assessment of Columns with Short Lap Splices Subjected to Cyclic Loads*. Murat Melek, John W. Wallace, and Joel Conte. April 2003.

PEER 2003/03 *Probabilistic Response Assessment for Building-Specific Loss Estimation.* Eduardo Miranda and Hesameddin Aslani. September 2003.

PEER 2003/02 *Software Framework for Collaborative Development of Nonlinear Dynamic Analysis Program.* Jun Peng and Kincho H. Law. September 2003.

PEER 2003/01 *Shake Table Tests and Analytical Studies on the Gravity Load Collapse of Reinforced Concrete Frames.* Kenneth John Elwood and Jack P. Moehle. November 2003.

PEER 2002/24 *Performance of Beam to Column Bridge Joints Subjected to a Large Velocity Pulse.* Natalie Gibson, André Filiatrault, and Scott A. Ashford. April 2002.

PEER 2002/23 *Effects of Large Velocity Pulses on Reinforced Concrete Bridge Columns.* Greg L. Orozco and Scott A. Ashford. April 2002.

PEER 2002/22 *Characterization of Large Velocity Pulses for Laboratory Testing.* Kenneth E. Cox and Scott A. Ashford. April 2002.

PEER 2002/21 *Fourth U.S.-Japan Workshop on Performance-Based Earthquake Engineering Methodology for Reinforced Concrete Building Structures*. December 2002.

PEER 2002/20 *Barriers to Adoption and Implementation of PBEE Innovations.* Peter J. May. August 2002.

PEER 2002/19 *Economic-Engineered Integrated Models for Earthquakes: Socioeconomic Impacts.* Peter Gordon, James E. Moore II, and Harry W. Richardson. July 2002.

PEER 2002/18 *Assessment of Reinforced Concrete Building Exterior Joints with Substandard Details.* Chris P. Pantelides, Jon Hansen, Justin Nadauld, and Lawrence D. Reaveley. May 2002.

PEER 2002/17 *Structural Characterization and Seismic Response Analysis of a Highway Overcrossing Equipped with Elastomeric Bearings and Fluid Dampers: A Case Study.* Nicos Makris and Jian Zhang. November 2002.

PEER 2002/16 *Estimation of Uncertainty in Geotechnical Properties for Performance-Based Earthquake Engineering.* Allen L. Jones, Steven L. Kramer, and Pedro Arduino. December 2002.

PEER 2002/15 *Seismic Behavior of Bridge Columns Subjected to Various Loading Patterns.* Asadollah Esmaeily-Gh. and Yan Xiao. December 2002.

PEER 2002/14 *Inelastic Seismic Response of Extended Pile Shaft Supported Bridge Structures.* T.C. Hutchinson, R.W. Boulanger, Y.H. Chai, and I.M. Idriss. December 2002.

PEER 2002/13 *Probabilistic Models and Fragility Estimates for Bridge Components and Systems.* Paolo Gardoni, Armen Der Kiureghian, and Khalid M. Mosalam. June 2002.

PEER 2002/12 *Effects of Fault Dip and Slip Rake on Near-Source Ground Motions: Why Chi-Chi Was a Relatively Mild M7.6 Earthquake.* Brad T. Aagaard, John F. Hall, and Thomas H. Heaton. December 2002.

PEER 2002/11 *Analytical and Experimental Study of Fiber-Reinforced Strip Isolators*. James M. Kelly and Shakhzod M. Takhirov. September 2002.

PEER 2002/10 *Centrifuge Modeling of Settlement and Lateral Spreading with Comparisons to Numerical Analyses***.** Sivapalan Gajan and Bruce L. Kutter. January 2003.

PEER 2002/09 *Documentation and Analysis of Field Case Histories of Seismic Compression during the 1994 Northridge, California, Earthquake.* Jonathan P. Stewart, Patrick M. Smith, Daniel H. Whang, and Jonathan D. Bray. October 2002.

PEER 2002/08 *Component Testing, Stability Analysis and Characterization of Buckling-Restrained Unbonded Braces™.* Cameron Black, Nicos Makris, and Ian Aiken. September 2002.

PEER 2002/07 *Seismic Performance of Pile-Wharf Connections.* Charles W. Roeder, Robert Graff, Jennifer Soderstrom, and Jun Han Yoo. December 2001.

PEER 2002/06 *The Use of Benefit-Cost Analysis for Evaluation of Performance-Based Earthquake Engineering Decisions*. Richard O. Zerbe and Anthony Falit-Baiamonte. September 2001.

PEER 2002/05 *Guidelines, Specifications, and Seismic Performance Characterization of Nonstructural Building Components and Equipment*. André Filiatrault, Constantin Christopoulos, and Christopher Stearns. September 2001.

PEER 2002/04 *Consortium of Organizations for Strong-Motion Observation Systems and the Pacific Earthquake Engineering Research Center Lifelines Program: Invited Workshop on Archiving and Web Dissemination of Geotechnical Data, 4–5 October 2001*. September 2002.

PEER 2002/03 *Investigation of Sensitivity of Building Loss Estimates to Major Uncertain Variables for the Van Nuys Testbed.* Keith A. Porter, James L. Beck, and Rustem V. Shaikhutdinov. August 2002.

PEER 2002/02 *The Third U.S.-Japan Workshop on Performance-Based Earthquake Engineering Methodology for Reinforced Concrete Building Structures*. July 2002.

PEER 2002/01 *Nonstructural Loss Estimation: The UC Berkeley Case Study.* Mary C. Comerio and John C. Stallmeyer. December 2001.

PEER 2001/16 *Statistics of SDF-System Estimate of Roof Displacement for Pushover Analysis of Buildings.* Anil K. Chopra, Rakesh K. Goel, and Chatpan Chintanapakdee. December 2001.

PEER 2001/15 *Damage to Bridges during the 2001 Nisqually Earthquake.* R. Tyler Ranf, Marc O. Eberhard, and Michael P. Berry. November 2001.

PEER 2001/14 *Rocking Response of Equipment Anchored to a Base Foundation.* Nicos Makris and Cameron J. Black. September 2001.

PEER 2001/13 *Modeling Soil Liquefaction Hazards for Performance-Based Earthquake Engineering.* Steven L. Kramer and Ahmed-W. Elgamal. February 2001.

PEER 2001/12 *Development of Geotechnical Capabilities in OpenSees.* Boris Jeremić. September 2001.

PEER 2001/11 *Analytical and Experimental Study of Fiber-Reinforced Elastomeric Isolators*. James M. Kelly and Shakhzod M. Takhirov. September 2001.

PEER 2001/10 *Amplification Factors for Spectral Acceleration in Active Regions.* Jonathan P. Stewart, Andrew H. Liu, Yoojoong Choi, and Mehmet B. Baturay. December 2001.

PEER 2001/09 *Ground Motion Evaluation Procedures for Performance-Based Design*. Jonathan P. Stewart, Shyh-Jeng Chiou, Jonathan D. Bray, Robert W. Graves, Paul G. Somerville, and Norman A. Abrahamson. September 2001.

PEER 2001/08 *Experimental and Computational Evaluation of Reinforced Concrete Bridge Beam-Column Connections for Seismic Performance*. Clay J. Naito, Jack P. Moehle, and Khalid M. Mosalam. November 2001.

PEER 2001/07 *The Rocking Spectrum and the Shortcomings of Design Guidelines.* Nicos Makris and Dimitrios Konstantinidis. August 2001.

PEER 2001/06 *Development of an Electrical Substation Equipment Performance Database for Evaluation of Equipment Fragilities*. Thalia Agnanos. April 1999.

PEER 2001/05 *Stiffness Analysis of Fiber-Reinforced Elastomeric Isolators.* Hsiang-Chuan Tsai and James M. Kelly. May 2001.

PEER 2001/04 *Organizational and Societal Considerations for Performance-Based Earthquake Engineering.* Peter J. May. April 2001.

PEER 2001/03 *A Modal Pushover Analysis Procedure to Estimate Seismic Demands for Buildings: Theory and Preliminary Evaluation.* Anil K. Chopra and Rakesh K. Goel. January 2001.

PEER 2001/02 *Seismic Response Analysis of Highway Overcrossings Including Soil-Structure Interaction.* Jian Zhang and Nicos Makris. March 2001.

PEER 2001/01 *Experimental Study of Large Seismic Steel Beam-to-Column Connections.* Egor P. Popov and Shakhzod M. Takhirov. November 2000.

PEER 2000/10 *The Second U.S.-Japan Workshop on Performance-Based Earthquake Engineering Methodology for Reinforced Concrete Building Structures.* March 2000.

PEER 2000/09 *Structural Engineering Reconnaissance of the August 17, 1999 Earthquake: Kocaeli (Izmit), Turkey.* Halil Sezen, Kenneth J. Elwood, Andrew S. Whittaker, Khalid Mosalam, John J. Wallace, and John F. Stanton. December 2000.

PEER 2000/08 *Behavior of Reinforced Concrete Bridge Columns Having Varying Aspect Ratios and Varying Lengths of Confinement.* Anthony J. Calderone, Dawn E. Lehman, and Jack P. Moehle. January 2001.

PEER 2000/07 *Cover-Plate and Flange-Plate Reinforced Steel Moment-Resisting Connections.* Taejin Kim, Andrew S. Whittaker, Amir S. Gilani, Vitelmo V. Bertero, and Shakhzod M. Takhirov. September 2000.

PEER 2000/06 *Seismic Evaluation and Analysis of 230-kV Disconnect Switches.* Amir S. J. Gilani, Andrew S. Whittaker, Gregory L. Fenves, Chun-Hao Chen, Henry Ho, and Eric Fujisaki. July 2000.

PEER 2000/05 *Performance-Based Evaluation of Exterior Reinforced Concrete Building Joints for Seismic Excitation.* Chandra Clyde, Chris P. Pantelides, and Lawrence D. Reaveley. July 2000.

PEER 2000/04 *An Evaluation of Seismic Energy Demand: An Attenuation Approach.* Chung-Che Chou and Chia-Ming Uang. July 1999.

PEER 2000/03 *Framing Earthquake Retrofitting Decisions: The Case of Hillside Homes in Los Angeles.* Detlof von Winterfeldt, Nels Roselund, and Alicia Kitsuse. March 2000.

PEER 2000/02 *U.S.-Japan Workshop on the Effects of Near-Field Earthquake Shaking.* Andrew Whittaker, ed. July 2000.

PEER 2000/01 *Further Studies on Seismic Interaction in Interconnected Electrical Substation Equipment.* Armen Der Kiureghian, Kee-Jeung Hong, and Jerome L. Sackman. November 1999.

PEER 1999/14 *Seismic Evaluation and Retrofit of 230-kV Porcelain Transformer Bushings.* Amir S. Gilani, Andrew S. Whittaker, Gregory L. Fenves, and Eric Fujisaki. December 1999.

PEER 1999/13 *Building Vulnerability Studies: Modeling and Evaluation of Tilt-up and Steel Reinforced Concrete Buildings.* John W. Wallace, Jonathan P. Stewart, and Andrew S. Whittaker, editors. December 1999.

PEER 1999/12 *Rehabilitation of Nonductile RC Frame Building Using Encasement Plates and Energy-Dissipating Devices.* Mehrdad Sasani, Vitelmo V. Bertero, James C. Anderson. December 1999.

PEER 1999/11 *Performance Evaluation Database for Concrete Bridge Components and Systems under Simulated Seismic Loads.* Yael D. Hose and Frieder Seible. November 1999.

PEER 1999/10 *U.S.-Japan Workshop on Performance-Based Earthquake Engineering Methodology for Reinforced Concrete Building Structures.* December 1999.

PEER 1999/09 *Performance Improvement of Long Period Building Structures Subjected to Severe Pulse-Type Ground Motions.* James C. Anderson, Vitelmo V. Bertero, and Raul Bertero. October 1999.

PEER 1999/08 *Envelopes for Seismic Response Vectors.* Charles Menun and Armen Der Kiureghian. July 1999.

PEER 1999/07 *Documentation of Strengths and Weaknesses of Current Computer Analysis Methods for Seismic Performance of Reinforced Concrete Members.* William F. Cofer. November 1999.

PEER 1999/06 *Rocking Response and Overturning of Anchored Equipment under Seismic Excitations.* Nicos Makris and Jian Zhang. November 1999.

PEER 1999/05 *Seismic Evaluation of 550 kV Porcelain Transformer Bushings.* Amir S. Gilani, Andrew S. Whittaker, Gregory L. Fenves, and Eric Fujisaki. October 1999.

PEER 1999/04 *Adoption and Enforcement of Earthquake Risk-Reduction Measures.* Peter J. May, Raymond J. Burby, T. Jens Feeley, and Robert Wood.

PEER 1999/03 *Task 3 Characterization of Site Response General Site Categories.* Adrian Rodriguez-Marek, Jonathan D. Bray, and Norman Abrahamson. February 1999.

PEER 1999/02 *Capacity-Demand-Diagram Methods for Estimating Seismic Deformation of Inelastic Structures: SDF Systems.* Anil K. Chopra and Rakesh Goel. April 1999.

PEER 1999/01 *Interaction in Interconnected Electrical Substation Equipment Subjected to Earthquake Ground Motions.* Armen Der Kiureghian, Jerome L. Sackman, and Kee-Jeung Hong. February 1999.

PEER 1998/08 *Behavior and Failure Analysis of a Multiple-Frame Highway Bridge in the 1994 Northridge Earthquake.* Gregory L. Fenves and Michael Ellery. December 1998.

PEER 1998/07 *Empirical Evaluation of Inertial Soil-Structure Interaction Effects.* Jonathan P. Stewart, Raymond B. Seed, and Gregory L. Fenves. November 1998.

PEER 1998/06 *Effect of Damping Mechanisms on the Response of Seismic Isolated Structures.* Nicos Makris and Shih-Po Chang. November 1998.

PEER 1998/05 *Rocking Response and Overturning of Equipment under Horizontal Pulse-Type Motions.* Nicos Makris and Yiannis Roussos. October 1998.

PEER 1998/04 *Pacific Earthquake Engineering Research Invitational Workshop Proceedings, May 14–15, 1998: Defining the Links between Planning, Policy Analysis, Economics and Earthquake Engineering.* Mary Comerio and Peter Gordon. September 1998.

PEER 1998/03 *Repair/Upgrade Procedures for Welded Beam to Column Connections.* James C. Anderson and Xiaojing Duan. May 1998.

PEER 1998/02 *Seismic Evaluation of 196 kV Porcelain Transformer Bushings.* Amir S. Gilani, Juan W. Chavez, Gregory L. Fenves, and Andrew S. Whittaker. May 1998.

PEER 1998/01 *Seismic Performance of Well-Confined Concrete Bridge Columns.* Dawn E. Lehman and Jack P. Moehle. December 2000.

ONLINE REPORTS

The following PEER reports are available by Internet only at http://peer.berkeley.edu/publications/peer_reports.html

PEER 2011/101 *Report of the Eighth Planning Meeting of NEES/E-Defense Collaborative Research on Earthquake Engineering.* Convened by the Hyogo Earthquake Engineering Research Center (NIED), NEES Consortium, Inc. February 2011.

PEER 2010/111 *Modeling and Acceptance Criteria for Seismic Design and Analysis of Tall Buildings.* Task 7 Report for the Tall Buildings Initiative - Published jointly by the Applied Technology Council. October 2010.

PEER 2010/110 *Seismic Performance Assessment and Probabilistic Repair Cost Analysis of Precast Concrete Cladding Systems for Multistory Buildlings.* Jeffrey P. Hunt and Božidar Stojadinovic. November 2010.

PEER 2010/109 *Report of the Seventh Joint Planning Meeting of NEES/E-Defense Collaboration on Earthquake Engineering. Held at the E-Defense, Miki, and Shin-Kobe, Japan, September 18–19, 2009.* August 2010.

PEER 2010/108 *Probabilistic Tsunami Hazard in California.* Hong Kie Thio, Paul Somerville, and Jascha Polet, preparers. October 2010.

PEER 2010/107 *Performance and Reliability of Exposed Column Base Plate Connections for Steel Moment-Resisting Frames.* Ady Aviram, Božidar Stojadinovic, and Armen Der Kiureghian. August 2010.

PEER 2010/106 *Verification of Probabilistic Seismic Hazard Analysis Computer Programs.* Patricia Thomas, Ivan Wong, and Norman Abrahamson. May 2010.

PEER 2010/105 *Structural Engineering Reconnaissance of the April 6, 2009, Abruzzo, Italy, Earthquake, and Lessons Learned.* M. Selim Günay and Khalid M. Mosalam. April 2010.

PEER 2010/104 *Simulating the Inelastic Seismic Behavior of Steel Braced Frames, Including the Effects of Low-Cycle Fatigue.* Yuli Huang and Stephen A. Mahin. April 2010.

PEER 2010/103 *Post-Earthquake Traffic Capacity of Modern Bridges in California.* Vesna Terzic and Božidar Stojadinović. March 2010.

PEER 2010/102 *Analysis of Cumulative Absolute Velocity (CAV) and JMA Instrumental Seismic Intensity (I_{JMA}) Using the PEER–NGA Strong Motion Database.* Kenneth W. Campbell and Yousef Bozorgnia. February 2010.

PEER 2010/101 *Rocking Response of Bridges on Shallow Foundations.* Jose A. Ugalde, Bruce L. Kutter, Boris Jeremic

PEER 2009/109 *Simulation and Performance-Based Earthquake Engineering Assessment of Self-Centering Post-Tensioned Concrete Bridge Systems.* Won K. Lee and Sarah L. Billington. December 2009.

PEER 2009/108 *PEER Lifelines Geotechnical Virtual Data Center.* J. Carl Stepp, Daniel J. Ponti, Loren L. Turner, Jennifer N. Swift, Sean Devlin, Yang Zhu, Jean Benoit, and John Bobbitt. September 2009.

PEER 2009/107 *Experimental and Computational Evaluation of Current and Innovative In-Span Hinge Details in Reinforced Concrete Box-Girder Bridges: Part 2: Post-Test Analysis and Design Recommendations.* Matias A. Hube and Khalid M. Mosalam. December 2009.

PEER 2009/106 *Shear Strength Models of Exterior Beam-Column Joints without Transverse Reinforcement.* Sangjoon Park and Khalid M. Mosalam. November 2009.

PEER 2009/105 *Reduced Uncertainty of Ground Motion Prediction Equations through Bayesian Variance Analysis.* Robb Eric S. Moss. November 2009.

PEER 2009/104 *Advanced Implementation of Hybrid Simulation.* Andreas H. Schellenberg, Stephen A. Mahin, Gregory L. Fenves. November 2009.

PEER 2009/103 *Performance Evaluation of Innovative Steel Braced Frames.* T. Y. Yang, Jack P. Moehle, and Božidar Stojadinovic. August 2009.

PEER 2009/102 *Reinvestigation of Liquefaction and Nonliquefaction Case Histories from the 1976 Tangshan Earthquake.* Robb Eric Moss, Robert E. Kayen, Liyuan Tong, Songyu Liu, Guojun Cai, and Jiaer Wu. August 2009.

PEER 2009/101 *Report of the First Joint Planning Meeting for the Second Phase of NEES/E-Defense Collaborative Research on Earthquake Engineering.* Stephen A. Mahin et al. July 2009.

PEER 2008/104 *Experimental and Analytical Study of the Seismic Performance of Retaining Structures.* Linda Al Atik and Nicholas Sitar. January 2009.

PEER 2008/103 *Experimental and Computational Evaluation of Current and Innovative In-Span Hinge Details in Reinforced Concrete Box-Girder Bridges. Part 1: Experimental Findings and Pre-Test Analysis.* Matias A. Hube and Khalid M. Mosalam. January 2009.

PEER 2008/102 *Modeling of Unreinforced Masonry Infill Walls Considering In-Plane and Out-of-Plane Interaction.* Stephen Kadysiewski and Khalid M. Mosalam. January 2009.

PEER 2008/101 *Seismic Performance Objectives for Tall Buildings.* William T. Holmes, Charles Kircher, William Petak, and Nabih Youssef. August 2008.

PEER 2007/101 *Generalized Hybrid Simulation Framework for Structural Systems Subjected to Seismic Loading.* Tarek Elkhoraibi and Khalid M. Mosalam. July 2007.

PEER 2007/100 *Seismic Evaluation of Reinforced Concrete Buildings Including Effects of Masonry Infill Walls.* Alidad Hashemi and Khalid M. Mosalam. July 2007.

The Pacific Earthquake Engineering Research Center (PEER) is a multi-institutional research and education center with headquarters at the University of California, Berkeley. Investigators from over 20 universities, several consulting companies, and researchers at various state and federal government agencies contribute to research programs focused on performance-based earthquake engineering.

These research programs aim to identify and reduce the risks from major earthquakes to life safety and to the economy by including research in a wide variety of disciplines including structural and geotechnical engineering, geology/seismology, lifelines, transportation, architecture, economics, risk management, and public policy.

PEER is supported by federal, state, local, and regional agencies, together with industry partners.

PEER reports can be ordered at http://peer.berkeley.edu/publications/peer_reports.html or by contacting

Pacific Earthquake Engineering Research Center
University of California, Berkeley
325 Davis Hall, mail code 1792
Berkeley, CA 94720-1792
Tel: 510-642-3437
Fax: 510-642-1655
Email: peer_editor@berkeley.edu

ISSN 1547-0587X